Applied Catalysis B: Environmental 334 (2023) 122853

Contents lists available at ScienceDirect

Applied Catalysis B: Environmental

journal homepage: www.elsevier.com/locate/apcatb

A roadmap towards sustainable anode design for alkaline water electrolysis

Tanveer ul Haq [a,*], Yousef Haik [b,c,**]

[a] Department of Chemistry, College of Sciences, University of Sharjah, P.O. Box 27272, Sharjah, United Arab Emirates
[b] Department of Mechanical and Nuclear Engineering, College of Engineering, University of Sharjah, P.O. Box 27272, Sharjah, United Arab Emirates
[c] Department of Mechanical Engineering, The University Jordan, Amman, Jordan

ARTICLE INFO

Keywords:
Anode degradation mechanism
High activity stability factor
Sustainable anode
Structural stability
Chemical stability
Mechanical stability
High corrosion resistance

ABSTRACT

Long-term anode durability with high intrinsic activity is crucial to deliver affordable green hydrogen by electrochemical water splitting. Current research mainly focuses on tuning the oxygen evolution reaction activity and efficiency, although the anode's structural, chemical, and mechanical sustainability at high geometric activity poses a significant challenge. In this review, anode degradation mechanisms based on surface reconstruction, agglomeration, and dissolution are described and discussed various strategies to design a durable anode with synergistic modulation of intrinsically reactive abundant active sites, efficient mass transfer, the fast rate for electron transportation, and gas evolution. Various strategies such as electronic modulation by cation, heteroatom doping, surface and structural optimization by defects engineering, heterostructure development and morphology tuning, aerophobic character, and strong catalyst support interactions are evaluated. Finally, we discussed the remaining stability challenges and set practical guidelines on how these potential strategies can be exploited to design stable high-output OER catalysts. With these insights, this review article will hopefully provide a roadmap for the rational design of a sustainable anode to make the water electrolysis process viable for scalable hydrogen production.

1. Introduction

Hydrogen is considered a very sustainable and promising alternative to traditional fossil fuels and a versatile energy carrier to tackle key energy challenges [1,2]. The current world's hydrogen demand is $150 billion, signaling the rising interest in green hydrogen as an energy carrier [3]. Over 95% of total hydrogen is formed by steam reforming of fossil fuels, accountable for 830Mt/yr carbon dioxide (CO_2) emission and causing serious threat to the environment [4]. Electrochemical water splitting is a practical approach to produce green hydrogen with high purity and zero carbon emission [5,6]. However, water electrolysis is a highly energy-intensive process, sharing less than 5% of the global hydrogen market due to its high capital expenditures [7]. The electricity capital expenses account for over 60% of the H_2 cost for renewable electricity if the electrolyzers sustainability operates for 4000 h (h). This is the dire need of society to tackle the required electricity consumption and capital expenditures of water electrolysis to make this process viable for massive green hydrogen production. This calls for the rational design of a cost-effective electrocatalyst to reduce capital expenditure with high intrinsic activity and high sustainability for thousands of hours a lifetime [8,9].

Electrochemical water splitting consists of two heterogenous half-cell reactions: anodic oxygen evolution reaction (OER) and cathodic hydrogen evolution reaction (HER) [10,11]. Both redox reactions imply the diffusion of reactants, successive adsorption-desorption of intermediates, and removal of the product in gaseous form at solid-liquid-gas triple-phase interfaces [12,13]. Currently, most active anode and cathode are composed of Ir/Ru-based materials and Pt group metals, respectively, while their high cost and scarcity obstruct commercial adoption [14,15]. An ideal electrocatalyst needs the following features: (1) Scalable synthesis of low-cost materials, (2) high intrinsic activity, (3) effective mass and electron transportation via short diffusion channels, (4) high structural, chemical, and mechanical durability [15,16]. From a practicable perspective, all these features should be fitted together in a single electrocatalyst. Low cost, activity, and stability are three significant merits that need to be considered for developing commercial electrocatalysts [17,18]. Recently, two strategies have been well established to boost the catalytic activity of an electrocatalyst:

* Corresponding author.
** Corresponding author at: Department of Mechanical and Nuclear Engineering, College of Engineering, University of Sharjah, P.O. Box 27272, Sharjah, United Arab Emirates.
E-mail addresses: thaq@sharjah.ac.ae (T. ul Haq), yhaik@sharjah.ac.ae (Y. Haik).

https://doi.org/10.1016/j.apcatb.2023.122853
Received 14 December 2022; Received in revised form 1 May 2023; Accepted 4 May 2023
Available online 6 May 2023

increasing the number and intrinsic activity of active sites [19–21]. To ameliorate the intrinsic activity of each active site, methods such as defects and phase engineering, multi-metal, and directional facet engineering, have been established [22–26]. Similarly, nanostructuring, fabrication of active sites with a 3D substrate, and its hybridization with conductive carbon ensure the maximum exposure of the active center for the adsorption-desorption of intermediates. These strategies work together to deliver high current density at low input voltage. The extensive reports published in recent years for designing earth-abundant electrocatalysts with impressive catalytic performance endorsed much progress in the direction of low cost and activity [27,28]. In the literature, limited reports are available that systematically focus on the durability of the anode, especially in industrial conditions. The catalyst with lower water oxidation performance having a slow degradation rate save enough energy cost after a longer operation time compared to the catalyst that demonstrates high OER efficiency but degrades faster [29, 30]. That is why, in a real application, the long-term sustainability of anode could carry even more weight than the significance of their activity and thus require more emphasis. The significant parameters that affect the anode durability are chemical transformation, structural disorders, and metal leaching (mechanical stability) during electrocatalysis at a high anodic potential [31,32].

In order to explore both the origin and solutions to the anode durability bottlenecks, this perspective comprehensively discussed the anode degradation mechanism and mitigation strategies. Chemical oxidation of the catalyst to inactive phase under high anodic potential is responsible for catalyst degradation [33]. Similarly, if surface reconstruction and structural disorders decrease the number of active sites, it causes catalyst instability [34]. Sometime O-O coupling occurs via lattice oxygen and induces structural instability [35,35]. In addition, metal dissolution and redeposition of dissolved ions compromise the Activity-Stability factor and substantially influence the durability of a heterogeneous catalyst [36,37]. Besides the degradation mechanism, recent innovative strategies for developing highly sustainable anode operating under industrial conditions are also discussed in this review. The mitigation strategies are electronic modulation to optimize the chemisorption energy of active sites for OER intermediate that increases the redox recyclability and sustains the catalyst in the active chemical phase [38–41]. Morphological optimizations avoid agglomeration, persist the number of active sites, and enhance the structural stability of the catalyst [42–44]. The super hydrophilic-aerophobic feature improved the charge and mass transfer, accelerated the bubble detachment to provide the maximum contact between electrolyte and active sites, and suppressed the support passivation [45,46]. Fabricating active sites on selective support decreases the metal dissolution rate and enhances overall stability [47,48]. By appropriately modifying the structure, component, dissolution, and redeposition, we believe this review will open up new endeavors for developing an anode with long-term durability for economic and massive green hydrogen production from water.

2. Figure of merits

Catalyst durability can be evaluated by directly measuring alteration in physiochemical properties (e.g., agglomeration or leaching of active sites) or by measuring the catalytic activity [49]. Usually, the activity declination is correlated to the catalyst's durability, but it does not always reflect the true sustainability of the active component [50,51]. Sometimes, catalyst leaching creates a rougher surface with a high specific surface area, provides additional active sites for the reaction, and boosts the catalytic activity [52–54]. Similarly, suppose the catalyst chemically transforms to a more active phase with a suitable electronic configuration concerning OER intermediates. In that case, it will increase the catalyst activity observed in Ni and Co-based oxides [55,56]. Although the unstable catalyst failure criteria are easy to determine by monitoring the sharp decrease in current density or ascending in the overpotential, the durability experiment parameters are varied significantly with no scientific justification.

Markovic and coworkers proposed activity and stability relation in terms of the Activity-Stability factor (ASF) that is more accurate and appropriate to evaluate electrode materials' intrinsic activity and stability [57]. ASF of any materials is the O_2 production rate and metal dissolution rate ratio. The rate of O_2 production can be expressed in geometric current density (j), while metal leaching or dissolution during water oxidation is equivalent to the current dissolution density (S (Eq. 1).

$$ASF = \left[\frac{J - S}{S}\right]_{\eta} \tag{1}$$

The material with high ASF is considered highly sustainable in practical application. Although Faradic efficiency is the kinetic parameter and provides insights into the ratio of activity and durability of active components, its accuracy is limited due to the involvement of both water and lattice oxygen in O-O coupling. The same group designed the Ir-based nanoporous architecture derived from the Ir_xOs alloy via a dealloying strategy and studied its ASF. The results demonstrate that the nanoporous morphology accelerates the Os dealloying rate, decreasing the Ir dissolution. The de-alloyed catalyst demonstrates a 30-fold higher ASF than benchmark Ir-based oxide due to its nanoporous surface structure effect rather than the electronic effect due to intermetallic bonding.

3. Anode degradation mechanism

3.1. Metal oxide corrosion

During the Oxygen Evolution Reaction (OER), the electrocatalyst can undergo several redox reactions involving the transfer of multiple electrons and protons. The electron transfer between the metal and the reaction intermediates can lead to the formation of M-O bonds, which can affect the catalytic activity of the electrocatalyst. However, under certain conditions, such as in basic or high potential electrolytes, the M-M bonds can be weakened, and the metal can dissolve in the electrolyte. The weakening of the M-M bonds and the dissolution of the metal in the electrolyte are related phenomena that can occur due to the oxidative dissolution of the electrocatalyst. This process involves the transfer of electrons from the metal surface to the reaction intermediates, leading to the formation of metal ions in the electrolyte. The metal ions can then react with the electrolyte and form soluble complexes, leading to the dissolution of the metal in the electrolyte. One mechanism by which the electron transfer between the metal and OER reaction intermediates can weaken the M-M bonds is by the formation of active oxygen species, such as hydroxyl radicals (OH*) and superoxide anions (O_2^-). These species can be formed on the surface of the catalyst by the reaction of water molecules with adsorbed intermediates or through direct interaction with the metal surface. The adsorbed intermediates can be hydroxide ions (OH^-) or oxygen-containing species, such as OOH* and O*. The reactive species can react with the metal surface, leading to the formation of metal-oxygen intermediates, which are unstable and can cause degradation of the M-M bonds. The weakening of the M-M bonds is a consequence of the partial transfer of electrons from the metal surface to the oxygen-containing species, resulting in the formation of metal-oxygen bonds. This process can be facilitated by the interaction of the oxygen-containing species with the M-M bonds, which can lead to the breaking of the bonds. As the metal-oxygen bonds are formed, the stability of the metal surface decreases, and the catalyst becomes more susceptible to dissolution in the electrolyte. The dissolution of the metal in the electrolyte can be accelerated by the interaction of the metal surface with the hydroxide ions (OH^-) in the electrolyte. The OH^- ions can interact with the metal surface and form metal-hydroxide complexes, which can further weaken the M-M bonds and promote the

dissolution of the metal in the electrolyte. The mechanism of electrocatalytic dissolution involves the formation and dissolution of metal oxide or hydroxide species on the surface of the catalyst during OER. The catalyst can undergo electrocatalytic dissolution due to the high potentials required for OER, which can exceed the thermodynamic stability of the metal oxide or hydroxide species formed during OER [58].

The electrocatalytic dissolution can occur in two steps. First, the surface of the catalyst undergoes oxidation during OER, which leads to the formation of metal oxide or hydroxide species. Second, these species can dissolve into the electrolyte due to the high potentials and reactive species generated during OER. The dissolution of metal oxide or hydroxide species can occur through several pathways. one pathway is the formation of intermediate species, such as metal oxyhydroxide, during OER. These species can undergo further oxidation and dissolution, leading to the loss of catalytic activity. The dissolution can occur due to the reaction of the intermediate species with protons or anions in the electrolyte. Moreover, the dissolution of transition metals during OER has been shown to depend on various factors, including the nature of the metal, the reaction environment, and the operating conditions. For example, studies have shown that the dissolution of iron in OER occurs through the formation of a highly soluble FeOOH intermediate, whereas the dissolution of nickel occurs due to the formation of a less soluble NiO species [59].

Binninger et.al., have proposed the following mechanism for the metal corrosion [60].

1. The cation M_{LOER}^{2n} that remains after the dissociation of LOER may dissolve in the electrolyte solution without any change in its oxidation state and subsequently move away from the electrode through diffusion. This phenomenon can result in a mass reduction of the metal oxide anode.
2. Under electrochemical conditions, the metal cation M_{LOER}^{2n+} can undergo oxidation to a higher oxidation number, resulting in an increased solubility in the electrolyte (Eq. 2).

$$M_{LOER}^{2n} \rightarrow M_{(aq)}^{(2n+m)+} + me^{-} \quad (2)$$

3. The electrochemical oxidation of the metal cation M_{LOER}^{2n+} can result in the formation of higher-valent cations with greater solubility in the electrolyte. The alkaline electrolyte solubilizes these higher-charge cations and undergo diffusion away from the electrode (Eq. 3).

$$MO_n \rightarrow M_{(aq)}^{(2n+m)+} + 1/2nO_2 + (2n+m)e^{-} \quad (3)$$

4. This cation cycle involves simultaneous oxidation of the lattice metal cation and oxygen anion, developing a 3-D boundary layer at electrolyte-metal oxide interface. This layer is referred to as the "hydrous amorphous layer" and offers specific active sites for intermediate adsorption. The LOER cation cycle induces dynamic changes in the hydrous amorphous layer but would not contribute to a mass loss. The electrode can be considered in a dynamic but stable state only if all metal cations participate in the cycle, and only those leaving the cycle to dissolve in the electrolyte will generate a mass loss of the electrode.
5. The metal oxide electrode endures a chemical process where oxygen anions are oxidized by a positively charged metal cations M_{LOER}^{2n+} and transfer them to the hydrous amorphous layer. This mechanism is comparable to the diffusion of created oxygen vacancies from the surface layer to the bulk of the metal oxide, thereby promoting the 3-dimensional expansion of the boundary layer.

3.2. Surface reconstruction

During the oxygen evolution reaction (OER), the surface of the electrocatalyst can undergo reconstruction, leading to a loss of activity. This reconstruction can occur due to the reaction of metal oxide electrocatalysts with protons generated during the OER. The Lux classification describes metal oxides as basic, and when they react with protons, they can become protonated and corrode, dissolve, or undergo amorphization [61]. Amorphous compounds refer to materials that lack long-range order and have a disordered atomic structure. These compounds can be formed through various processes, such as rapid quenching or precipitation from solution. In the case of transition metal dissolution during OER in alkaline environments, the amorphous compounds can form due to the rapid and uncontrolled growth of metal oxide or hydroxide species on the surface of the catalyst. The rapid growth of these species can result in the formation of disordered, amorphous compounds instead of ordered crystalline structures [62].

Firstly, the disordered atomic arrangement of amorphous compounds can result in a high degree of disorder and structural defects, making them more susceptible to dissolution in alkaline environments during OER. The formation of structural defects and disordered atomic arrangements can result from the rapid nucleation and growth of metal oxide or hydroxide species on the surface of the catalyst. The rapid growth of metal oxide or hydroxide species can result in structural defects and disordered atomic arrangements due to the inability of the metal atoms to pack together in an ordered manner. Secondly, the dissolution of amorphous compounds can occur due to the formation of reactive intermediates, such as metal oxyhydroxide species. These oxyhydroxide species can undergo further oxidation and dissolution, leading to the loss of catalytic activity. For example, the dissolution of iron-based catalysts during OER has been attributed to the formation of amorphous FeOOH species, which can undergo further oxidation to form Fe2O3 and dissolve in alkaline environments. Finally, the dissolution of amorphous compounds can be influenced by the composition and structure of the amorphous compound itself. For example, amorphous compounds with a higher concentration of metal ions or a higher degree of structural disorder are more susceptible to dissolution in alkaline environments during OER. The dissolution of amorphous compounds can also be influenced by the presence of other species in the electrolyte, such as anions or organic compounds, which can interact with the metal oxide or hydroxide species and affect their stability [63].

Self-healing oxygen evolution catalysts (OECs) can regenerate themselves with a repair rate greater than or equal to the damage rate. This regeneration is achieved when an external bias is applied to the OEC, which drives the regeneration process, preventing the degradation of the catalyst. The catalyst's ability to self-heal depends on various factors, such as electrolyte concentration, temperature, applied current and potential, and mass transport conditions [64].

3.3. Catalyst surface blocking

Catalyst surface blocking during water splitting refers to a phenomenon in which unwanted species cover or secure the catalyst's surface, thereby reducing or inhibiting its ability to catalyze the desired chemical reaction. During the OER process, unwanted species, such as adsorbed intermediates or reaction products, can accumulate on the catalyst surface, eventually leading to surface blockage. These species can include hydroxyl groups (OH^-), oxygen-containing species (O*, OOH*), and metal oxide species (MO*, M-OH*), among others. As the catalyst surface becomes blocked, the number of active sites available for the OER reaction is reduced, resulting in decreased OER activity. In severe cases, the catalyst may become completely inactive, preventing the OER reaction from occurring altogether [65].

Several strategies can be employed to prevent or mitigate catalyst surface blocking during water splitting. These include using catalysts with high surface area, modifying the catalyst surface with functional

groups that repel unwanted species, employing electrochemical methods such as electrode potential cycling to remove surface species, and using catalysts that are resistant to surface blocking, such as nickel-iron oxides [65].

3.4. Active sites agglomeration

The internal surface of the catalyst is not exposed to the electrolyte and not participating in redox reactions; only the unsaturated surface atom of the catalyst can serve as an active component and facilitate the intermediate's adsorption-desorption [66]. Nanostructuring is a well-established strategy to maximize the number of active sites and the intrinsic activity of each active site. Ideally, the distance between two active centers should be less than the Vander wall radii of O_2, where a low activation barrier is associated with the O-O coupling. At such a close distance, nanostructures with high surface energy are intrinsically unstable and become bigger due to Ostwald ripening; the existing particles serve as a nucleation center for the redeposition and growth of dissolved ions and increase the particle size distribution (PSD) [67]. During redeposition or reprecipitation, other nucleation centers, e.g., defects in the support, facilitate the nanostructure growth, block the active sites, and decrease the electrocatalyst's specific surface area. In the catalyst with abundant active sites, particle size increases due to sintering, where particles in the vicinity of each other are contacted, become bigger in size, and decrease the surface energy. The particle agglomeration usually is due to the corrosion of supporting materials and weak catalyst support interaction [68,69].

3.5. Support passivation

During the water oxidation in the harsh electrolyte at high anodic potential, a semi or nonconductive oxide layer is formed, decreasing the effective contact of the water molecule with the underlying support, and impeding the current flow. This layer may be directly grown over the support materials or onto the top of the catalyst surface. The reduction in the contact area between the electrode and electrolyte needs more positive input voltage to deliver the same geometric activity that further accelerates the catalyst's deactivation.

During OER, transition metals demonstrate the continuous variation of the electronic structure and valance state, which lead to the metal dissolution and its leaching from the underlying support. Cherevko et al. examined the dissolution of different precious metals Ru, Ir, Pd, Rh, Pt, Au, and Ag in alkaline conditions (0.05 M NaOH); the experimental findings revealed that the water oxidation activity increases in the order of Au<Pt<Pd<Ag<Rh<Ir<Ru, while metals dissolution rate also increases in the order of Au<Pd<Pt<Rh<Ir<Au<Ag and Ru [70]. These materials transform to destabilized form at high anodic potential, where their polar index value matches with the water and loses its stability. It has been investigated that the benchmark rutile type RuO_2 chemically oxidizes to RuO_4^{2-} and is dissolved in solution [71]. Similarly, another state of art catalyst, i.e., IrO_2, also suffers from the same problem of chemical oxidation and does not sustain the high current density for an extended period [72]. Although metal dissolution has been observed for the transition metal (e.g., Ni, Co, and Fe) based catalysts, their durability is sufficiently higher than the noble metals [73]. Markovic group investigated the Activity-Stability trends for monometallic 3d transition metals (M-O_xH_y; M=Fe, Co, and Ni) [74]. The catalysts were stabilized over the Pt surface with reasonable control over reactive site coverage and possess a high roughness factor. The ASF for the designed catalysts was elucidated in a highly pure KOH electrolyte to evade the contamination effect in the electrochemical response. The O_2 gas production to metal dissolution has been monitored using a stationary probe rotating disk electrode (SPRDE) coupled to an ICP-MS spectrometer. The comparative analysis of ASF at 1.7 V vs. RHE revealed the following trend for the activity Fe O_xH_y > CoO_xH_y > NiO_xH_y, which is the opposite trend inspected for OER stability. After five cyclic polarization curves, the Fe-based catalyst reveals a considerable drop in the OER activity due to its higher dissolution rate, leading to a reduction in active metal sites. Both polarization and steady-state analysis demonstrated the long-term durability of Ni-based catalysts without noticeable degradation due to a slow dissolution rate. Because ASF is a metric that evaluates the gas production rate for a given quantity of dissolved specie, the higher ASF represents the higher conversion rate with respect to time. Based on this assumption, the author attributed the higher ASF to the Ni-based catalyst despite its poor efficiency per geometric area. The authors have incorporated these active sites with other transition metals and evaluated the ASF. The ICP-MS results revealed that Cu interconnected with NiO_xH_y showed high stability in a given potential window compared to pristine CuO_xH_y. The authors suggested that high activity and stability of active sites by increasing the intrinsic activity and suppressing the metal dissolution is the practical way to enhance the ASF. The Ni and Cu precursor with Fe contamination revealed higher ASF due to Fe active sites and prevention of metal dissolution due to interfacial interaction between metal d orbitals.

Recently, researchers have substantially explored metal oxides (spinel's, perovskite, and rutile), boride, chalcogenides, pnictides, and carbides. Jaramillo and coworkers investigated the activity and stability of Co and Ni-based electrocatalysts (CoO, CoPi, Co-FeO_x, NiO, Ni-CeO_x, Ni-CoO_x, Ni-CuO_x, and Ni-FeO_x, for water oxidation [75]. It has been observed that in alkaline conditions, Co-FeO_x, and IrO_x were unstable. The slow dissolution of Co-FeO_x was attributed to the spinel-type structure, causing the reduction of the number of active metal centers and loss of catalytic efficiency after 2 h of continuous operations.

4. O-O Coupling Pathway

The O-O coupling route in water oxidation plays a critical role in the sustainability of active sites. The reaction pathway for water oxidation defines the dissolution rate and catalyst durability. Aside from establishing strategies for utilizing highly efficient and sustainable electrocatalysts, research on OER mechanisms and O-O coupling pathway is also significant in recognizing the actual active phase on the catalyst surface. Fig. 1A revealed a universally accepted mechanism of OER in alkaline media, known as the adsorbate evolution mechanism (AEM). In the 1st step, hydroxyl anion diffuses towards the anode, adsorbed on the active sites (M) by one-electron oxidation, and turns into an M-OH intermediate. Then M=O intermediate is formed on active sites from the removal of coupled electron and proton (H^+). In AEM, M=O intermediate interact with OH- ion and forms an oxyhydroxide (M-OOH) intermediate via one-electron oxidation, and the proton-coupled electron transfer process is again initiated, which leads to the O-O coupling and regenerating the active sites for cyclic reaction (Eqs. 4–7). In contrast to AEM, Fig. 1b depicts another OER reaction pathway (lattice oxygen oxidation mechanism, LOM), without adsorbate energy scaling limitations, which occurs only when two adjacent oxidized oxygen can substitute a portion of sacrificial metal oxygen and hybridize oxygen holes by themselves [76]. In LOM, two metal sites are responsible for O-O coupling, which is desorbed as O_2 from metal ions (Eqs. 4–5,8–9) [77].

$$M + OH^- \rightarrow M - OH + e^- \quad (4)$$

$$M - OH + OH^- \rightarrow M = O + e^- + H_2O \quad (5)$$

$$M = O + OH^- \rightarrow M - OOH + e^- \quad (6)$$

$$M - OOH + OH^- \rightarrow M + H_2O + e^- + O_2 \quad (7)$$

$$M = O + M = O \rightarrow M - O - O - M \quad (8)$$

$$M - O - O - M \rightarrow 2M + O_2 \quad (9)$$

[35,78] Grimaud et al. used in situ isotope labeling mass spectrometry to evaluate many perovskite OER catalysts. They discovered that O2

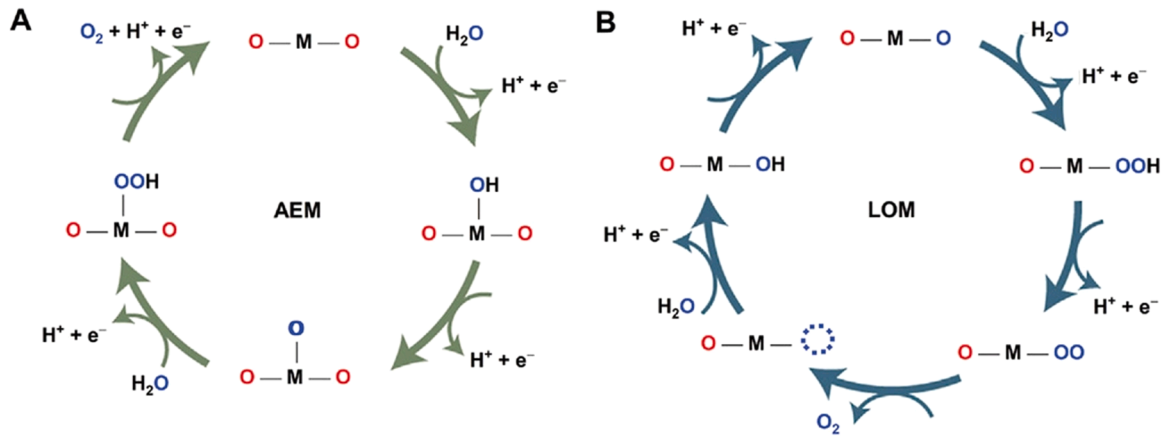

Fig. 1. (A) Adsorbate evolution mechanism and. B) Lattice oxygen oxidation mechanism. M represents the active sites
Reproduced with permission from ref [76]. Copyright 2022, Wiley

production during OER could be attributed to lattice oxygen for some efficient catalysts [79]. Catalysts with lattice oxygen exchange, such as $La_{0.5}Sr_{0.5}$-CoO_3-d and $SrCoO_3$-d, showed pH-dependent OER activity, whereas those without, such as $LaCoO_3$, demonstrated pH-independent OER activity. This may be due to the mechanistic difference for O-O coupling between AEM and LOM. Density functional theory (DFT) calculations revealed that non-concerted proton-electron transfer steps are feasible on perovskites with higher activity and possess stronger metal-oxygen covalency. Similar trends have also been revealed in oxyhydroxide and spinel oxide system [80,81].

The OER proceeds on one active site in conventional AEM, and the activity is highly dependent on the chemisorption energy of OER intermediates. Ideally, all steps should proceed on the catalyst surface with the same free energy (G) magnitude at U = 0. (U: external potential). However, because of the linear correlation of OER intermediates in AEM, the binding of *OH and *OOH is closely coupled with the energy gap of 3.2 eV (ΔG*OOH-ΔG*OH) [82,83]. Because this scaling connection defines the lower limit of the OER at 370 mV, breaking such a scaling relationship is critical for enhancing OER kinetics [84]. Recently, researchers have reported different electronic and structural modulations to optimize ΔG*O, ΔG*OH, and ΔG*OOH to bind O-intermediates that are neither too strong nor too weak, according to the Sabatier principle [85]. The efficient tactics are foreign elements substitution, vacancy generation, strain tuning, and surface engineering, etc [86–88].

Binninger et al. investigate the catalyst durability and follows the lattice oxygen and conventional adsorbate route during the OER by considering the thermodynamic model [60]. Suppose free reaction enthalpies are considered thermodynamically during the reaction pathways. In that case, this leads to a fixed relation of both routes for dissolution because AEM and LOM share the reaction intermediates. However, LOM is not limited to the adsorption energy scaling relationship and surpasses the theoretical limitation of AEM for OER activity by providing a distinct pathway for O-O coupling. Recent findings demonstrated the probability of bulk oxidation by LOM and the development of 3-D surface oxides regime on active sites of many electrocatalysts. The metal cations in LOM either recombine with the OH^- ions from the electrolyte and return to their original state or dissolve if dissolution is kinetically favored over recombination and decreases the ASF. A thermodynamic study revealed that the LOM route has the potential to decrease the activation barrier for O-O coupling, but the involvement of lattice oxygen could also lead to catalyst instability. Binninger et al. model recommends the replacement of oxygen anions with high oxidation potential anions or reducing the mobility of oxygen anions to prevent the dissolution and LOM for the high sustainability of the anode [60].

5. Electronic optimization

5.1. Cation doping

The electronic structure of active sites defines its position relative to the fermi energy level, modulates the potential energy barrier for O-O coupling and remarkably impact the activity and stability of active sites. An electronic modification of active sites by increasing or decreasing the electronic cloud around active components is a realistic approach to optimize the chemisorption energy and increases the redox recyclability of active sites [89]. The intermediate adsorption and desorption rate depends on the metal d band position relative to the Fermi level, as Norskov's theorem explains. The electronic features of active components could be well controlled by tuning the nature, location, and density of dopants in the parent framework. Markovic and coworkers investigated the activity-stability trends for water oxidation on conductive metals (M) hydroxide/oxyhydroxide (O_xH_y) cluster and Fe containing M-O_xH_y (M= Fe, Co, Ni, and Cu [74]. The experimental results demonstrated that Fe dissolution and redeposition at the Fe-containing electrolyte-host interface establish dynamically durable Fe active sites. These dynamically stable active sites surpass the limitations enforced by the thermodynamic instability of oxide materials at anodic potentials and give a general descriptor for catalyst activity and stability. The authors used in-situ ICP-MS and observed that pure Cu active sites in pristine Cu-O_xH_y form reveal limited stability in OER potential window compared to the Cu active sites in Ni-Cu O_xH_y. At the same time, Fe insertion further enhanced the Faradic efficiency and catalyst durability by decreasing the dissolution rate. The promoted ASF was attributed to the synergistic intermetallic interaction, modulated the electronic structure, enhanced the number of dynamically stable active sites, and reduced the potential energy barrier for O-O coupling. The author's findings unveiled that the efficient way to enhance the ASF value for anodic materials is to attain high intrinsic activity and stability concurrently. The same group investigated the origin of the ultra-stable and active components of an electrocatalyst $La_{1-x}Sr_xCoO_3$ (LSCO) [90]. The detailed investigation revealed that Co sites chemically transform to Co-OOH that interact with the electrolyte's trace quantity of Fe specie and generate dynamically sustainable active components. The chemical oxidation of Co to Co-OOH triggers the Fe interaction, modulates the electronic distribution, suppresses the Co dissolution, and increases the stability 10-fold compared to the nanoscale cobalt hydroxide structure. The current dissolution density (S) calculations show that the Co-active site's interaction with La and Sr decreases the metal dissolution rate from 23 pg $cm^{-2}s^{-1}$ to 1.8 pg $cm^{-2}s^{-1}$. Density functional theory (DFT) calculations revealed that LSCO interactions enhanced the Co-OOH active sites by the free energy of 0.3 eV compared to the Co-OOH

stabilized over Pt. The authors have estimated the ASF that shows the 3-time improvement after La and Sr doping. The authors proposed a model for the electronic conduction between perovskite oxide and alkaline water interface, which allows the chemical oxidation of TM-hydroxide/oxy(hydroxide) shell around the perovskite core, and their interaction with the Fe to create dynamically stable active sites to promote the OER. The electronic density can be manipulated by changing the dopant nature and composition and stabilizing the active sites. The authors suggested that the relative stability of active sites depends on the electronic contributions, and epitaxial strain needs further exploration to develop a sustainable anode. Recently, it has been investigated that the electronic interaction between Cu nanoclusters (NCs) and CoS fabricated over Cu foam enhanced the electrochemical activity and durability of active sites for water oxidation (Fig. 2A) [91].

The spectroscopic investigation demonstrated that during water oxidation at the high anodic potential, the Cu and Co metals available on the top surface chemically oxidized to corresponding Cu-O and Co-O, preventing the inner structure, and enhancing the corrosion resistance of the material (Fig. 2B-F). Electrochemically activated catalysts revealed high catalytic efficiency compared to the pristine Cu and Co-based oxides. Based on XAFS analysis, authors reported that the Co-O component exposed towards electrocatalysis has the least coordination number of 2, possesses a highly disordered structure, and sustained the high current density during continuous alkaline water electrolysis. The synergy between Cu and Co prevents the semi- or non-conducting layer formation, maintains the maximum contact area at the electrode-electrolyte interface, and suppresses the metal dissolution, subsequently increasing the ASF (Fig. 2G,H). Recent findings demonstrated that earth-abundant monometallic Fe catalysts reveal limited activity and stability. Menezes and coworkers reported an intermetallic strategy to increase the intrinsic activity and durability by developing the $FeSn_2$ anode (Fig. 2I) [92]. The catalyst has structural disorders, provides abundant active sites, and increases the ASF. Compared to the pristine Fe catalyst, metal dissolution was not observed for $FeSn_2$, and the sustainability is attributed to the abundant active sites with high intrinsic activity per active site, which deliver the high current output at low input voltage and shield the active sites from passivation. It has been reported that crystalline αFe-O(OH) can resist solvation at high overpotential compared to the amorphous phase and needs low input voltage to cross the energy barrier for O-O coupling. The high ASF factor has been attributed to the surface reconstruction/modulation of active sites, where Sn can be leached under anodic bias, oxidized, and stabilized the Fe in its more active form, i.e., αFe-O(OH). During the OER, Fe $^{\delta+}$ oxidized to $Fe^{2+}(OH)_2$ and then transformed to αFe-O(OH) as an active component for water oxidation. The experimental findings suggested that the regular arrangement of αFe-O(OH) directly relates to the structural ordering of the $FeSn_2$ core, leading to the surface modification to the crystalline phase (Eq. 10).

$$FeSn_2 + 15OH^- \rightarrow Fe^{III}O(OH) + 2[Sn^{IV}(OH)_6]^{2-} + 11e^- + H_2O \quad (10)$$

The electronic modulation by intermetallic interaction improves the activity factor by tuning the metal d band center relative to O 2p orbitals, providing optimized chemisorption energy, and preventing metal dissolution due to strong outer orbitals interaction. Huang et al. reported the impact of catalytically inactive $Zn^{2+}(d^{10}$; no empty orbital is available for catalysis) on the Co-OOH catalyst [80]. The Zn incorporation creates accessible oxygen nonbonding state with different local configurations. The experimental and theoretical investigations demonstrated that specific local configuration and the presence of oxygen vacancies are responsible for regulating the reaction pathway for O-O coupling (Fig. 2J-P). The authors suggested that the LOM reaction mechanism is sustainable if two oxidized oxygen atoms (present at a distance closer than the van der Waals radii) hybridize their oxygen vacancies without sacrificing active site-O 2p hybridization. The specific local configurations dictate the reversible oxygen refiling process and define the durability of the catalyst. The atomic orbitals of O 2p participate in M-O bond formation in MOOH, causing M-O bonding and antibonding state, and the difference between bonding and antibonding states, known as change transfer energy, depends on the orbital energy of oxygen ions and metal.

Moreover, the electrochemically active late transition metal (Fe, Co, Ni, and Cu) oxide further split the antibonding states with one filled lower Hubbard band (LHB) and one empty upper-Hubbard band (UHB) due to d -d coulomb interactions (U). The Coulomb interactions have an inverse relation with the orbital size and hence strongly depend on the oxidation state of metal (i.e., the magnitude of effective nuclear charge defines the orbital volume). In MOOH, i.e., charge transfer energy is more than the d-d coulomb interaction, the LHB 1st oxidizes with a high valance charge of metals after the initial OH attack. The enhanced valance state of metals decreases the metal orbital energy due to effective nuclear charge and increases the d-d coulomb interactions, leading to charge transfer energy lower than the coulomb interactions and LHB penetrating the M-O bonding state. Because electrons are oxidizing from the M-O bonding band, it decreases the bonding order and destabilizes the catalyst's structure. Researchers unveiled that the catalyst should meet the two necessary conditions to accelerate the LOM with structural and mechanical sustainability. (1) incorporation of a buffer band from oxygen nonbonding state, so M-O preserved its initial bond order even during the oxidation process, and (2) high covalency of the M-O bond to suppress the probability of electron removal from LHB. The authors reported that the interaction of CoOOH with the catalytically inactive metal (Zn) increases the Co-O covalency, creates the accessible oxygen nonbonding states, and sustains the high current density for a long time without degradation. Chemical oxidation of metal during OER to inactive phase is a critical challenge that accelerates the metal dissolution and decreases the ASF. Electronic modulation by doping the selective metal into the parent framework is a promising route to increase the redox recyclability of the active metal. In addition, it has been explored recently that the presence of a vacant 4 f orbital in rare earth metals can dwell/diffuse with the d orbital, and thus the electron could turn into a valance electron which promotes the electronic conduction between rare earth metals [93]. In other reports, it has been explored that doping of small amount of rare earth metals alter the electronic properties of composite materials and subsequently enhance the catalytic activity and sustainability [94–96]. In our recent report, we have fabricated Gd doped CoB nanosheets for electrochemical water oxidation [97]. The XPS and Fermi level UPS spectra analysis demonstrated that Gd doping alters the surface electronic structure of Co active sites. The electrochemical evaluation analysis suggested that a small and controlled amount of Gd exponentially enhances the electrochemical performance in terms of high TOF, decreasing Tafel slope and small charge transfer resistance (less resistive). More promisingly, we observed that after Gd doping, the Tafel slope drastically decreased from 70 mV/dec to 40 mV/dec, which indicates that the M-OOH formation is the rate-determining step. It means that Gd doping can even change the reaction pathway. The enhancement of reaction kinetics accelerates the gas desorption rate, decreases the metal dissolution, and enhances the Activity-Stability factor (ASF). Yu and coworkers examined the Ce impact on Co oxides' catalytic activity and durability [98]. The structural analysis revealed that Ce doping partially disordered the Co oxide structure, increasing the activity and durability of the Co-active component. The spectroscopic study demonstrated that Ce interaction with the Co modulated the surface electronic structure and enhanced the charge transfer kinetics. In both samples (Co_3O_4 and $Co_{3-x}Ce_xO_4$), Co is present in a divalent state (Co^{2+} and Co^{3+}), but the Ce interaction increases the Co^{2+}/Co^{3+} ratio. The Co active sites available in the + 2-valance state easily transform to Co-OOH under anodic bias, function as actual active centers, and return to their original state after O-O coupling and increases the metal redox recyclability. The deep insight spectroscopic analysis revealed that the Ce-containing samples retain the Co^{2+}/Co^{3+} ratio during the OER and maintain the high current

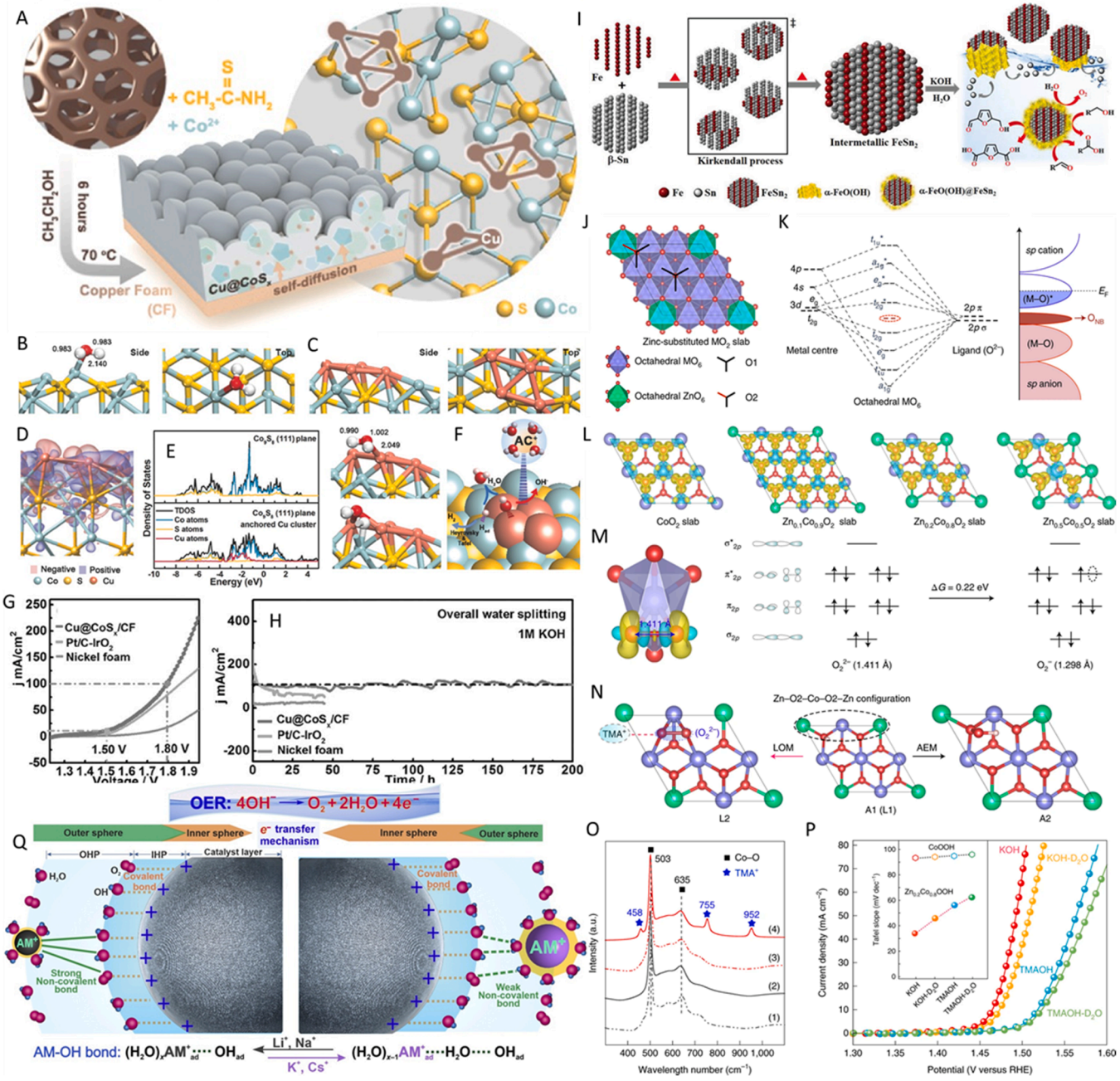

Fig. 2. (A) Systematic presentation of Cu@CoS_x/CF synthesis at low temperature involving CoS_x films formation at CF along with Cu species inter diffusion (B) Water molecule structure adsorption on Co_9S_8 (111) plane surface (C) Stabilization of four atom Clusters of Cu on Co_9S_8 (111) plane surface (D) Charge density difference inside clusters of heterogeneous Cu@Co_9S_8; Blue and red regions depicts depletion and accumulation of electrons (E) Computed density of states (DOS) of Co_9S_8 (F) Systematic illustration of water molecule adsorption, dissociative adsorption and reorientation on clusters of Cu@Co_9S_8 (111)n plane (G) Comparative two-electrode polarization curve of Cu@CoS_x/CF- Cu@CoS_x/CF couple, Pt/C-IrO_2 couple and nickel foam(NF)-(NF) couple in 1 M KOH for water electrolysis (H) Time versus current density curve at 1.8 V applied voltage for water electrolysis. (I) Systematic illustration of intermetallic FeS_2 ordered structurally along with close packing of atomic Sn and Fe. Copyright 2020, Wiley-VCH. (J) Model of Zn-substituted MO_2. Green, red and purple balls denote zinc, oxygen and metal atoms (K) Schematic ONB formation by molecular orbital energy diagram extrapolation for octahedral MO_6; Fermi level presented by EF (L) and projected (DOS) (M) Thermodynamic stabilities between species of O_2^- and O_2^{2-}; Blue and yellow colors show charge depletion and accumulation, with 0.015 eÅ^{-3} isosurface value (N) Schematic $O2^{2-}$ species chemical recognition utilizing TMA^+ as a probe (O) Raman spectrum of CoOOH (1 and 2) and $Zn_{0.2}Co_{0.8}$OOH (4 and 3) electrodes. First, operation of 1 and 3 at the open-circuit potential, while 2 and 4 at 1.45 V potential Vs RHE, in 1 M TMAOH electrolyte. Then, washing of electrodes with purified water and acetone for measurement of ex situ Raman analysis (P) Tafel slopes and polarization curves of $Zn_{0.2}Co_{0.8}$OOH in 1 M KOH and TMAOH dissolved in H_2O (99%), respective. (Q) Systematic illustration of alkali metal cations adsorption for enhanced oxygen evolution reaction.
(a) Reproduced with permission from ref [91]. (b) Reproduced with permission from ref [92]. (c) Reproduced with permission from ref [80]. (d) Reproduced with permission from ref [99]. Copyright 2021, Elsevier.

density where the gases were produced. Redox transformation of $Ce^{3+/4+}$ was observed after Ce interaction with the Co, and oxygen vacancies were observed in the sample. A considerable proportion of Ce^{3+} endorsed the oxygen vacancies creation that introduces the band gap state due to the formation of unpaired d electrons, enhancing the interaction between the antibonding state of the active component and the O 2p orbital. The results further suggested that the Ce^{3+} coupling with Co^{2+} strengthens the Co-O π bonding due to electronic delocalization and accelerates the charge transfer from Ce to Co, accelerates the intermediate adsorption-desorption, and decreases the metal dissolution.

A recent investigation revealed that alkali metals' interaction with transition metals changed the electronic structure and enhanced the durability of the catalyst. Chuang and coworkers studied the interfacial interaction between alkali metals and transition metals and electric double structure to investigate the influence of alkali metal cation on water oxidation (Fig. 2Q) [99]. Their experimental results revealed that the activity of IrO_x and $NiCo_2O_3$ decreases in the sequences $K^+ > Cs^+ > Na^+ >$ and $Li^+ >$ due to the interaction strength of non-specifically adsorbed alkali metals cation (AM^+ ads)and specifically adsorbed OER intermediate in the electric double structure. The authors found that the selective quantity of K^+ in the amorphous IrO_2 facilitates the LOM and increases the reactivity of active sites, improving the catalyst's durability by stabilizing the unstable iridium oxyhydroxide phase. The interfacial covalent and noncovalent interactions and formation of EDL structure define the activity and stability of exposed active sites. The deep investigation demonstrated that reactant (OH^-), OER intermediate (OH*, O*, OOH*), and product (O_2) have been adsorbed in the inner Helmholtz plane (IHP) of EDL and proton-coupled electron transfer reaction proceeds via an inner sphere mechanism (ISM), where OER intermediates strongly interact with the exposed active components. To maintain the surface energy of EDL, the solved alkali metals cation reached the outer Helmholtz plane (OHP) and stabilized the intermediates. Because water molecule is ultra-stable and high energy is needed to dissociate the O-H bond. Studies unveiled that noncovalent interaction between alkali metal cation and OH intermediate leads to the complex cluster formation, weakens the O-H bond, and prevents the active sites' dissolution.

5.2. Heteroatom doping

Heteroatom doping has been recognized as a promising method to regulate the catalyst's electronic structure, increase the intrinsic activity of active sites, and enhance the ASF. Doping heteroatoms into an electrocatalyst introduces the charge redistribution, modulates the surface and electronic structure, boos the electroconductivity, and optimizes the chemisorption energy, thereby providing dynamically active and stable sites to catalyze the reaction [100]. Moreover, foreign element doping substantially impacts the physicochemical properties, such as increasing the roughness factor and specific surface area and, consequently, exposing additional reactive centers for electrolyte concentration and impeding the nonconductive layer formation at a high anodic potential. Benefiting from these surface and electronic structure merits, researchers extensively explore the different heteroatom impacts on the activity and stability of the catalyst. Results demonstrated that heteroatom doped catalyst revealed higher activity and stability than the pure counterpart. Xie group investigated the impact of N anion doping in Ni_3S_2 electrode materials for overall water splitting [101]. The findings revealed that N doping enhanced the specific and electrochemical active surface area, accelerated the electronic conduction, optimized the chemisorption energy (ΔG-H_2O), enhanced the reaction kinetics, suppressed the metal leaching, and enhanced the sustainability of active sites in alkaline conditions. The authors have conducted the 1st principal calculation to interrogate the intrinsic behavior of active sites after N doping. The density of states for both N-doped Ni_3S_2 and pristine Ni_3S_2 shows continuity around the Fermi level, implying the inherent metallic character of both catalysts. However, after N doping, the DOS strength increases near the Fermi level, suggesting that the anion's introduction ameliorates the electronic conduction and concentration of the charge carrier and enhances the electrochemical performance of the catalyst. Furthermore, the higher electrical conductivity suppresses the growth of the semi/nonconductive layer and increases the long-term durability of the catalyst. The authors assigned the high intrinsic activity and sustainability to the following factors: (1) Higher electrical conductivity is brought about by the addition of anion N atoms, which dramatically boosts the DOS near the Fermi level and can assist in enhancing the electron transport and ultimately catalytic activity, (2) N doping increased the structural defects enlarged the specific surface area that sustains the high current density at low input voltage, (3) The DFT calculations revealed that the catalyst-H* state and catalyst-H_2O state could quickly arise on the surface of the N anion-Ni_3S_2 catalyst, which would ultimately increase the overall performance, (4) The anion introduction also increases the charge and mass transfer kinetics, highly needed for the stable electrode.

Provided that phosphorus (P) has smaller electrical negativity of 2.19 than oxygen (3.5), nitrogen (3.04), and sulfur (2.58), P doping is anticipated to successfully change the transition metal's electronic conformation, resulting in an inherently increased water splitting activity. Transition metal oxides have gained considerable attention as potential water-splitting catalysts due to their appealing catalytic performance in alkaline medium. Still, they are constrained by minimal active site exposure and poor electrical conductivity that trigger the chemical transformation of active sites to inactive phase and lose the durability of the catalyst. For example, Zhang et al. fabricated a P-doped Ni-Mo aerogel metal-aerogel gelation process followed by a P introduction [102]. The catalyst demonstrated good catalytic performance for oxidation (OER) and reduction (HER) reactions, which needed a small overpotential to drive a high geometric activity. The remarkable performance and sustainability of active sites were attributed to the P-doped 3D metal aerogel structures possessing abundant active sites, high charge and mass rate of transportation needed low activation energy for O-O coupling. The results unveiled that P addition redistributes the electronic structure around the active component, optimizes the bond strength of active sites and intermediates, and reduces the potential energy barrier for water splitting. DFT calculations further supported the experimental results, showing that P doping and Mo interaction with the Ni active sites optimized the D band DOS of Ni and the bond coordination between active sites and intermediates, promoting intermediate adsorption and stabilization and increasing the ASF.

A recent investigation revealed that most transition metals (e.g., Ni and Co) are chemically oxidized to higher valance states that act as real active components for water splitting. The redox recyclability of metals is responsible for the long-term sustainability of the anode. Researchers unveiled that the specific content of heteroatom not only increases the exposure of active sites with high intrinsic activity but also accelerates the metal chemical transformation to the actual active phase and shields the excessive oxidation of metals and their leaching from the current collector. Xu group reported that P doping negatively shifts the redox potential of Co-based electrode, promotes the redox reaction and self-reconstruction during the electrochemical reaction responsible for the stability of active sites [103]. At anodic potential, P oxidizes to PO_4^{3-}. The detailed characterization suggested that P doping modulate the electronic structure of the catalyst, accelerate the growth of actual active component on the surface of the catalyst (Co-OOH)and also trigger the morphological evolution due to its self-construction property, and increases the durability of cobalt in harsh alkaline condition at high anodic potential (Fig. 3A-I). Similarly, Liu et al. investigated that P incorporation optimizes the chemisorption energy ($\Delta GH^*/\Delta H_2O^*$), provides additional active sites, and increases the electrical conductivity of the catalyst [104]. Interestingly, it has been observed that P triggers the Ni oxidation to its more active phase and increases the Ni^{3+}/Ni^{2+} ratio, facilitates the OH^- attack, stabilizes the OOH intermediate and

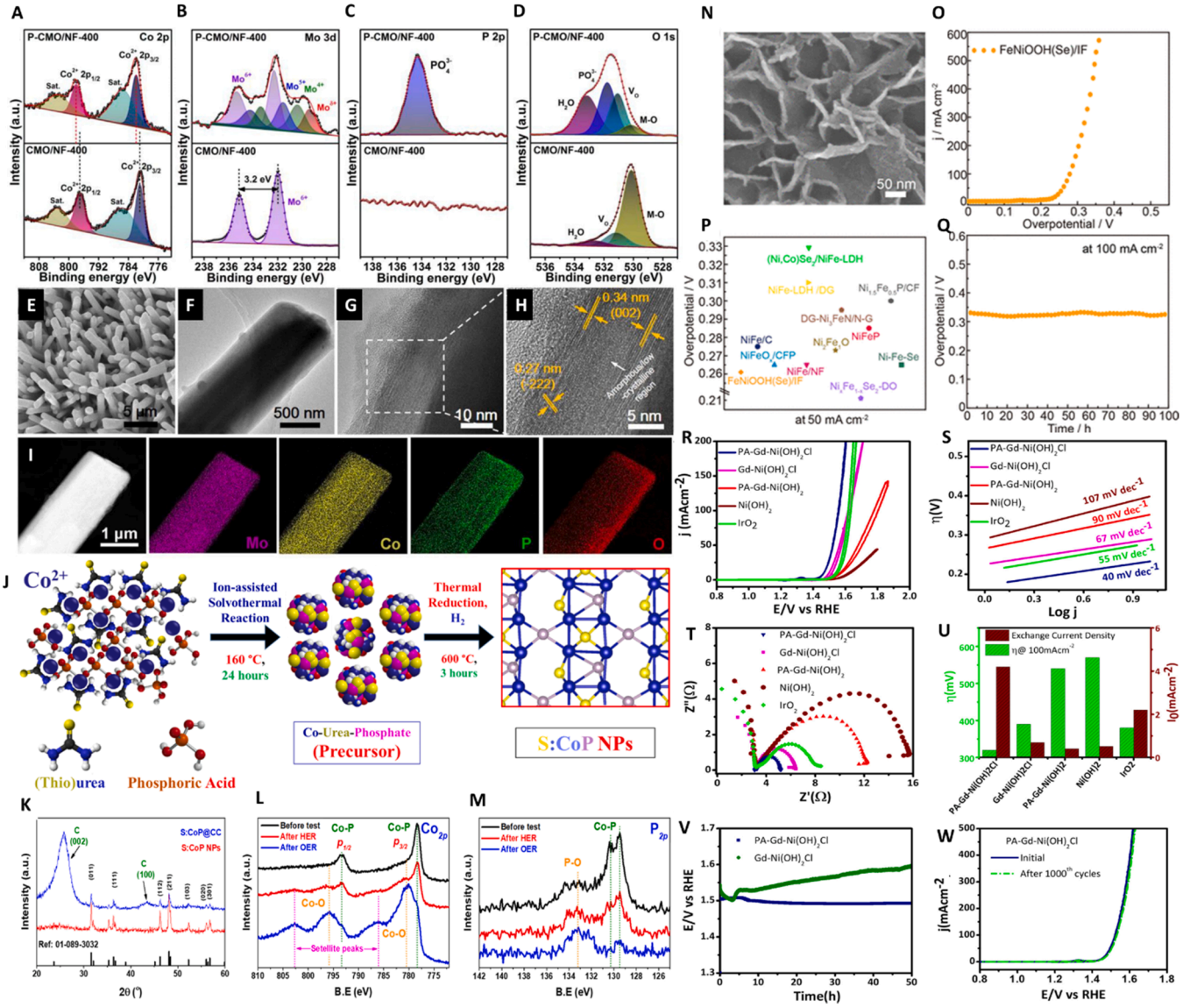

Fig. 3. High-resolution XPS spectra of (A) Co 2p, (B) Mo 3d, (C) P 2p and (D) O 1 s for synthesized electrocatalysts. (E) SEM image, (F) TEM image and (G, H) HRTEM images, (I) HAADF-STEM image and the corresponding elemental mapping images for P-CMO/NF-400. (J) Schematic presentation of thiourea-phosphate-assisted with synthesis of S-doped CoP nanoparticles (S:CoP NPs) (K) XRD, XPS spectra for (L) Co 2p (M) P 2p. (N) SEM images of FeNiOOH(Se)/IF. (O) LSV curves of FeNiOOH(Se)/IF. (P) Overpotential comparison of FeNiOOH(Se)/IF and state-of-the-art OER catalysts. (Q) Chronopotentiometric curve of FeNiOOH(Se)/IF. (R) Cyclic voltammogram, (S) Tafel plots, (T) EIS, (U) exchange current density vs overpotential graph for PA-Gd-Ni(OH)$_2$Cl, Gd-Ni(OH)$_2$Cl, PA-Gd-Ni(OH)$_2$, Ni(OH)$_2$, and IrO_2, (V) chronopotentiometry at 100 mA cm^{-2} for PA-Gd-Ni(OH)$_2$Cl and Gd-Ni(OH)$_2$Cl, and (W) Stability test of PA-Gd-Ni(OH)$_2$Cl in 1 M KOH solution.
(a) Reproduced with permission from ref [103]. (b) Reproduced with permission from ref [98]. (c) Reproduced with permission from ref [112]. (d) Reproduced with permission from ref [93]. (i) Copyright 2022, Elsevier. (j) Copyright 2018, Elsevier. (l) Copyright 2019, American Chemical Society

desorption of gases molecules, highly needed for effective contact of electrolyte with the underlying support subsequently for the long-term stability of the electrode.

Like P, Sulfur also has the same physical and chemical properties and has the potential to tune the electronic and surface structure of TM catalyst and increases the reactivity and stability for water splitting. The adsorption energy of oxygen-based intermediates in the OER mechanism is an objective metric to comprehend the ASF throughout the redox process. Notably, the adsorption capacity of OER intermediates is inversely correlated with the energy barrier (ΔG). The catalyst with a high energy barrier needed high input voltage for O-O or H-H coupling triggers metal leaching, structural accumulation, and support passivation. Researchers demonstrated that S doping remarkably reduces the potential energy barrier for O-O/ H-H coupling and governs the sustainability of the electrode material. Feng group performed DFT calculation to probe the impact of S dopant in Ni-Fe-P-based catalyst [105]. The authors deduce from experimental and theoretical results that the active sites should be where Ni replaces Fe in the discrete units. The results show that S introduction remarkably tunes the Gibbs free energy for four steps (OH*, O*, OOH*, O_2). The S addition improved the adsorption ability of Ni sites for OOH* and reduced the energy barrier associated with the rate-determining step from 3.04 eV to 2.86 eV. According to theoretical calculations and experimental findings, S doping can successfully adjust the ΔG value for intermediates formation on Ni atoms to a desirable value and exhibit an improved OER performance (Figure). The authors calculated the 3D charge density difference and Bader charge numbers of the atoms in S-Ni-Fe-P intermediates with OH*, O*, and OOH* to better understand how the electronic distribution degree changes at the interface between the Ni sites and OER intermediates during the OER process. Due to more effective nuclear

charge (high electronegativity), S and P have lower energy orbitals than TM, i.e., Ni and Fe, and electrons preferably transfer from the higher orbital energy of metals to the lower orbital energy of S after coordination. S anions capture the electronic density from the active sites and stabilize metals in a high valance state, decreasing the activation barrier for O-O coupling and sustaining the stability of the catalyst. Lee's group reported the S-doped CoP catalyst for overall water splitting possessed high ECSA, low charge transfer resistance, and good sustainability in an alkaline medium (Fig. 3J-M) [106]. The durability of the active sites was assigned to the aerophobic characteristics of the catalyst that accumulate a negligible quantity of gas bubbles and provides exposed active sites for intermediate adsorption. The results unveiled that S doping significantly enhanced the aerophobicity of the CoP. Recently, we have reported S doped Cu_2O-CuO nanoneedles array as a free-standing anode for unpurified seawater oxidation [107]. The catalyst demonstrates abundant active sites with high intrinsic activity per active site, high electrical conductivity, and a fast rate for ions and electrons transfer at the electrode-electrolyte interface. The catalyst has very high corrosion resistance and sustained the high current density without degradation. The S 3p orbital boosts Cu metallic environment by intensifying the states deep into the conduction and valance band near the Fermi level to some extent. This doping also localized the electron population in the Cu 3d orbital near the Fermi level and reduced the oxidation state [106]. The high-resolution XPS spectrum of Cu 2p without S substitution endorsed that most of the surface Cu is in a 1 + valance state. However, the S substitution prevents the excessive oxidation of the catalyst and accelerates optimum adsorption between $OH^{\bullet}$ or H^{+} and the central metal ion, which precedes the O_2 production from intermediates [108]. The redox states of the metals have been determined with XPS before and after catalysis and deconvoluted using 'AVANTAGE-XPS software. Interestingly, there is no notable change in the content of the S atoms even after the OER stability tests in seawater, suggesting that the promotional effect of sulfur remains strong throughout the OER. These results indicate the surface oxidation or partial adsorption of oxygen-containing groups under long-term OER reaction, which is consistent with the behavior of hetero atom doped transition metal in the form of metal hydroxide/oxyhydroxide with metal redox. So, based on our experimental results after a long-term stability test and comparison with the literature, we assumed that the S-$Cu^{2+/3+}$ redox couple might be the active phase to govern OER. In addition, the stable performance under long-term OER conditions also supports the periodicity of the metal redox couple. For further justification, we also recorded inductively coupled plasma optical emission spectroscopic (ICP-OES) measurements of KOH electrolytes after 20 h of continuous electrolysis. The results demonstrate that sulfur specie is not present in the electrolyte solution, suggesting that sulfur species retain as the inherent part of hybrid material and act as an active phase rather than dissolving in the electrolyte as observed for another non-oxide-based catalyst [109,110]. The recent findings suggested that oxygen-deficient surface oxides (Cu-O_x) formed in situ through electrochemical oxidation catalyzed the process. However, the promotional effect of S remaining in the oxidized catalyst is equally effective by assisting in situ formed metal oxo-/-hydroxide OER active sites on the surface of S: Cu $_x$ O., Another interesting phenomenon in the S doped catalyst, is the leaching of S from the catalyst lattice induces self-reconstruction of the catalyst surface and chemically evolved to the most active component and increases the ASF. Chen et al. reported the S-doped Ni-Fe LDH and revealed that during the OER process, all the S was removed from the catalyst, and the original small sheets were transformed into the Ni-doped Fe-OOH nanosheets, which possess higher catalytic activity and stability [111]. The author's findings show that S presence has a critical role in the original catalyst's structural rearrangement and chemical transformation. The electrochemical results revealed that S doping decreases the charge transfer resistance, provides additional active sites, and catalyzes the water oxidation at low potential. The OER process of oxides through the participation of lattice oxygen exhibits typical pH-dependent activity on the RHE scale due to the non-concern between the hydroxide affinity and electron transfer kinetics at the catalyst/electrolyte interface. Therefore, more understanding of the electrocatalytic mechanism and associated intermediates for the as-prepared catalysts could be gained by studying the pH dependence on OER activity. The results demonstrated that S doping and leaching-induced structural rearrangement triggered the LOM and destabilized the water molecule and its interaction with the active sites. Wan group probed that Se doping substantially increases the intrinsic activity and sustainability of the catalyst due to the involvement of 4p orbitals, which could dwell the electrons and improves the electronic conduction [112]. They have synthesized Se-doped Fe-OOH anode via an electrochemical activation strategy having vertical 3D nanosheets-like morphology that provides abundant active sites to stabilize the intermediates and catalyze the reaction at low input voltage. Se doping boosts the intrinsic activity of adjacent active areas and increases the aerophobicity of the active component (Fig. 3N-Q). The theoretical calculations demonstrated that Se substitution at different places (at the top and lattice oxygen) in the Fe-OOH structure showed different catalytic behavior. Selenium was substituted with oxygen at the top and in the subsurface of Fe-OOH (Se-1 and Se-2) to interrogate the dopant effect in the lattice structure. The energy change profile was estimated for different OER intermediates, i.e., OH*, O*, OOH*, where the formation of oxyhydroxide intermediate exhibited the highest energy barrier and was considered the rate-determining step. The free energy calculations revealed that Se doping drastically reduces the activation barrier from 3.20 eV to 1.45 and 1.83 eV Se-1 and Se-2, respectively. This reduction in the activation barrier accelerated the reaction kinetics and impeded the support passivation usually observed at a high anodic potential. Similarly, Zhu et al. reported that Se doping enhanced the electronic conduction, promoted the charge transfer kinetics at the solid-liquid boundary, and promoted the activity and stability of the catalyst [113]. Se doping tailored the surface structure of the catalyst providing additional active sites and increasing the number of reactive components and corrosion resistance of the catalyst. The author's studies show that Se's presence triggers the formation of an ultrathin amorphous layer that increases polarizability, destabilizes the water molecule, and facilitates intermediate adsorption. This amorphous layer overcomes the structural and mechanical instability of the catalyst due to its self-reconstruction and healing characteristics. Se-doped Co_3O_4 @CeO_2 revealed good catalytic activity and durability for overall water splitting [114]. Theoretical investigations revealed that Se doping improves the water adsorption performance and enhances the reaction kinetics for sluggish OER. In addition, the authors demonstrated that Se doping enhanced the density of states near the Fermi level and improved the intrinsic metallic property responsible for the catalyst's long-term durability. Furthermore, the Se doping changed the electronic structure of Co3O4, improving the electronic conduction due to the hybridization of Co 3d orbital, O 2p orbital, and Se 3p orbital. This p-p hybridization improves the water-splitting performance on the catalyst's surface and increases the catalyst's chemical durability.

Researchers unveiled that a strong association of electronegative elements with metal facilitated charge transport across the electrode-electrolyte interface [115]. The high electronegative character pulls the electronic density away from metal, provides abundant electrophilic active sites to uplift the OER intermediate formation and stabilization at low overpotential. Liang et al. have reported developing a Ni-Fe oxyfluoride system through electrodeposition followed by an anodization strategy [116]. The free energy profile revealed the limiting potentials of 1.074, 0.481, and 0.364 V associated with the kinetically sluggish oxyhydroxide intermediate formation for Ni-O, Ni-Fe-O, and Ni-Fe-OF, respectively. The much smaller limiting potential after F doping was attributed to the effective charge transfer effect of Fe^{3+} on Ni^{2+} due to the high electronegative character of F. The F doping increases the reactivity of active sites, create strong electronic interaction between the different metallic component of the catalyst, and enhances the structural

stability and corrosion resistance. In addition, the anionic substitution of F- with the oxide enhanced the electrical conductivity and suppressed the support passivation. Similarly, Han et al. reported the nickel−cobalt fluoride oxide for water oxidation [117]. Their investigation has shown that F substitution increases the specific surface area of the catalyst and unsaturated coordination responsible for the high activity and stability of the catalyst. The DFT calculation demonstrated the presence of an extra electron in each elementary step during the OER at the adsorbate-adsorbent interface. More specifically, adsorbates withdraw the electronic population from the Co, which causes a buildup of electron density close to the adsorbates while also depleting electrons at the Co atoms' interfacial Co atoms. Importantly, because the bottom "F" atoms have a strong electronegativity, electrons from the Co atom are also transferred to those atoms, increasing the active sites' reactivity. The theoretical calculations unveiled that DOS increases near the Fermi level after F substitution, and the electrons are freely involved in the conduction band, decrease the charge transfer resistance, and facilitate the charge transfer at electrode-electrolyte interfaces, resulting in high activity and stability of the active sites.

Li Song and his coworkers reported a new class of cobalt oxychloride as a pre-catalyst for OER with unique features that allows a gradual phase reconstruction during catalysis [118]. As a result of the lattice Cl species being etched under oxidizing potentials, it was discovered that the catalyst might exhibit continuous reconstruction-enhanced activities. Combining operando XANES and EXAFS investigations with HAADF-STEM imaging and DFT calculations revealed that coordinatively unsaturated Co serves as a real active center for intermediate adsorption and desorption, and this atomic level coordination is responsible for the high activity and stability of the catalyst. This self-reconstruction behavior enhanced the structural flexibility of the catalyst that regulates the surface structure according to the reaction condition, especially at a high anodic potential where immense gases are produced. In our recent report, we have systematically revealed that Cl incorporation enables Gd-Ni $(OH)_2$ catalyst to reach higher geometric activity compared to its counterpart with the long-term sustainability [93]. Low charge transfer resistance and support of high current density in a sharp potential window were observed to verify the inherent activity of the catalyst after Cl incorporation and meanwhile providing a large number of exposed electrochemical active sites mainly responsible for the sustainability of active sites. The stable performance under long-term OER conditions also supported the periodicity of the metal redox couple. Our experimental and theoretical calculations revealed that Cl presence facilitates firm adhesion and electrical contact with underlying support, which are worth considering in the stability of transition metal-based catalysts (Fig. 3R-W).

Although significant progress has been achieved in enhancing the efficiency of heteroatom-doped catalysts, many of the catalysts demonstrate durability for a short period (<100 h) and don't meet the commercial requirement of thousands of hours. Nonetheless, the chemistry and mechanism of heteroatoms in water splitting stability remain uncertain, and this area has yet to receive much attention. Potentiodynamic cycling of the heteroatom-doped catalyst during the OER process typically involves surface rebuilding or elemental leaching. In general, higher covalence in metal oxides and their derivatives produces more oxygen vacancies, lowering bulk stability and potentially leading to surface amorphization by heteroatom leaching. In an electrolyzer, the flowing electrolyte could wash away the leached metal ions, eventually deteriorating the electrode and the electrolyzer. Under harsh oxidizing conditions, the sustainability of these vacancies is a primary concern in enhancing the stability of electrode materials [76]. Wang et al. used an ingenious technique to stabilize the oxygen vacancies (V_O) by adjusting the coordination numbers by filling the oxygen vacancies with P heteroatoms, resulting in a remarkable activity by changing the electronic structure [119]. According to detailed structural research, oxygen vacancies produced in V_O-Co_3O_4 disrupted the Co^{3+} (Oh)-O link, and more electrons entered the octahedral Co 3d orbital than the tetrahedral Co 3d orbital. After filling P at the vacancy site, electrons transferred out of the Co 3d states, leaving more Co^{2+} (Td) than Co^{3+} (Oh) in PCo_3O_4, indicating that the Co^{2+} (Td) site dominates the catalytic capacity. The P-filled Co_3O_4 demonstrated exceptional HER, OER, and total water-splitting performance. Therefore, systematic research integrating in-situ techniques and theoretical calculations is required to unveil heteroatoms' fundamental role and chemistry in heteroatom-modified electrodes for enhancing water-splitting durability, particularly under anodic conditions.

5.3. Defects engineering

The critical factor in controlling the activity, selectivity, and durability of the active component on the surface of the catalyst is to modulate the relationship between reaction kinetics and intermediate adsorbed on the active sites [120]. The intrinsic defects are commonly identified as real active sites because of tuned surface and electronic properties in the local structure. Defect engineering induced a high electronic state at the topological region and tuned the ASF [121]. This has been demonstrated through a combination of theoretical calculations and experimental findings, which show that active sites for various electrochemical reactions are induced by particular defect types due to specifically desired reactant binding energies for each electrochemical response. Furthermore, most transition metals band gaps or electronic states close to the Fermi level can also be tuned through crystal strain, which defects can induce at the edges or basal plane [122]. Therefore, defects engineering has been widely used to boost active sites' intrinsic activity and sustainability. As is well known, defects can be classified based on the dimensions, i.e., 0-D point defects (doping and vacancy), 1-D line defects (dislocation), 2-D planar defects (e.g., grain boundaries), and 3-D volume defects [123,124]. However, in electrocatalysis, researchers can further investigate the line and surface defects in the materials based on their understanding of the point defect model. Defects, for instance, can contribute to the production and conversion of reaction intermediates by influencing the adsorption activation energy of reactant molecules and the dissociation energy of the product molecules during water splitting [125]. Additionally, theoretical studies showed that defect-enriched materials closer to the Fermi level could improve electrical conductivity, further controlling the electronic structure and enhancing the stability and catalytic activity [126]. In metal compounds or non-metal materials, point defects can be further divided into three representative configurations: (1) metal atomic doping induced defective coordination structure, (2) nonmetallic (anions such as B, N, P, and S) vacancies, (3) vacancy defects or reconstruction [24].

Atomic defect engineering is a practical method to adjust the atomic structure of host materials and then achieve electronic structure regulation [127]. Previous studies have shown that layered double hydroxides (LDHs) are typically made up of brucite-like layers with trivalent metal cations (M^{3+}), which are atomically dispersed and tunable over a wide range, isomorphously replacing some of the bivalent metal cations (M^{2+}) that were previously octahedrally coordinated by hydroxide ions. Song and coworkers demonstrated; how atomic V replacement could change the electronic structure of pyrite NiS_2 from its typical semiconductive properties to metallic properties [128]. Extensive experimental investigations and DFT calculations have confirmed the semiconductor-to-metal transition. Notably, XAS measurements revealed that the electron transfer between doped V heteroatoms and Ni sites was the source of NiS2's electronic structure reconfiguration and responsible for active sites' high activity and stability. Similarly, the Mu group developed a defective RuO_2/TiO_2 heterostructure by replacing one Ru atom from the top surface, showing considerably higher catalytic activity and sustainability than a non-defective counterpart [129]. DFT calculation demonstrated that after heterostructure formation, electrons were transferred towards the upper RuO_2 layer from the bottom TiO_2 layer and created highly charged Ru, which increases Ru's chemical

stability and suppresses its leaching at a high anodic potential. The Ru atoms located in the surrounding defects possessed more positive electrons due to Ru vacancy, induced charge delocalization, and decreased the activation barrier for O-O coupling. Theoretical investigation revealed that RuO_2/TiO_2 and defective-RuO_2/TiO_2 are metallic, indicating a high electrical conductivity, in contrast to pristine TiO_2 with a narrow band gap. As a result, altering the electronic structure of Ru by creating a hybrid RuO_2/TiO_2 interface and adding defects to RuO_2 is thermodynamically possible. When defective RuO_2/TiO_2 is compared to RuO_2, the D-band center of the Ru d orbital moves to a low energy level, indicating that the interaction between adsorbed oxygen species and Ru sites is weaker and favorable for OER. In general, the RuO_2/TiO_2 hybrid interface can modify RuO2's electronic state, optimize the adsorption energy of intermediates in the key OER steps, and stabilize the OER intermediates to benefit the sustainable water-splitting process. An advanced La-doped RuO_2 electrocatalyst has been fabricated using a synergistic method that combines oxygen vacancies and heteroatom doping [130]. The synergistic effect of La doping and oxygen vacancies contributes to the obtained La-doped RuO_2's long-lasting and high electrocatalytic performances for OER and HER. DFT calculation revealed that the energy barrier for RuO2 at U = 0 V was 2.46 eV and considered the rate-determining step (RDS) (*OOH to O_2). After adding the La element, the reaction's intermediate state's binding energy has been optimized, and the third step (*O to *OOH) is discovered to be RDS. Compared to RuO_2, the calculated binding energy of La-doped RuO_2 for RDS is lower at 1.94 eV. RuO_2 has a higher free energy barrier than La-doped RuO_2 at U = 1.23 V (overpotential = 0 V).

Additionally, all of the primary steps on the surface of La-doped RuO_2 became downhill when U = 1.94 V (overpotential = 0.71 V), but there is still an uphill step on the surface of RuO_2. It demonstrated that La-doped RuO_2 has higher OER activity, supporting the experimental findings. These results suggested that the defects engineering effectively modifies the D-band structure of Ru centers, lowers the energy required for substance adsorption, encourages substance desorption on the La-doped RuO_2, and enhances the sustainability of the electrocatalyst.

Surface defect engineering is regarded as a promising strategy to increase the effectiveness of water splitting because the defect sites control the electronic and surface structure of catalysts and have an impact on the coordination environment of the active component, which is favorable to accelerate the reaction kinetics at the electrode-electrolyte interface and stabilize the OER intermediates, increasing the effectiveness of the OER. The defects present in the electrocatalysts increase the unsaturation, leading to dangling bonds and altering the valence state of the nearby metal centers, destabilizing the water molecule, lowering the adsorption energy, and enhancing the sustainability of active sites. The vacancy is lattice defects that comprise substitutional atoms, interstitial atoms, and vacancy. Because of the atomic energy ups and downs, there is always enough energy to overcome the bound particles; yet it is feasible to migrate elsewhere, leading to the initial equilibrium position node. Huang et al. have developed a defective P-doped NiS_2 structure with sulfur vacancies via a Prussian-blue-analogue-sacrificed strategy followed by P substitution (Fig. 4A-I) [122]. The X-rays analysis revealed that S vacancies control the defects in the structure and modulate the electronic structure of the catalyst. The electrochemical results unveiled that the optimized strength of S vacancies and P content enhanced the water oxidation performance, and the catalyst sustained high geometric activity at low input voltage. For OH*, O*, and OOH*, each step's adsorption Gibbs free energies have been estimated to interpret the origin of the samples' catalytic activity. A recent investigation revealed that the OER process's conversion of O* to OOH* species served as the rate-determining step for pure NiS_2 (Fig. 4L-P). A high overpotential during the OER process is mainly due to the intermediates' strong adsorption on the surface of NiS_2 and caused the high energy barrier. Modifying the intermediate adsorption on Ni sites by P-doping and sulfur vacancy introduction reduces the required energy barrier. The predicted limiting barrier was Vs-P-NiS_2, P-NiS_2, and NiS_2, in that order (U = 1.23, G = 1.17 eV, 1.49 eV, and 1.71 eV, respectively). The Vs-P-NiS_2 exhibited the highest theoretical OER activity due to defective sites governing high stability. The authors considered the DOS to examine the changes in electronic structure following P-doping and the insertion of sulfur vacancies to learn more about improving OER activity. NiS_2 has an estimated bandgap of 0.38 eV, typical semiconductors. The bandgap is decreased to 0.01 eV for P-doped NiS_2 bulk, demonstrating that P doping has improved the conductivity of the NiS_2 crystal.Additionally, compared to pure NiS_2, the D-band center of Ni in Vs-P-NiS_2 and P-NiS_2 was marginally displaced to the low-energy level, indicating a lower affinity for *OH, *O, and *OOH on the catalytic surface. As a result, and by the experimental findings, the reaction barrier of the rate-determining step was reduced clearly. S-doped highly porous Co-S films have been fabricated on Ni foam (Co-S-x/NF), and the defective catalyst acts as high-performance bifunctional electrocatalysts for overall water splitting in alkaline environments [131]. The free-standing Co-S films display extremely effective electrocatalytic activity and outstanding durability for both OER and HER, at high geometric activity, because of high structural integrity and suitably exposed active sites located in the defective surface (Fig. 5A-K). Vacancy defects and porous structure ensured the fast charge/mass transfer from an active phase surface to the underlying support and mitigated the support passivation. As more ECSAs proliferate and structural defects result from the S-doping effect, the catalytic reaction kinetics are markedly accelerated with increased intrinsic activity. Additionally, it has been demonstrated that during OER, the near-surface Co-S phases can transform into oxygen deficiency-rich Co-O/OH species, which are genuine active species, to assure its exceptional OER activity and durability.

Introducing defects in the underlying support is a promising way to enhance active sites' mechanical and structural durability due to strong interfacial interaction. The intimate interaction between the active component and defective support stabilized the active sites and mitigated the support passivation. Hou group developed defective Ni-Fe LDH supported Ru single atom revealed high activity and sustainability for water oxidation (Fig. 5L) [126]. The surface and structural defects introduced via acid etching demonstrated a high specific surface area to stabilize the highly energetic Ru atoms and catalyze the electrochemical reaction at low input voltage (Fig. 5M-O). The X-ray absorption fine structure (XAFS) spectroscopy and spherical aberration-corrected transmission electron microscope have been utilized to validate the defects, and the result revealed that defective local atomic structure of Ni-Fe LDH provide nucleation sites for the growth of Ru sites. The author used DFT modeling to calculate the free energy for concerted proton-coupled electron transfer steps, where defective Fe and Ni edge sites in Ni-FE LDH were considered reactive components (Fig. 5P-R). The Ni-Fe interfacial interaction promoted the RDS from O* formation to OOH*. Surprisingly, the Gibbs free energy calculated for Ru sites were higher than the pristine Ni and Fe site with the 1.71 eV and was not in agreement with the recent findings. The authors then considered the Ru-O reaction sites and proposed these moieties as actual reaction centers stabilized by defective Ni-Fe LDH with the overpotential of 0.38 eV. From both theoretical and experimental results, it has been concluded that the synergetic promotion between Ru sites and defective Ni-Fe LDH is crucial to accelerate the O-O coupling with high sustainability.

Recent findings demonstrated that surface defects modulate the chemisorption energy of intermediates and trigger the dissociation of reactant molecules during water electrolysis. Theoretical results also unveiled that the material with high surface defects closer to the Fermi level possesses short diffusion channels for ions migration and suppresses the support passivation. The surface reconstruction in defects-induced electrocatalysis enhanced the roughness factor and sustainability of active sites [132]. In a recent report, it has been demonstrated that dual defects in Co_3O_4 nanostructure due to F doping and oxygen

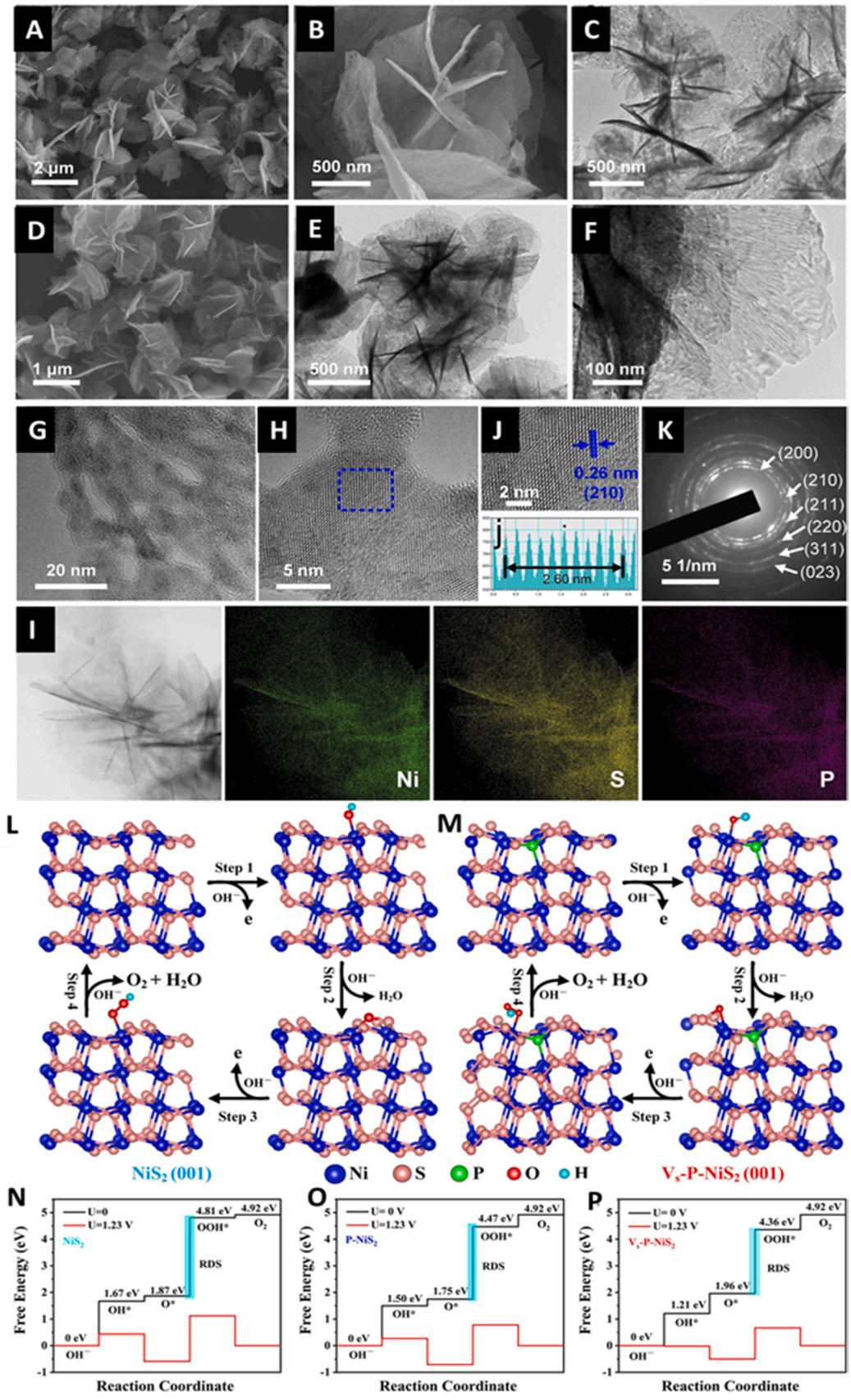

Fig. 4. Structure characterization and morphology of catalyst. (A,B) Typical SEM images (C) TEM image (D) SEM image of pure NiS_2 sample (E,F) TEM images (G) Magnified TEM images (H, I) High-resolution TEM (J) integrated pixel intensities of P-NiS_2-500 (taken from the blue dotted rectangle in panel (K) SAED patterns and Elemental map of the P-NiS_2-500 catalyst. Schematic illustration of H_2O activation, OH* , OOH* , O*intermediates formation, and O2 evolution processes (L) On pure NiS_2 and (M) V_s-P-NiS_2. The calculated Gibbs free-energy presentation diagram for 4-OER steps (N) On pure NiS_2, (O) P-NiS_2 and (P) V_s-P-NiS_2. The light blue part indicates rate-determining step (RDS).
Reproduced with permission from ref [122]. Copyright 2021, Elsevier.

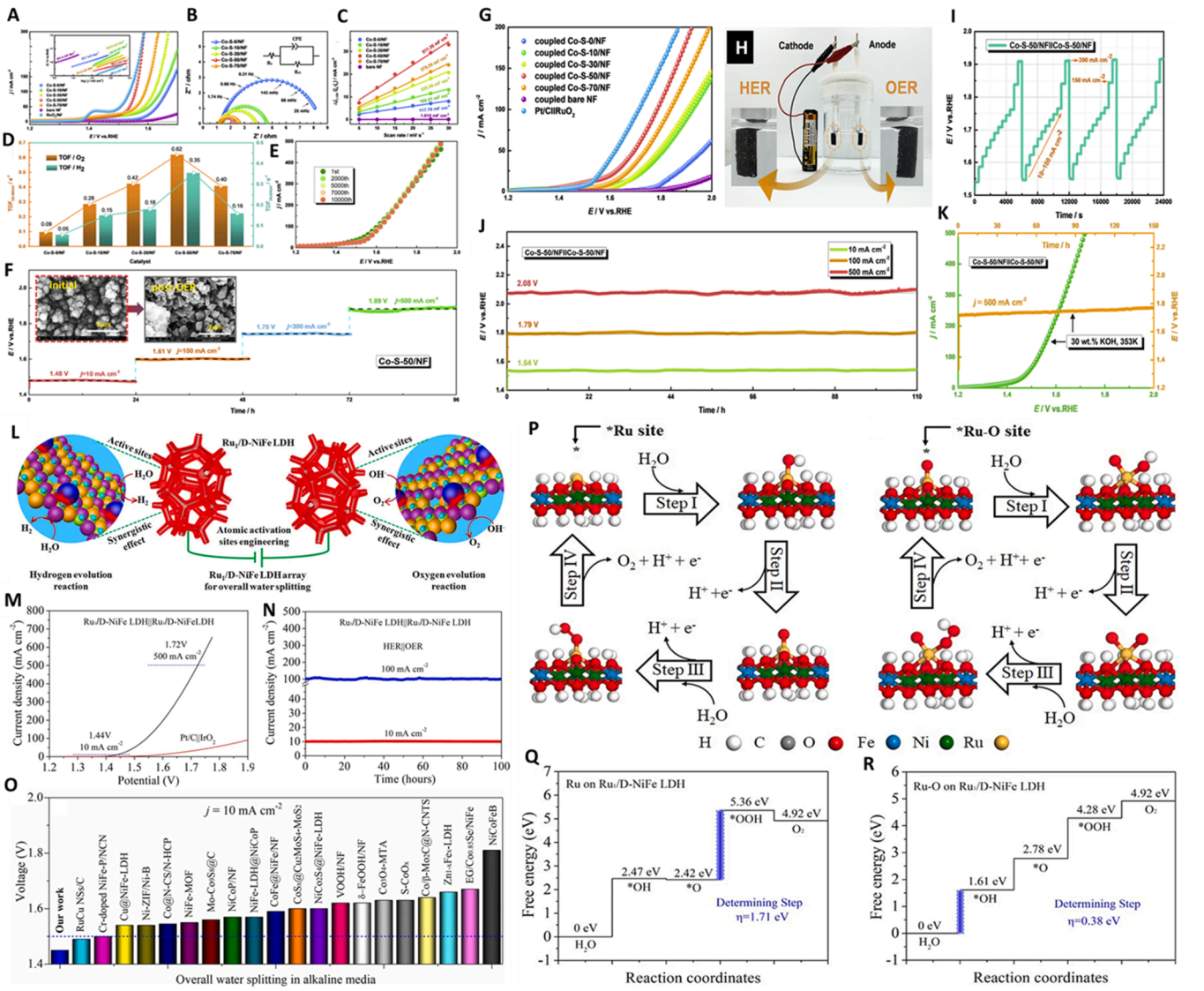

Fig. 5. (A)IR corrected LSV for Co-S-x/NF, RuO_2/NF, and NF at a slow scan rate of 5 mV s^{-1} and the inset shows the corresponding Tafel plots obtained from linear fitting). (B) EIS spectra, recorded at η = 350 mV. (C) Double layer capacitance graph at 1.13 V potential Vs. RHE. (D) TOF for Co-S-x/NF recorded at η_{OER} = 350 mV and at η_{HER} = −200 mV. (E) Polarization curves of Co-S-50/NF before and after successive 2000, 5000, 7000, and 10,000 CV cycles between − 0.20 V and 0.20 V vs. RHE with a sweep rate of 100 mV s^{-1}. (F) Stability curves for the Co-S-50/NF constant geometric activity of 10, 100, 300, and 500 mA cm^{-2} for each 24 h. The inset SEM images reveal the structural transformation of Co-S-50/NF after 24 h long-term OER electrolysis at j = 10 mA cm^{-2} in 1.0 M KOH (G) Polarization curves of the coupled Co-S-x/NF (as indicated), RuO_2/NF||Pt/C/NF and bare NF for overall water splitting at 5 mV s^{-1} scan rate (H) Overall water electrolysis in 2-cell configuration at a cell voltage of 1.5 V. (I) Multi-current process of Co-S-50/NF||Co-S-50/NF, with the current density stepping from 10 mA cm^{-2} to 200 mA cm^{-2} per 1000 s (J) constant current electrolysis (CCE)curves of Co-S-50/NF||Co-S-50/NF attained at j = 10, 100, and 500 mA cm^{-2} for each 110 h. (K) Polarization (green, at a scan rate of 5 mV s^{-1}) and CCE (orange) curves of the coupled Co-S-50/NF for overall water electrolysis under a J of 500 mA cm^{-2} for 150 h in 30 wt% KOH. Copyright 2019, Elsevier (L) A Schematic representation of water splitting in a two-electrode configuration, (M) polarization curves by a two-electrode system, (N) CCE test of Ru_1/D-NiFe LDH with J of 10 and 100 mA cm^{-2} at 1.44 and 1.54 V, and (O) Cell voltages comparison at 10 mA cm^{-2} for Ru_1/D-NiFe LDH with reported bi-functional electrocatalysts. (P) Pictorial representation of OER mechanism (Q) Gibbs free energy diagram for Ru (R) Gibbs free energy diagram for Ru-O sites. (a) Reproduced with permission from ref [131]. (b) Reproduced with permission from ref [126]. (R) Copyright 2021, Nature Publishing Group.

vacancy enhanced the self-healing features of active sites, promoted the OOH intermediate adsorption, and accelerated the O-O coupling. The F leaching introduces surface reconstruction and creates real active sites that remarkably trigger the OH^- adsorption, and sustainability of active sites [133]. The dynamic reconstruction of the catalyst introduces a high degree of defects, reduces the activation barrier, and enhances the catalyst's structural sustainability. The surface reconstruction of the catalyst can be measured in terms of the triggering condition, the reconstruction rate, and the degree of conversion [134]. The external potential which causes surface reconstruction, temperature and electrolyte content is referred to as the triggering condition. The reconstruction rate denotes the degree of difficulty in driving the reconstruction process. Accelerating the reconstruction rate allows for the rapid formation of rich active sites, which aids in enhancing water electrolysis efficiency. The degree of reconstruction could represent the conversion rate of pre-catalysts [135]. By increasing the degree of reconstruction, more pre-catalyst components can be converted into active species, resulting in a deeper reconstructed layer, a large number of active sites, and a high pre-catalyst utilization rate. Because the reconstruction process is fundamentally a chemical reaction, the intrinsic qualities of the pre-catalyst, as well as the reconstruction conditions, will influence the reconstruction process. Furthermore, dynamic structural development would modify the inherent features of newly generated species (e.g., composition, microstructures, metal valence

state, defect level), which are connected to catalytic efficiency [136].

The surface defects could modulate the reconstruction behavior and, thus, the structure of the pre-catalyst, thereby enhancing the catalytic performance and sustainability. In addition, partial dissolution is considered a common driving force for reconstructing the active phase. Therefore, the catalyst should be designed with high defect density and strong linkage with underlying support to promote the reconstruction, which governs high efficiency and durability.

6. Morphology optimization

6.1. Core-shell nanostructure

The available active sites and catalyst consumption can be controlled by modifying the shape of OER catalysts. The stability and activity of an OER catalyst are significantly influenced by mass transport phenomena such as gas desorption and bubble detachment, which are determined by the electrochemically active surface area [137]. Fundamental research examining the efficiency of a catalyst's isolated crystal facets has assisted in understanding and advancing the design of catalysts for electrochemical reactions [138]. The same approaches are being used to better understand the OER, for example, by customizing the exposed facets of nanostructured catalysts to improve their performance [139]. Strain engineering is one of the promising routes to enhance the sustainability of an electrocatalyst by modifying the atom's internal spacing to alter the electronic and surface structure [140]. Recent investigations revealed that one percent strain could cause the d band center to move by around 0.1 eV, strengthening the bond between surface adsorbates and catalytically active sites [141]. Lattice strain can now be introduced using heteroatom substitution, substrate-induced, and lattice mismatch. Lattice strain can be produced by creating a lattice mismatch between two metals, either by synthesizing core-shell structures or carefully removing atoms from an alloy [142,143]. However, it is inevitable to incorporate interface-synergistic effects between various components, which also affect the catalytic activity and stability. Mainly, strain effects caused by the structure or electron transfer between two components are the interactions in core-shell nanostructures that are advantageous for sustainable electrocatalysis [144]. Due to a lattice mismatch with the core lattices, the strain effect occurs when the geometry of the shell atoms is squeezed or expanded. In general, tensile strain reduces the surface atoms' coordination numbers, which results in a smaller bandwidth and an upshifted d-band center [145,146]. In contrast, compressive lattice strain causes the broadening of bands and the d-band center to migrate downward. The d-band center location is sensitive to the antibonding states below the Fermi level; therefore, the above shifting can effectively change the bindings of adsorbates. The more robust bonds with *OH intermediates are caused by the upshifting, and vice versa [147].

Core-shell nanostructure affords the following unique features.

1. The robust shell protects reactive cores, mitigates the aggregation by avoiding the sintering or Ostwald ripening phenomena during the catalyst development and electrocatalysis, and enhances the resistance of the active core against corrosion in acidic or basic conditions [148].
2. Strong interactions between the components of the core and shell allow for the alteration of the electronic/chemical configurations of active sites, which is crucial to enhancing intrinsic activity and optimizing the binding of reaction intermediates. In core-shell nanostructures, the lattice strain of the shells and the interfacial electronic redistribution can change the d-band centers to suitably fulfill the reaction kinetics and enhance the chemical stability of the catalyst [149].
3. Abundant active sites in core-shell nanostructure with variable electronic configurations are anticipated to effectively interact to accommodate the numerous primary steps of water-splitting reactions [150].

One of the most important advantages of the core-shell nanostructure is its much-improved sustainability and recyclability during catalysis. Although the strong metal-support connection improves the durability of traditionally supported catalysts, the highly energetic NPs may migrate and agglomerate when exposed to harsh electrolytes at a high anodic or cathodic potential. Recent findings demonstrated that when metal nanoparticles are enclosed in inorganic nano-shells or nanopores, migration and coalescence due to sintering or Ostwald ripening phenomena are reduced to a more significant extent [151]. Metal nanoparticles could be significantly restricted in their migration and coalescence when enclosed in inorganic nano-shells or nanopores due to spatial structural confinement, which is responsible for the structural durability of active sites. Encapsulation, particularly in the core-shell arrangement, ensures that the metal nanostructure in the core has the greatest possible interfacial area with the shell materials. Catalytic performance can be dramatically improved if the interactions are carefully adjusted [152].

For highly effective and durable OER catalysts, the Strasser group introduced a novel catalyst/support couple concept that combines an electrochemically dealloyed Ir-Ni core and IrO_x shell concept with mesoporous corrosion-resistant oxide support [148]. This idea has based on the kinetically frustrated oxidized Ir shell formation, which produced outstanding OER activity at low noble metal content and allowed the active NPs to be dispersed. The high surface area mesoporous structure of the support also gave the catalysts excellent corrosion resistance. The authors concluded that the core-shell water-splitting catalyst supported 2.5 times higher O-O coupling rate on the electrolyzer level while demonstrating negligible activity loss during 20-hour continuous electrolysis in contrast to various Ir benchmark materials. Realistic PEM electrolyzer anodes might be coated with a couple of nanostructured core-shell catalysts and mesoporous support to enhance the overall sustainability and corrosion resistance. The core-shell catalyst/oxide support concept has been considered a practical approach to reducing the number of scarce elements in catalytic nanoparticles. Similarly, Zhu et al. reported that core-shell structure could accelerate the charge transfer, enhance the bubble detachment and gases desorption rate, increases the exposed specific surface area with high intrinsic reactivity, and significantly improve the ASF (Fig. 6A) [153]. The author's designed core-shell electrocatalysts, i.e., Ni-Co/Ni-Co−OH and Ni-Fe/-Ni-Fe−OH, via gas templated electrodeposition strategy. The developed Ni-Co/Ni-Co-OH and Ni-Fe/Ni-Fe-OH exhibit outstanding activity toward the HER and OER in 1 M KOH, respectively, especially at high current densities necessary for industrial applications. The water electrolyzer built of Ni-Co/Ni-Co-OH and Ni-Fe/Ni-Fe-OH has the potential to catalyze the water splitting at 1 A cm^2 for at least 300 h without significantly degrading performance, and it only needs a cell voltage of 1.74 V to achieve 500 mA cm^{-2} in two electrode configurations. The authors attributed the high electrocatalytic activity and sustainability to the distinct core-shell heterostructures, where the surface hydroxides provide many active sites, and the inner alloy facilitates electron transport with high corrosion resistance (Fig. 6B-K). Core-shell nanostructure construction is a practical way to optimize the chemisorption energy and stabilize the intermediate with optimum adsorption energy responsible for the catalyst's high intrinsic activity and stability. Recently, core-shell nanostructure with Au core and $AuIr_2$ shell has been constructed, which revealed 4.6 times higher intrinsic activity compared to commercial Ir-based catalyst [154]. The catalyst sustained high current density for 40 h without noticeable degradation and revealed high structural and mechanical durability. X-ray analysis revealed the electronic interaction between Ir and Au, which shows the electronic redistribution after core-shell formation. The theoretical and experimental study validates that a partially oxidized surface has more optimum energy to stabilize the OER intermediate and enhance the reaction

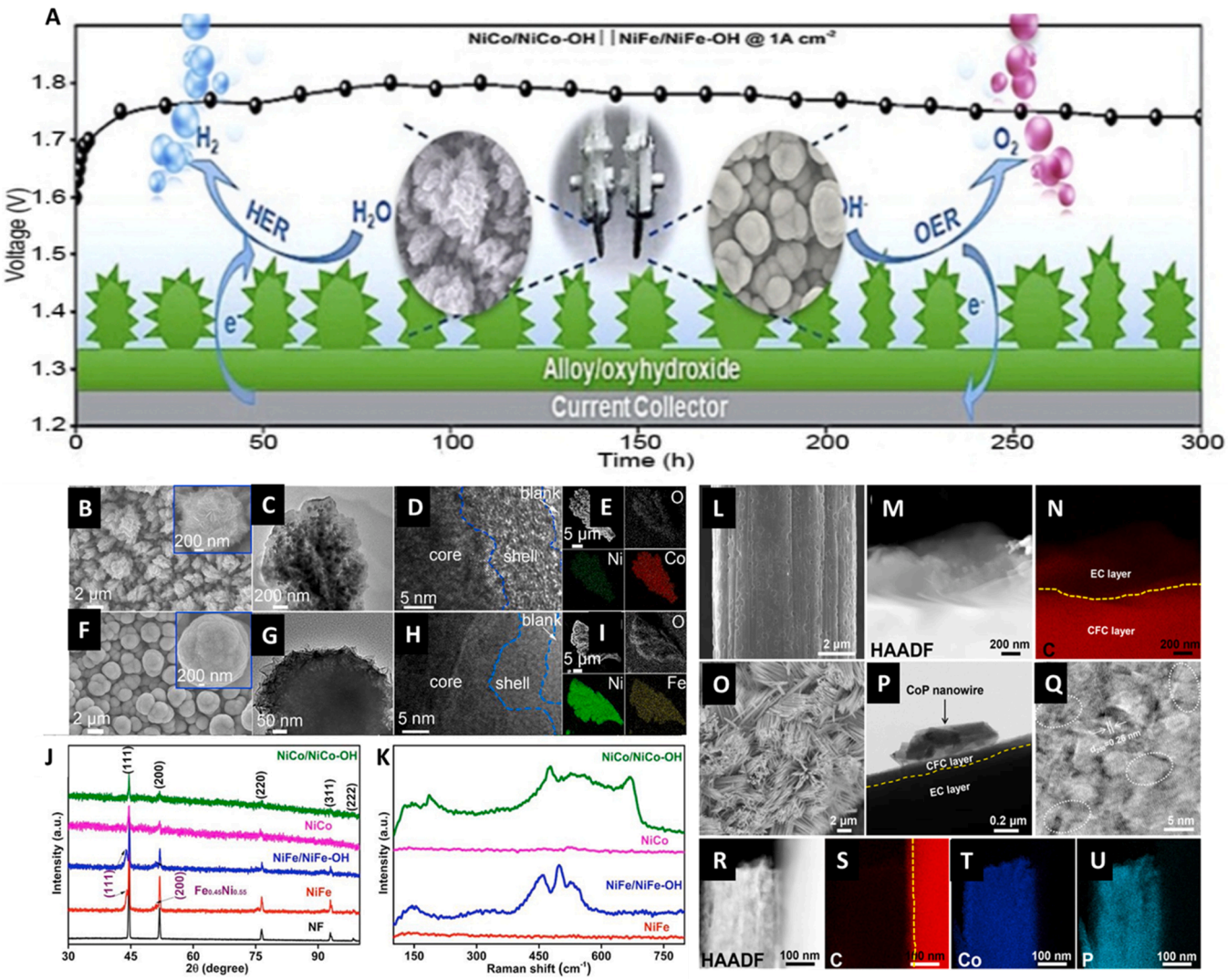

Fig. 6. (A) Graphical abstract illustrating that NiCo/NiCo−OH and NiFe/NiFe−OH composite overall water splitting at 1000 mA cm^{-2} for at least 300 h at a low cell voltage; Structural characterization of the alloy/oxyhydroxide core-shell electrocatalysts. (B, F) SEM, (C,G) TEM, and (D, H) HRTEM images and (E, I) elemental maps of the NiCo/NiCo−OH (B-E) and NiFe/NiFe−OH (F-I). (J) XRD patterns and (K) Raman spectra of electrode. Morphological characterization of CFC@EC and CFC@EC/CoP. (L) SEM image of CFC@EC. (M and N) EDS mapping of CFC@EC depicting core–shell structure. (O) SEM image of CFC@EC/CoP. (P) TEM image of CFC@EC/CoP with core-double-shell engineering. (Q) HRTEM image of CFC@EC/CoP displaying distortion and lattice fringes of CoP (R-U) EDS mapping spectra. Copyright 2021, Elsevier.
(a) Reproduced with permission from ref [153]. (b) Reproduced with permission from ref [155]. (j) Copyright 2020, Elsevier

kinetics compared to the metallic surface. Each elementary step of OER must have a relatively small free energy change at the usual equilibrium potential for OER for the electrocatalytic system to cross the energy barrier at low input voltage. The DFT calculations showed that the intermediates' excessively high binding affinities result in a large overpotential for the OER on clean metallic surfaces.

In contrast, the partially oxidized surfaces possessed a substantially lower binding affinity and had high ASF. Additionally, there is a chance to boost activity even more by creating a hybrid material that has been partially oxidized. The partially oxidized core-shell surfaces attain a better equilibrium for intermediates binding and thus demonstrate a higher OER activity than the simple hybrid surfaces. Yang et al. developed a monolith architecture of carbon fiber cloth core-shell structure supported by transition metal compounds, revealing high activity and sustainability for water splitting [155]. Different transition metals compounds, including Ni_3S_2, Ni_3N, Ni-Co-LDH, CoS_2, and Ni-Mn-LDH integrated with the core-shell structure were examined for water splitting, and the catalysts revealed high geometric activity at low input voltage and demonstrated high structural, chemical, and mechanical durability at the high potential in alkaline medium. The author's findings suggested that numerous lattice distortions and potent electrical interactions between the metal cations and substrate are made possible by designing the core-shell structure (Fig. 6L-U). The lattice distortions expose more active sites, increase the intrinsic activity of active sites, and are responsible for long-term durability. Recent findings revealed that the development of core-shell nanostructure provides abundant exposed active areas, ensures effective contact between water molecules and active components, and mitigates the nonconductive layer formation. In addition, the core-shell structure offered a distinctive way for the electrolyte diffusion, enhanced the bubble detachment rate and gas desorption from the active sites due to lattice strain, and enhanced the charge and mass transfer kinetics at the electrode-electrolyte interface (Fig. 7A-L) [156].

Researchers found that core-shell structures avoid the agglomeration of nanostructure due to van der Waals forces of attraction, particularly observed in 2D nanosheets. Han and coworkers constructed a core-shell structure via the homogenous growth of $MoSe_2$ nanosheets on conductive MOF to prevent the aggregation of sheets and trigger the charge and

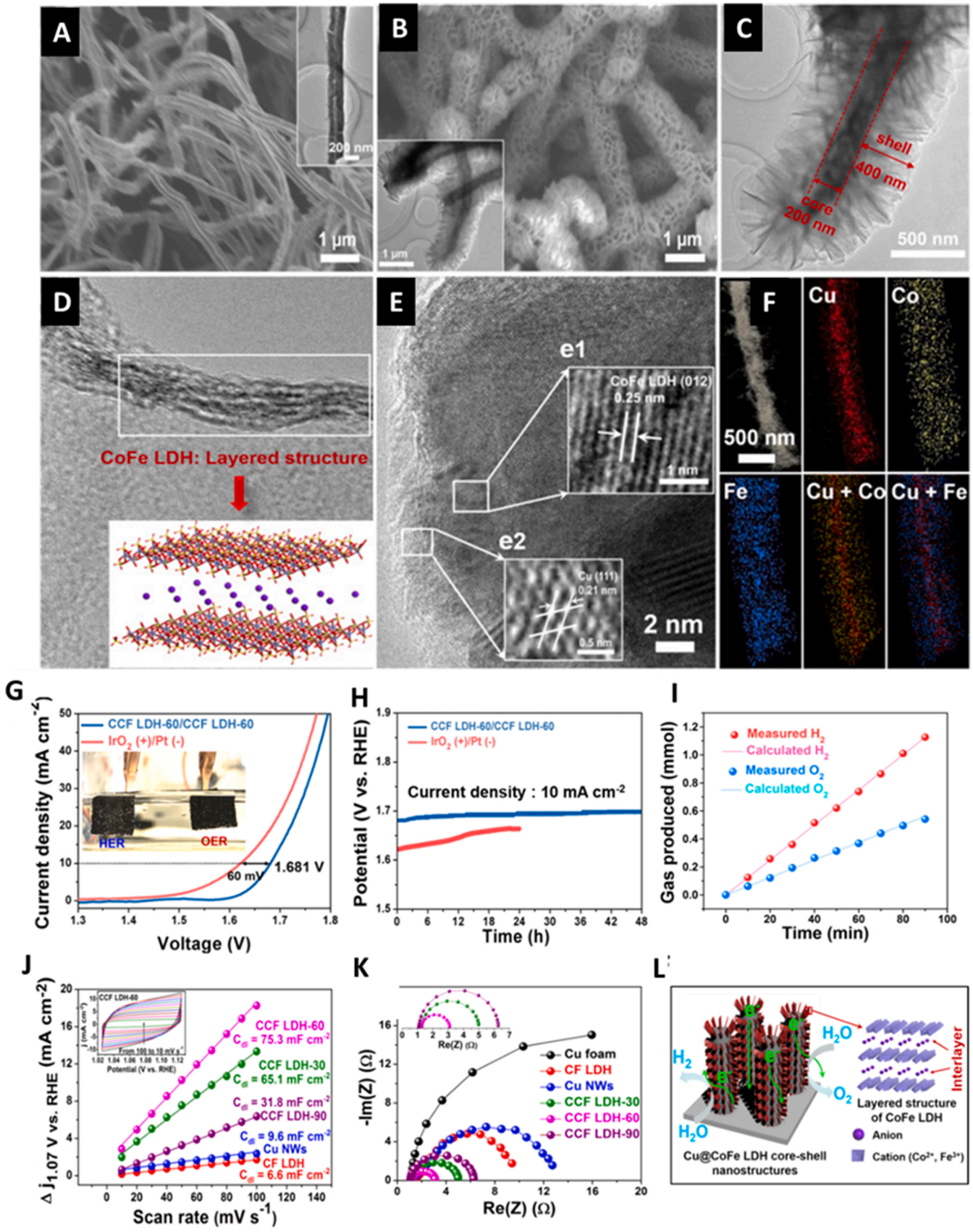

(caption on next page)

Fig. 7. SEM images of (A) Cu NWs and (B) CCF LDH-60. (The insets include TEM images.) (C) TEM images of CCF LDH-60. (D) HRTEM image of CCF LDH-60 to depict CoFe LDH layered structure (E) Lattice fringes (The inset in d is a structural model of CoFe LDH. (e1) and (e2) in e are the corresponding enlarged parts of the square) (F) DF-STEM image of CCF LDH-60 and the Elemental mapping.(G) Overall water electrolysis polarization curves with CCF LDH-60 composite as both cathode and anode at of 2 mV s^{-1} scan rate (The inset is the optical photograph indicates O_{2and} H_2 bubbles formation on electrodes.) (H) Chronopotentiometry curves of CCF LDH-60 at a constant current density of 10 mA cm^{-2} in a two-electrode setup. The state-of-art IrO_2 (+)/Pt (−) are experimented side by side as in G and H. (I) Experimental and theoretical amounts of H_2 and O_2 by the CCF LDH-60 electrode at a fixed 40 mA cm^{-2} current density (J) Capacitive currents as a function of scan rate and (K) Nyquist EIS plots (overpotential = 250 mV). The inset in (j) is the CV curve of CCF LDH-60 at multiple scan rates and in (K) is enlarged EIS plots of composite. All the tests were done in 1 M KOH electrolyte. (L) Schematic presentation of structural characteristics for Cu@CoFe LDH core-shell hierarchical nanostructured composite.
Reproduced with permission from ref [156]. Copyright 2017, Elsevier.

mass transfer at the interfacial boundary highly needed for the sustainable electrode [157]. The multiple active sites for hosting the 2D nanoflakes of $MoSe_2$ on the vertically oriented and well-separated Co-MOF nanowalls boosted the final active sites for the redox process. Interestingly, it has been noted that during the hydrothermal synthesis of $MoSe_2$, Co-MOF was changed into $CoSe_2$, which was broken through the conductivity barriers of Co-MOF. Additionally, the electroactive sites that come from decorating the $CoSe_2$ nanowalls with $MoSe_2$ nanoflakes were improved. $MoSe_2$ nanosheets served as an active nano-surface material for electrochemical interactions with electrolyte ions in the developed MOF-$CoSe_2$ @$MoSe_2$ nanostructure, where the core of MOF-$CoSe_2$ nanowalls creates conductive unidirectional pathways using low scattering electron transfer between the $MoSe_2$ nanosheets and carbon cloth (CC). Reactive reaction sites could be employed more effectively in core-shell structures with short ion diffusion pathways because $MoSe_2$'s porous 2D nanosheets permit close contact with the electrolyte. Uniquely created CC/MOF-$CoSe_2$ @$MoSe_2$ two-dimensional nanostructure combines the advantages of various phases and creates a strong interface connection between the MOF--$CoSe_2$ shell's outer and the central core, which is used for OER and HER electrochemical activities in alkaline media. With hydrothermal, sulfurization, and in situ electrochemical tuning processes, Liu and coworkers created a new trimetallic Ni-Fe-V disulfide @ amorphous Ni-Fe hydroxide core-shell heterostructure electrocatalyst for the OER [158]. The catalyst possessed the following merits: (1) The formation of a favorable electron configuration of active sites (either Ni or Fe sites) on the surface of the shell is favored by the strong synergistic interaction between the core (Ni-Fe-V disulfide) and shell (amorphous Ni-Fe hydroxide). (2) Co-doping the metallic Fe and V could improve the electronic conductivity of the NiS2 core, accelerating the electronic transfer during OER. The trimetallic $Ni_{0.70}Fe_{0.10}V_{0.20}S_2$ core-shell nanostructure demonstrated the best OER activity compared to mono-/bi-metallic core catalysts, according to electrochemical measurements with similar mass loading. The catalyst was fabricated on hydrophilic-treated carbon paper (CP) and created an integrated 3D electrode with a large loading mass and good conductivity to determine the precise composition and enhance the overall OER performance and stability of the material. As a result, the core-shell structure demonstrated exceptional overall OER performance and stability. Wang et al. explored a variety of lattice-strained homogeneous NiS_xSe_{1-x} nanosheet/nanorod hybrids [143]. computational and experimental results verified that the generated lattice strain in NiSxSe1-x could reduce the metal D-orbital overlap and bring the D-band center closer to the Fermi level, which enhances intrinsic electronic conductivity and optimizes reaction pathways/energy barriers, thereby significantly improving the electrocatalytic properties. Following equation has been used to calculate lattice strain (τ) (Eq. 11).

$$T \quad NiS_xSe_{1-x} = \left|\frac{a-\bar{a}}{\bar{a}}\right| \times 100\% \tag{11}$$

Where a is the lattice strain of dopant and ā is that of pristine Ni-Se and NiS.

OER goes through a four-electron step process in an alkaline medium. The adsorption energies of OER intermediates adsorbed on various samples have been estimated at various constant potentials. An appropriate contact strength between the active sites and reaction intermediates is essential for OER activity. The predicted energy barriers for limiting reactions decent from $NiS_{0.5}Se_{0.5}$ (τ = 2.7%, 1.59 eV) to NiS (= 0%, 2.69 eV), Ni-Se (τ = 0%, 2.58 eV), $NiS_{0.23}Se_{0.77}$ (τ = 1.8%, 1.77 eV), $NiS_{0.76}Se_{0.24}$ (τ = 1.6%, 2.03 eV) at zero potential. Therefore, among all the samples under investigation, the $NiS_{0.5}Se_{0.5}$ with a lattice strain of = 2.7% has the most favorable OER kinetics, proved by experimental results. Other than that, $NiS_{0.5}Se_{0.5}$ exhibits a greater density of state (DOS) near the Fermi level than other samples, suggesting enhanced electron mobility in the sample with a lattice strain of = 2.7% for rapid charge transport, which is another significant factor in the remarkable catalytic reactivity. The author's findings unveiled that the 2p electronic orbit arrangement of active metal sites are affected by lattice strain. When the lattice strain increases, the D-band center changes to a favorable position relative to the Fermi level. The D-bandwidth also reduces as the lattice strain increases. According to this finding, the created strain causes the change in electrical characteristics that results in a smaller metal D-orbital overlap, a narrower bandwidth, and a more positive D-band center. The lattice strain resulted in reduced bandwidth and an upshift in the D-band center. Antibonding d states would move upward with the upshift of the D-band center, accompanied by a decrease in the occupation, which will boost the adsorption contact with reaction intermediates, favoring increased activity and stability.

6.2. 2D materials

In addition to the internal atomic structure (d band position relative to EF), the external structure (crystallization, morphology, etc.) has a critical role in modulating the reaction energy barrier, adsorption/desorption activation, and chemisorption energy and controlling the dynamics of electrochemical process [159]. Among different surface or geometric structures, 2-D nanomaterials (e.g., nanosheets, nanoflakes, nano meshes, nanoplates) have been recognized as more efficient and sustainable electrocatalysts for driving water electrolysis due to abundant unsaturated atoms, high specific and electrochemically active surface area and densely occupied edges and defects [160]. Additionally, it has been revealed that exposing highly active facets can significantly increase the intrinsic activity of 2D nanostructures [161]. Additionally, the unique strain effect and ligand impact within the 2D nanostructures may also help further to promote the intrinsic activity and durability of an electrocatalyst [162]. The following are the unique merits of 2D catalysts: 1) The abundant exposed active sites are present in the ultrathin 2D nanostructure, which has a large specific surface and an atomic thickness [163]. 2) The 2D nanostructure has many defects, and unsaturated metal sites can facilitate the adsorption and desorption of reaction intermediates by providing the optimum chemisorption energy [164]. 3) The 2D nanostructure has distinct electronic structures at the atom level, decreases the free energy of fundamental steps in the HER and OER processes, decreases the charge transfer resistance at a solid-liquid boundary, and offers short diffusion channels for ions migration [165]. 4) The extensive surface area of the ultrathin 2D nanostructure makes them the perfect platforms for combining other catalytic materials, further adjusting the states of electronic structures and enhancing electrochemical behavior, i.e., heterostructures constructed with various catalysts that each have unique intrinsic

advantages [166,167]. Tian's group suggested a complex O-anion doping method to enhance the electrocatalytic performance of CoP nanosheets toward the overall water splitting in an alkaline medium (Fig. 8A-H) [168]. The experimental and DFT simulations revealed that the proper insertion of O into CoP could significantly modify its electronic structure and change the adsorption-free energies of reaction intermediates, enhancing the HER and OER activities. The simulation results showed that when the oxygen dopant was added, the electronic states of the O-CoP catalyst near the Fermi level appeared to rise, indicating a more significant charge carrier density and favorable charge transfer during the electrocatalytic processes of the O-CoP catalyst. In the alkaline electrolyte, the O-CoP nanosheets with an optimized O incorporation display compelling bifunctional performances; for HER and OER, respectively, overpotentials of 98 and 310 mV are needed to deliver a current density of 10 mA cm^{-2}. Furthermore, the O incorporation is thermodynamically favorable in 2D nanosheets due to the unique in-plane electron transfer mode. The low coordinated edges, steps, and kinks facilitate the intermediate adsorption and decrease the kinetic barrier. Additionally, the O-CoP nanosheet catalyst could function as both an anode and a cathode to build a two-electrode electrolyzer that provides a total water-splitting current density of 10 mA cm^{-2} at a cell voltage of just 1.60 V with impressive stability. Similarly, Co, Fe co-doped $NiSe_2$ nanosheets have been fabricated by structural transition using Fe, Co co-doped $Ni(OH)_2$ nanosheets as starting point through the vapor deposition technique [169]. The investigation revealed that compared to single-cation-doped or pure $NiSe_2$, the dual-cation inclusion could alter the lattice and produce stronger electronic interaction, increasing the active site exposure and optimizing the adsorption energy of reaction intermediates. The $Fe_{0.09}Co_{0.13}$-$NiSe_2$ porous nanosheet electrode exhibited good catalytic activity and needed a low overpotential to drive high geometric activity with long-term durability. The 2D nanomaterials heterojunction also exhibits improved catalytic capability and stability for water splitting in alkaline electrolytes due to the interface nanosheet structure with many defects. The nanosheet interface allows the electrolyte penetration to the underlying support and avoids the support passivation [170]. Yang et al. have designed 2D amorphous $FePO_4$ nanosheets vertically grown on Ni foam and used inner and outer structural engineering strategies to modulate the external structure of electrocatalysts (Fig. 8J-O) [171]. The amorphous $FePO_4$ nanosheets with disordered structures have a low-energy d band center and reduced Gibbs free energy, responsible for high electrocatalytic activity and sustainability (Fig. 8P-R). Based on the experiment and DFT results, the authors concluded that the following factors are responsible for the high sustainability and activity of the catalyst. (1) the amorphous structure encourages the adsorption of reaction intermediates on surfaces and may lower the binding energy between the OER reaction intermediates and the electrode surface, reducing the activation barrier and avoiding the support passivation at a high anodic potential. (2) The 2D morphology offered abundant active sites with high intrinsic activity and short diffusion channels for ions migration responsible for high structural and chemical durability. (3)The Ni introduction enhanced the electrical conductivity and altered the electronic structure with optimum chemisorption energy stabilized the OER intermediates.

Given that 2D structure considerably enhances the electrochemically active area, the fabrication of single- and few-layered 2D nanosheets has shown promise in improving catalytic activity [172]. But irreversible restacking of 2D nanosheets during processing and manufacture blocks the active sites, provides a more challenging electrolyte diffusion pathway, and compromises sustainability, which is still a significant

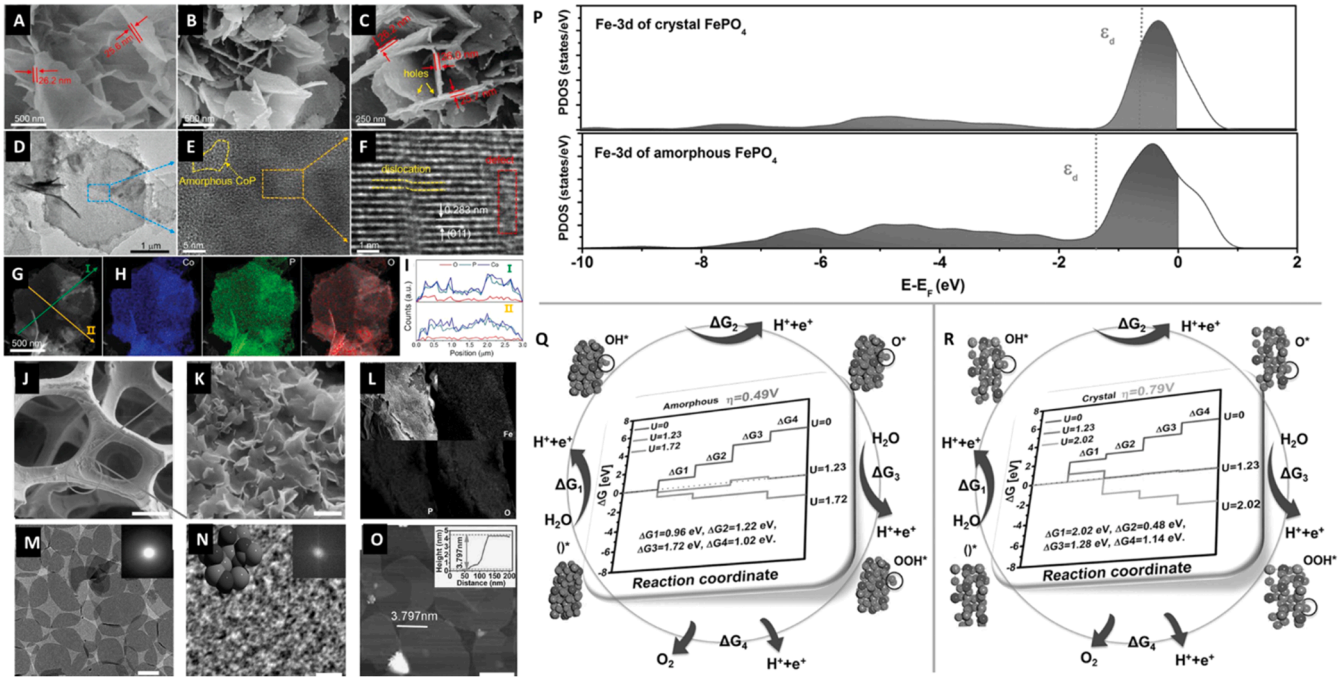

Fig. 8. (A) $Co(OH)_2$ nanosheets starting SEM images (B,C) SEM images, (D) TEM image, (E,F) HRTEM images, (G) HAADF-STEM image, (H) Elemental mapping images, and (I) EDX line-spectra of as-converted O-CoP-2 nanosheets. Copyright 2019, Wiley VCH (J) Low-magnification and (K) SEM images of high-magnification for amorphous $FePO_4$ nanosheet at NF. Scale bar in (J) 100 nm (K) 2 μm (L) Elemental mapping of P, O, and Fe for nanosheets of amorphous $FePO_4$ (M) TEM and (N) HRTEM image of amorphous $FePO_4$ nanosheet. Scale bar in (M) 500 nm (N)5 nm, Insets of (M) and (N) are FFT pattern, SAED pattern and structural model of amorphous $FePO_4$ nanosheet. (O) AFM image of amorphous $FePO_4$ nanosheet. The scale bar in (O) is 500 nm. (P) Calculated PDOS of the d band of the Fe atoms in $FePO_4$. Fermi level is set as zero and the d band center is marked with a pink dashed line. (R) OER mechanism scheme on the $FePO_4$ surface. The inset of (Q) and (R) depicts a free-energy landscape in comparison to an ideal composite (dashed line). For amorphous $FePO_4$, as shown in (P), reaction 3 is a potential-limiting step. At potential > 1.72 V, all intermediate steps are thermodynamically feasible. As shown in (R), for crystal $FePO_4$, reaction 1 is the potential-limiting step. For U > 2.02 V, all steps are thermodynamically favorable.
(a) Reproduced with permission from ref [161]. (b) Reproduced with permission from ref [171]. Copyright 2017, Wiley VCH

challenge. On the other hand, Holey/porous nanomaterials have more active areas and continuous mass/charge transport pathways due to their interconnected open architectures and structural stability. Yu and coworkers developed the metallic $NiCo_2Se_4$ (NCS) holey nanosheets with a monoclinic phase, demonstrating high intrinsic reactivity and robustness for water oxidation [173]. NCs holey nanosheets have better catalytic activity and long-term durability for OER because of their metallic composition, synergistic interaction between Ni and Co atoms, and the holey structure of linked nanoparticles. The holey nanosheets acquired enhanced cycle stability low barrier for O-O coupling and driving the electrochemical reaction with high sustainability. The density functional theory (DFT) calculation and experimental findings demonstrated that the $NiCo_2Se_4$ exhibited good catalytic activity due to the highest hydroxyl ion absorption energy. Due to the synergistic

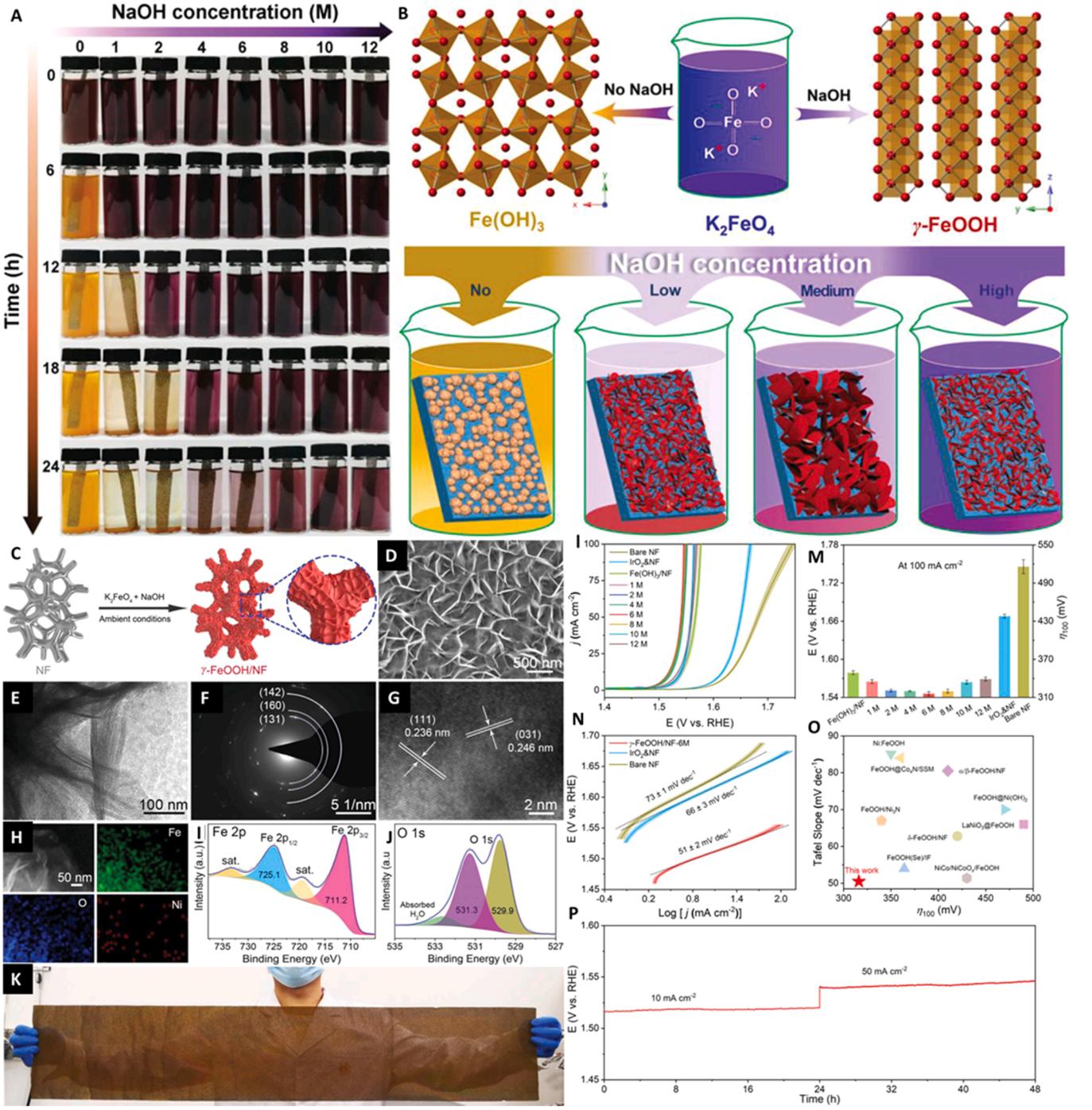

Fig. 9. (A) Time-dependent discoloration behaviors of K_2FeO_4 with various NaOH concentrations. (B) Pictorial presentation for K_2FeO_4 hydrolysis pathway and controlled mechanisms of γ-FeOOH NAs. (C) Scheme of synthesis of γ-FeOOH/NF. (D) SEM, (E) TEM, (F) SAED, (G) HRTEM, and (H) HAADF-STEM and EDS mapping images of γ-FeOOH/NF. (I,J) High-resolution Fe 2p and O 1 s XPS spectra of γ-FeOOH/NF. (K)Synthesis of γ-FeOOH/NF with 100 × 20 cm^2 geometric size (L) Polarization curves (M) overpotential/potential at 100 mA cm^{-2} for γ-FeOOH/NF-X, $Fe(OH)_3$/NF, IrO_2&NF, and bare NF. (N) Tafel plots of γ-FeOOH/NF-6 M, IrO_2&NF, and NF. (O) Comparison of η_{100} and Tafel slope of γ-FeOOH/NF-6 M. (P) Chronopotentiometry curve of γ-FeOOH/NF-6 M at constant current density of 10 and 50 mA cm^{-2}. The shaded area and error bars represent the standard deviations for twenty independent measurements.
Reproduced with permission from ref [175]. Copyright 2021, Wiley VCH

interactions between Ni and Co atoms, holey nanosheet structure, and metallic properties of ternary selenide, these materials exhibited exceptional electrocatalytic performance. First, the metallic properties enhance the OER kinetics by favoring the proton-coupled electron transfer (PCET) between the catalyst and the current collector. Second, a holey nanoarchitecture could increase the interaction between reactants, active sites, and electrolyte diffusion. The 2D shape offers a direct path for the easy release of generated O_2 bubbles and the facilitation of electrolyte penetration. Interconnected nanoparticles could be found inside the holey structure to help with electron transfer and improve the electrocatalyst's structural stability. Because of their altered electronic system and mixed valence states, the synergistic effect of Ni/Co atoms can further enhance electrocatalytic activity and sustainability. Qu et al. have developed Ru-doped Ni-Fe-P nanosheets directly grown over Ni foam via hydrothermal method followed by phosphorization [174]. As it has been produced, the material is a superb bifunctional catalyst with strong stability for both exceptional HER and OER activities. Low overpotentials of 242 mV for OER (@100 $mAcm^{-2}$) and outstanding stability in 1.0 M KOH solutions were used to demonstrate good performance. Based on XPS and Bader charge analyses, Ru doping is crucial in controlling electron density to enhance catalytic activity. Combining the results of the experimental and computational investigations, the authors concluded that the catalytic capability has significantly improved by a reduction in free energy following the addition of trace Ru, which increases the number of active sites and enhances the intrinsic activity of the original active sites. Furthermore, the hierarchical nanosheets that provide a large surface area and more exposed sites, the smaller contact resistance and faster charge transfer between the catalyst and the substrate, and the synergistic effect of Fe and Ni are all factors that contribute to the high catalytic activity and excellent durability. Wang et al. developed a highly controllable hydrolysis method to fabricate large-scale γ-Fe-OOH nanosheets directly grown over Ni foam with structural stability and corrosion resistance (Fig. 9A-K) [175]. The experimental results show that the nanosheets have low charge transfer resistance and sustainability to catalyze the water oxidation reaction. The DFT calculation suggested that Ni foam electrochemically oxidizes to γ-Ni-OOH would cause charge accumulation on the Fe sites of -Fe-OOH nanosheets, enhancing the adsorption of OER intermediates for water splitting (Fig. 9L-P). The high intrinsic activity and structural and mechanical durability of the catalyst were credited to the following factors: (1) In addition to ensuring good electrical contact to speed up the electron/charge transfer, the -Fe-OOH nanosheets grown directly on NF also provide additional active sites without any conducting agent or binder. (2) The mechanical resilience of the arrayed structure prevents the electrocatalyst from aggregating and increases ECSA for effective electrochemical reactions. (3) Aligned pores on the -Fe-OOH 2D structure produce a super hydrophilic surface that makes it easier for electrolytes to penetrate and creates channels for O_2 bubble detachment. iv) The -Ni-OOH produced in situ due to the electro oxidation of NF during OER encourages the charge to build up on the Fe sites of the -Fe- OOH NAs, which facilitates intermediate adsorption and significantly increases catalytic activity. By interstratifying the exfoliated nanosheets, bifunctional 2D superlattice electrocatalysts comprising alternating layered double hydroxide (LDH) and transition metal dichalcogenide (TMD) hetero layers has been reported [176]. The catalyst revealed firm electrical contact at the interface and showed excellent long-term durability and low overpotential. After interstratification with MoS_2 nanosheets, the chemical stability of LDH was noticeably improved. The 2D nanosheet assembly's beneficial effects can be attributed to improved electrical conductivity, an enhanced affinity for reaction intermediates (OH^- and H^+), suppressed charge transfer resistance, and the presence of multiple active sites because of strong interfacial electronic coupling and noticeable surface expansion. Notably, optimal intermediate adsorption with the active sites can increase the activity, selectivity, and durability of the electrocatalyst, and this optimum adsorption, in turn, depends on the metal's orbital energy level and electronic structure being compatible with the incoming intermediates, the population of the electron density, and the surface engineering of the catalyst. We have recently reported that Au-supported Gd-doped CoB amorphous sheets developed via the electrodeposition route have shown substantial activity and sustainability for water oxidation [97]. The amorphous nanosheets facilitated the electrolyte penetration and accelerated the desorption of gas molecules. Energy valence bond theory states that the hyper-electronic d orbitals and unoccupied 4 f orbitals of rare earth metals can diffuse one another, making it easier to arrange the orbitals in the right way for the catalysis required in OER processes. The addition of "B" from the electrochemical activity significantly improves the catalytic activity of the Gd-doped Co film for OER, particularly against corrosion and chemical transformation. We also deduced from high TOF, FE, and long-term durability tests that a smooth film of Au and controlled incorporation of Gd allow for the uniform growth of nanosheets with a distinctive texture, significantly increasing the overall catalytic potential, preventing catalyst poisoning and, ultimately imparting extra stability even at a high anodic potential.

Similar to this, Liu et al. have described an easy and scalable process for creating a hybrid network of mesoporous nanosheets made of Co_3O_4 and $Co_3(PO4)_2$ [177]. The porous nanosheet structure with oxygen vacancies and $Co_3(PO_4)_2$ that received electrons from Co_3O_4 demonstrate exceptional performance for oxidizing water. According to the author's description of the synthesis process, Guanosine 5-monophosphate (GMP) was first broken down into guanine, pentose, and phosphate ions in hydrothermal conditions (Eq. 12).

$$C_{10}H_{12}O_8N_5P^{2-} + 2H_2O \rightarrow C_5H_{10}O_5 + C_5H_5N_5O + PO_4^{3-} + H^+ \quad (12)$$

Pentose has been dehydrated before organic residue has been carbonized to create the carbon phase (Eq. 13).

$$C_5H_{10}O_5 \rightarrow 5C + 5H_2O \quad (13)$$

Then, through electrostatic interactions or coordination mechanisms, the hydrophilic surface of the carbon phase initiates the adsorption of Co^{2+} ions. Guanine hydrolysis acts as a pH buffer, increasing the concentration of OH- ions and CO_3^{2-} ions in the process (Eqs. 14–15).

$$Co^{2+} + OH^- + 0.5CO_3^{2-} + 0.11H_2O \rightarrow \mathrm{Co}(OH)_1(CO_3)_{0.5}0.11H_2O \quad (14)$$

$$Co^{2+} + 2PO_4^{3-} \rightarrow CO_3(PO_4)_2 \quad (15)$$

Co_3O_4's acidity has increased due to the electrical contact with $Co_3(PO_4)_2$, which causes Lewis' base to become destabilized through acid-base interaction and lowers the potential kinetic barrier for O-H bond breakdown. The intrinsic activity of active sites increases and accelerates the charge transfer conduction due to the electronic interaction at the 2D nanosheet interface. According to recent research, pure cobalt oxide has weak electronic conductivity and performs less well as an electrocatalyst because there aren't as many active sites exposed. Because of the structural and morphological imperfections at the interface boundary, the small grain size increased the exposed surface area, changed the electronic conduction of Co by changing its D-band center, and sped up the kinetics of the electrochemical reaction. The reaction center chemisorption energy is optimized by the structural and morphological optimization with increased oxygen vacancies, which also lowers the metal dissolving rate and increases the ASF [178].

6.3. 3D hierarchical nanostructures

In principle, abundant active sites with high intrinsic activity, the maximum contact area between electrolyte and electrode, and higher bubbles desorption rate are crucial to enhance the ASF of the heterogeneous catalyst. Nanostructuring is a widely applicable strategy to strengthen the number of active sites. Still, it does not certainly infer the

increment in catalytic performance because the charge diffusion pathway has sometimes been cut off. The 3D hierarchical nanostructure has a unique figure of merits as it provides maximum exposure to active sites while maintaining a robust interconnected structure, endorses excellent charge carrier mobility, and ensures active sites' structural and mechanical durability [179]. Kong et al. have fabricated carbon textile-supported 3D hierarchical $NiMo_3S_4$ nanoflowers that demonstrated higher catalytic activity and durability in alkaline solutions [180]. The Ni incorporation in Mo-S modulated the surface structure at the atomic scale, created substantial surface defects that act as active centers, and impressively enhanced the activity and stability of the material. The 3D hierarchical $NiMo_3S_4$ nanostructure has a high specific surface area, offers short diffusion channels for mass and ions migration, improves the contact portion at the electrode-electrolyte interface, and delivers a higher current density at a small input voltage. In addition, the 3D hierarchical structure enhanced the electronic conduction by increasing the DOS at the Fermi level and ensuring the support stability under high anodic potential [180]. Similarly, a 3D hierarchical hybrid electrocatalyst has been fabricated by embedding the Co_9S_8 nanosheets into vertically aligned Ni_3S_2 nanosheets and evaluating its electrochemical performance for overall water splitting. The heterointerface in a 3D hierarchical architecture obtained high specific surface area, efficient diffusion channels, and strong interlinkage with the underlying support, sustainably catalyzing the OER and HER at low input voltage. Furthermore, the theoretical investigations unveiled that 3D structures facilitate the interface reconstruction during the intermediate adsorption and gas desorption process and retain the structural features of the active sites due to strong coupling interconnection. These strong interfacial interactions sustained the electrochemical conversion process under intermittent solar input energy and presented commercial interest [181].

The 3D porous conductive substrate is highly beneficial to enhancing the water splitting kinetics, offers high energy active center for the nucleation and growth of nanostructure, minimize the probability of support passivation and non-conducting layer formation in alkaline condition at high anodic potential, and contributes to the overall durability of electrode material. Co-Ni-P nanostructure encapsulated in 3D N enriched holey carbon fabricated over Ni foam revealed excellent catalytic activity and durability [182]. The robustness and superior electrochemical performance were attributed to the following features of the catalyst: (1) Bi-metallic phosphide nanostructure increases the DOS near the Fermi level, enhances the metallic character of transition metal active sites that facilitates the electronic conduction across the interface, optimized the chemisorption energy of active sites, preferably adsorb the reaction intermediates offering low thermodynamic barrier for O-O and H-H coupling and suppress the non-conducting oxide layer formation on the surface. (2) The heteroatom doping, i.e., N, regulates the coordination number of active sites, introduces the surface defects, and provides steric hindrance to the active sites in the lattice that alleviate the agglomeration phenomena during the pyrolysis and electrochemical process [183]. (3) The nanoporous N-doped carbon structure facilitates the active center exposure, electrolyte penetration, intermediate adsorption, and additional adsorption sites for O-O coupling and overcoming the mass transfer limitation. The in situ formed carbon shell around the metal active sites enhanced the corrosion resistance of hybrid material and saved the active sites from stress or pitting corrosion during water electrolysis.

Lee group employed a simple hydrothermal strategy followed by controlled selenization for the rational development of Ni foam supported 3D hierarchical oxygenated nickel tungsten selenide [184]. The designed catalyst demonstrated a nanoporous network with large active centers enriched with oxygenated intermediates and operated at low cell voltage to deliver a higher current density in the water electrolysis process. The 3D hierarchical structure with homogenous mesopores across the network improved the water diffusion, stabilized the intermediates, and triggered the gas desorption from the active center to vacate the operational phases for incoming cyclic reaction. The surface structure of the catalyst stabilized the Se in a metallic lattice, and the Se-O bond enhanced the metallic content in the hybrid material and reduced the charge transfer resistance at the electrode-electrolyte interface. The free-standing characteristic of the hybrid material elevates the polymeric binder need, enhances the exposure of active sites, decreases the metal leaching probability at higher current density, and enhances the ASF. The 3D hierarchical structure facilitates the chemical transformation of the reactive component to the most active phase because of maximum effective contact at the electrode-electrolyte interface that enhances the self-healing property of active center extended in a 3D manner and this active phase construction around the pre-catalyst decreases the chance of metal leaching at a high anodic or cathodic potential. 3D hierarchical nanostructure composed from Co-Ni carbonate hydroxides and copper nitride on copper foam accelerates the dual phase transformation during water electrolysis, offers a hydrophilic surface for electrolyte penetration, large electrochemically active surface area for intermediate adsorption and resistance-free channels for electron conduction at interface collectively enhanced the reaction kinetics and durability of an electrocatalyst (Fig. 10 A-J) [185]. Based on experimental results, authors have reported that a 3D hierarchical structure with heterointerface stabilized the highly entropic nano sites, suppressed the accumulation, and maintained the structural features of the catalyst in an electrochemical reaction. The 3D open architecture is beneficial for mass migration without developing a nonconductive layer and suppressing the blockage of the active center due to bubbles accumulation. The 3D surface structure accelerates the formation of the passive layer, i.e., CuO and CoOOH, via dual phase transformation, decreases the metal leaching rate, and sustains the electrochemical process for a long time.

2D planner current collectors not only have limited active centers due to improper contact of electrolyte with the electrode but also impede the gas desorption, causing non-negligible extra potential, especially at a high geometric activity where immense gas molecules are produced. However, a 3D substrate with a micro or mesoporous framework exhibits high specific surface area, electrical conduction, and excellent structural, chemical, and mechanical durability [186]. Yu et al., $Ni(OH)_2/Fe_2O_3$ heterointerface via a scalable route where the 3D hierarchical structure demonstrated outstanding operation stability and sustained the high current density for more than 1500 h without noticeable degradation (Fig. 11A-F) [187]. Based on theoretical and experimental investigations, authors have attributed the sustainable behavior of catalyst to the following merits: (1) The direct growth of active centers on the current collector without using any conducting agent or polymeric binder promotes the electrolyte diffusion and mass migration at the solid-liquid interface and ensure the higher conduction of electrons. (2) The tight interlinkage of 3D structure with a wide distribution of pores in the micro and mesopore range ensures the hydrophilic and aerophobic surface, which is conducive for electrolyte infiltration, and gas removal enhances the corrosion resistance of the active component. (3) The strong interfacial coupling between the different components of hybrid material triggers the water molecule destabilization, increasing the OER sluggish kinetics and durability of the catalyst. The 3D hierarchy stabilized the active sites, prevented them from aggregation, and maintained the catalytic performance in cyclic operations.

7. Aerophobic electrode

In electrocatalysis, overcoming long-term catalyst degradation and maintaining high activity is a significant issue. Non-noble alkali or rare-earth element components' dissolving in harsh electrolytes has been identified as the primary degradative process of mixed oxides. Although gas bubbles have long been thought to be capable of mechanically harming the materials they surround, little attention has been paid to the role that developed bubbles play in the degradation of electrocatalytic

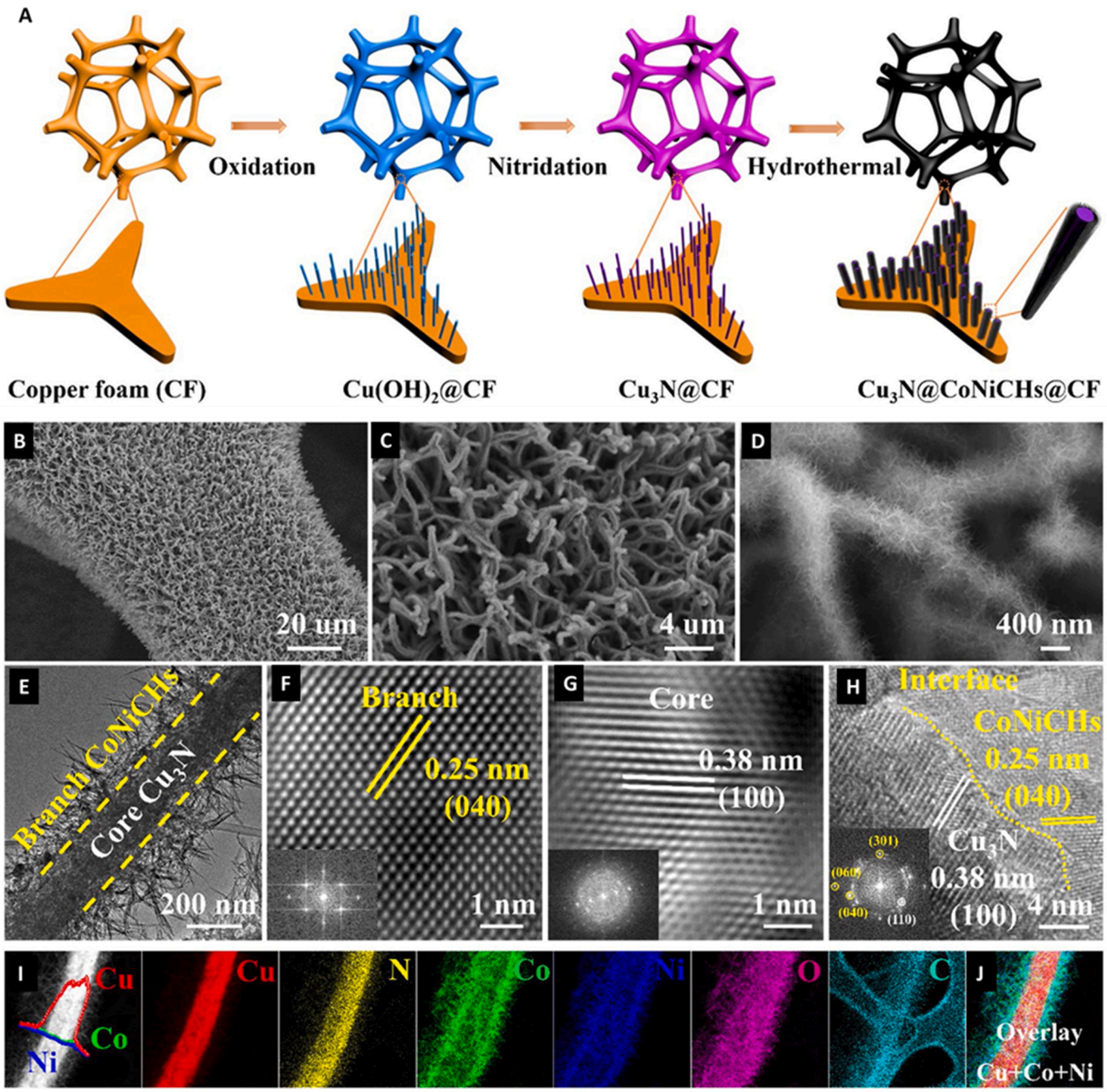

Fig. 10. (A) Systematic illustration for the development of 3D hierarchical Cu_3N @ CoNiCHs@CF. Physical characterization of 3D hierarchical Cu_3N @ CoNiCHs@CF (B-D) SEM images at different magnifications. (E) TEM image. (F-H) HRTEM images and inserted SAED patterns (I) STEM image of Cu_3N @ CoNiCHs and its elemental mapping images. (J) Elemental mapping of Cu, Co, Ni elements.
Reproduced with permission from ref [185]. Copyright 2021, Elsevier.

materials [188]. The gas bubbles generated during electrocatalysis substantially impact the reaction kinetics, intrinsic reactivity, and sustainability of electrode materials. At a gas-evolving electrode, a bubble typically goes through four stages in its life cycle: nucleation, growth, coalescence, and detachment [189]. Nucleation is the stochastic formation of a cluster of gas molecules from a solution supersaturated with dissolved gas [190]. Following nucleation, the bubble keeps expanding by absorbing additional dissolved gas molecules. The buoyant force acting on the bubble grows as it develops [191]. Finally, the bubble is elevated and eventually separates from the electrode surface when the buoyant force is powerful enough to overcome the adhesion force keeping it there [192]. Two bubbles coming into contact, whether on the electrode or in the solution, causes coalescence, which lowers the total surface energy. As the nucleation starts, it alters the dissolved gas bubble's concentration and disturbs the equilibrium at the solid-liquid boundary [193]. These gas bubbles accumulate on the electrode surface, block the active component, impede the proper contact of electrolyte with the underlying support and trigger the support passivation [194]. During the growth, coalesce, and desorption processes from the active sites, it changes the mass transfer rate of the reactant and product. It also imparted ohmic resistance in the electrolyte after desorption from the active sites and altered the solution path via the electrolyte [29].

Cao group has developed porous Ni/Ni-Fe-Mo-O_x nanoplates grown over Ni foam, revealing highly sustainable water-splitting performance (Fig. 12A-O) [195]. Based on experimental results, authors attributed the catalyst efficiency to the following factors; (1) The oxygen vacancies

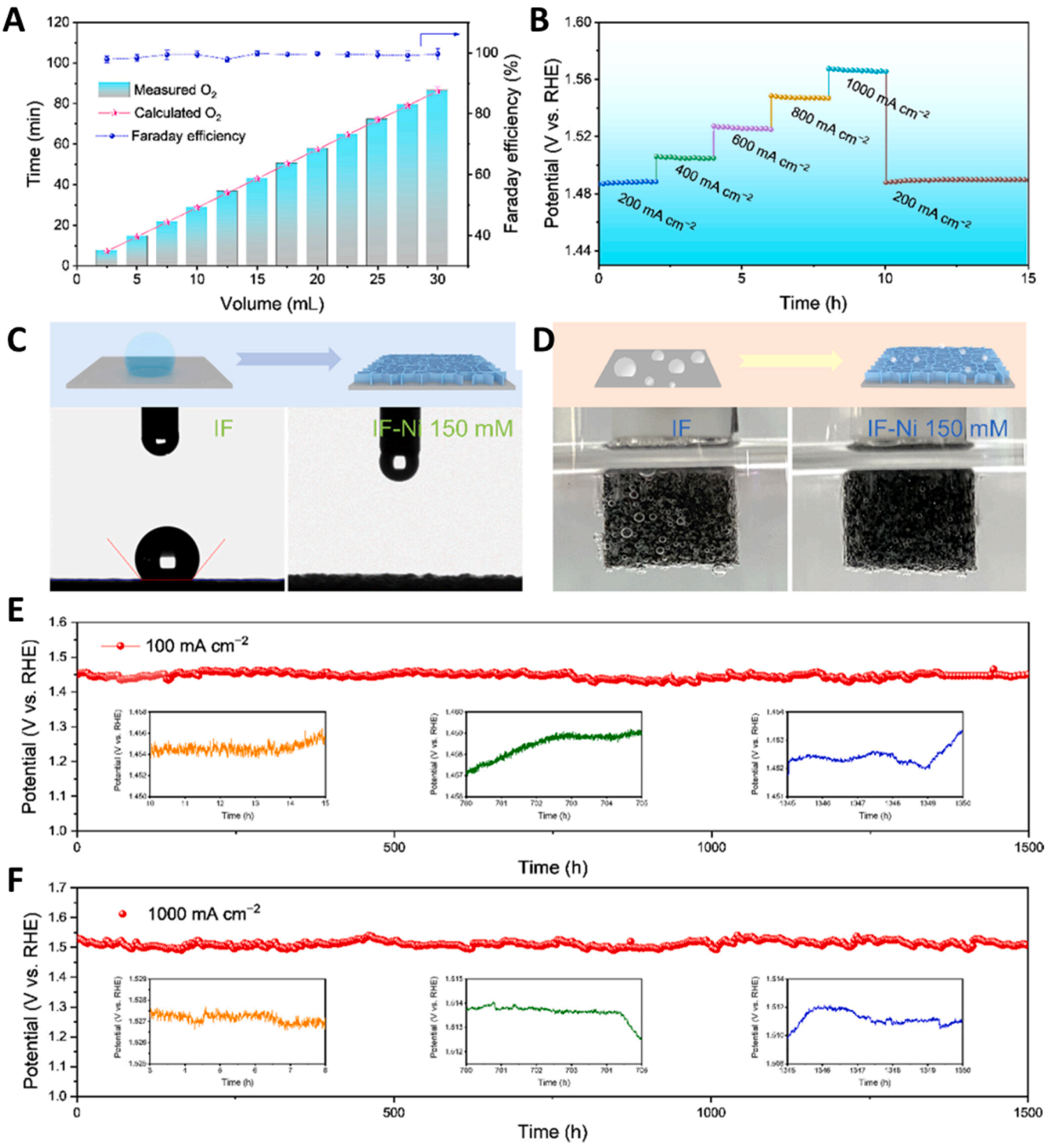

Fig. 11. Electrochemical evaluation of $Ni(OH)_2/Fe_2O_3$/IF(a) Faraday efficiency (b) Stability test at different geometric activity for up to 15 h. The schematic illustration and digital images of (c) wettability. (d) oxygen bubbles in contact with the surfaces of $Ni(OH)_2/Fe_2O_3$/IF and IF. (e, f) Stability of the of $Ni(OH)_2$/Fe2O3/ at 100 and 1 A cm^{-2}.
Reproduced with permission from ref [187]. Copyright 2022, American Chemical Society.

in amorphous Ni/Ni-Fe-MoO_x^- modulated the d band center position relative to fermi level, optimized the chemisorption energy of active component and stabilized the OER intermediates at low input potential, (2) The conductive substrate provides the efficient charge transfer pathway and suppress the non-conductive layer formation, (3) the hydrophilic and aerophobic porous surface structure offers the short diffusion channels and accelerate the mass transfer kinetics, (4) porous free-standing electrode with aerophobic characteristics enhanced the mechanical durability of catalyst and prevented the active sites leaching from the substrate at high current density. The hydrophilic and aerophobic features are needed in an efficient catalyst to facilitate water adsorption and gas desorption to increase the reaction kinetics and catalyst durability. Recently, FeCoNiP@C catalyst supported over metallic Ni has been explored for water splitting. The catalyst revealed

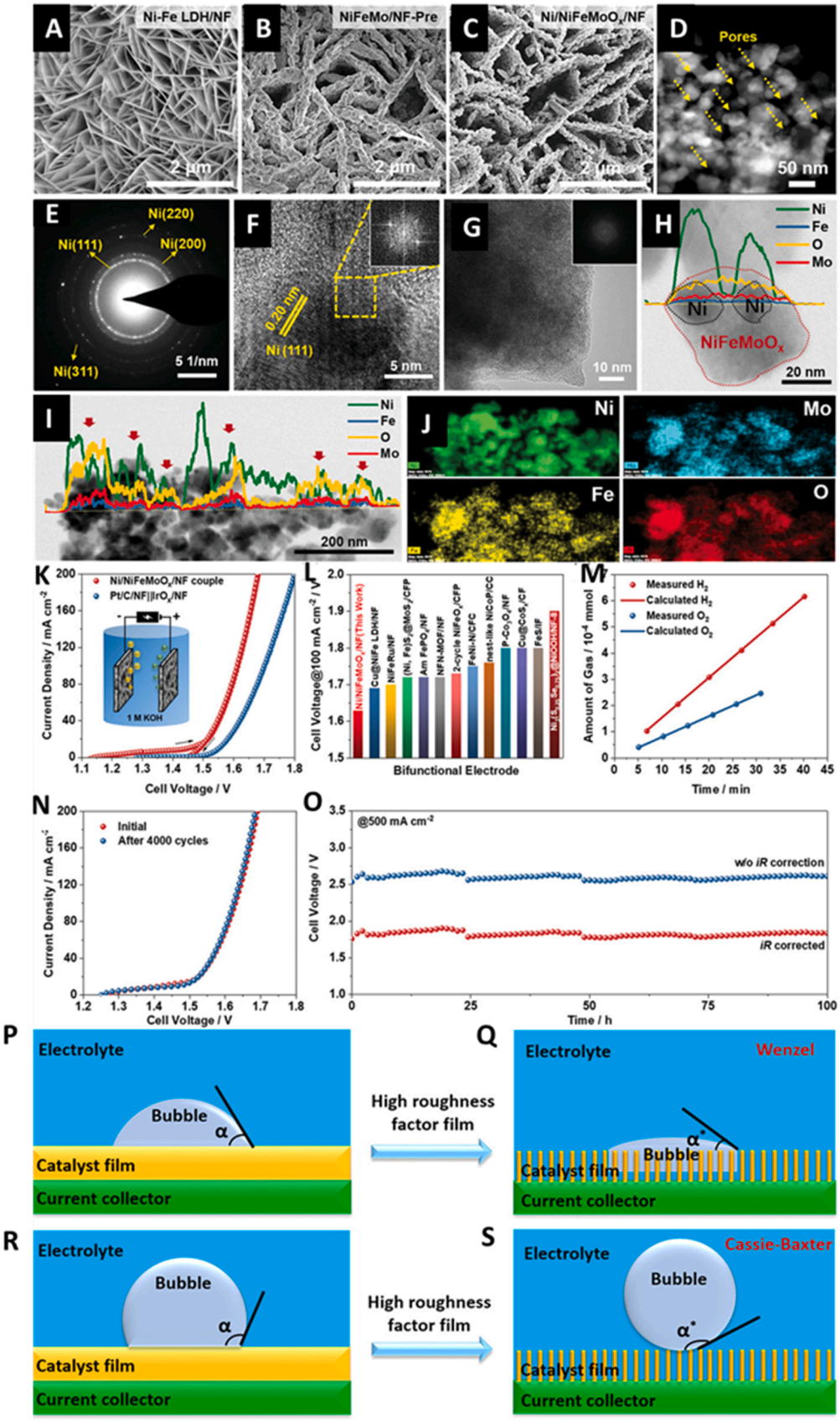

Fig. 12. SEM images of (A) Ni–Fe LDH/NF, (B) NiFeMo/NF-Pre, and (C) Ni/NiFeMoO$_x$/NF. (D) HAADF-STEM image and (E) Electron diffraction pattern of Ni/NiFeMoO$_x$/NF. HRTEM images of (F) Ni nanoparticle (G) NiFeMoO$_x$. (H–J) Elemental distribution of Ni/NiFeMoO$_x$/NF. The inset in panels (F) and (G) display the fast Fourier transform (FFT) pattern of the corresponding image. Red arrows in panel (I) show locations of NiFeMoO$_x$ particles (K) Polarization curves (iR-corrected) of Pt/C||IrO$_x$ electrolyzer and Ni/NiFeMoO$_x$/NF and in 1 M KOH. (L) Cell voltage comparison of Ni/NiFeMoO$_x$/NF with other electrodes: NiFeRu LDH/NF, Cu@NiFe LDH/NF, Am FePO$_4$/NF, (Ni, Fe)S$_2$ @MoS$_2$/CFP, NFN-MOF/NF, FeNi-N/CFC, two-cycle NiFeO$_x$/CFP, nest-like NiCoP/CC, P-Co$_3$O$_4$/NF, FeS/IF, Ni$_3$(S$_{0.25}$Se$_{0.75}$)$_2$ @NiOOH/NF-8 and CF-Cu@CoS$_x$/CF (M) O$_2$/H$_2$ collected amount comparison for Ni/NiFeMoO$_x$/NF. (N) Polarization curves of Ni/NiFeMoO$_x$/NF electrolyzer before and after 4000 potential cycles between 1.2 and 1.887 V (iR uncorrected). (O) Chronopotentiometry of Ni/NiFeMoO$_x$/NF electrode at 500 mA cm^{-2}. Schematic presentation of bubble contact angle dependence on surface roughness at given intrinsic aerophilicity: (P) flat aerophilic surface, (Q) rough aerophilic surface, (R) flat aerophobic surface (S) rough aerophobic surface.

(a) Reproduced with permission from ref [195]. (b) Reproduced with permission from ref [198]. Copyright 2018, American Chemical Society. (0) Copyright 2019, Wiley VCH.

high intrinsic activity and durability for water oxidation [196]. The superior performance of the catalyst has been assigned to the following merits: (1) The conductive Ni foam current collector and metal phosphide-based active components evade the mass transport limitation due to strong conductive adhesion. The nanoarray morphology accelerates the nucleation and coalescence of bubbles formation and, subsequently, its desorption from the active sites to vacate the sites for cyclic reaction. (2) The high specific surface area of microscale amorphous structure with optimum adsorption energy increases the reactivity of active sites. (3) The N-doped carbon matrix stabilizes the active sites via strong σ and π bonding, improves the catalyst's mechanical robustness, and avoids leaching in a harsh electrolyte. (4) The thin oxyhydroxide layer on the catalyst's surface triggers the OH^- attack and initiates the water dissociation with low input energy. (5) The hydrophilic-aerophobic surface triggers water adsorption and gas desorption, prevents support passivation, and enhances the structural and chemical durability of the anode during water oxidation. The wetting capacity of the electrolyte and the speed with which bubbles form on the electrode surface are released during the water-splitting process have a substantial impact on the activity of the catalysts [197]. A "dead zone" will form on the electrode surface if there is a strong bond between the electrode and the bubbles, preventing the diffusion of the electrolyte and lowering the exposure of the active sites (Fig. 12P-S) [198]. Therefore, by altering the electrode's wettability to make it super hydrophilic, which can enhance electrode wettability, and super aerophobic, which can accelerate bubble release, the efficiency, and stability of water splitting can be effectively increased. In addition, recent research has demonstrated that building micro-nano structures on flat substrates or hydrophobic coating materials can influence the wettability of electrodes, affecting the dynamics of bubbles such as heterogeneous nucleation, bubble growth, bubble layer thickness, and bubble departure size [199–202]. It was discovered by Wang et al. that the water-splitting performance on porous electrodes is susceptible to wettability because the larger bubble dimensions reduce the reaction area of the porous electrode [198]. In addition to the high roughness factor to exposed selective active components for electrochemical reactions and surface wettability to increase the effective contact portion between electrode and electrolyte are the efficient tactics to improve the durability of catalysts, a suitable wettability modifier is crucial. Yao et al. revealed that hydroxylated multiwalled carbon nanotubes (CNTs) have high electrical conductivity, thermal stability, specific surface area, and flexible surface wettability [188]. They have developed a Co_9S_8--Ni_3S_2 heterojunction anchored on CNTs grown on Ni foam through a hydrothermal process and evaluated its electrochemical performance for water splitting. This multistage arrangement can reveal more of the electrode's active regions, improving the efficiency of intermediate adsorption and gas desorption. Additionally, the electrode's architecture gave it super hydrophilic and super aerophobic qualities that sped up the transfer of electrolytes that had been adsorbed on the surface and significantly reduced the adhesion of evolving gas bubbles to the electrode surface, enhancing the electrode's durability.

A recent investigation revealed that metal dissolution and surface corrosion of transition metals are unavoidable under normal anodic conditions. The chloride ions in electrolytes trigger metal corrosion, especially in a humid environment, where O_2 from air or water initiates the metal hydroxide formation. The maximum exposure of active components is crucial in accumulating the side reaction and catalyzing the water oxidation at low input potential. The super hydrophilic and aerophobic characteristics accelerate the O_2 desorption from the active component, increase the intimate contact between electrode and electrolyte, and suppress the metal leaching. It has been found that surface structure manifestation to control the hydrophilicity and aerophobicity to achieve the favorable wettability and bubble release rate at the electrode surface enhanced the reaction kinetics, O-O coupling rate and operational durability of the catalyst [189]. The gas bubbles pined or aggregated on the electrode surface, specifically at a high current density where immense gases are produced, block the diffusion channels, suppress the exposed active sites, and increase the internal resistance of the catalyst. Shao and coworkers investigated the influence of nano architecture morphology for electrolyte diffusion and bubbles detachment by considering the Ni-Fe oxyhydroxide nanosheets with flower-like clusters grown over NF [203]. The author revealed that the morphology substantially impacts the hydrophilicity and aerophobicity of active sites and controls the reaction kinetics. In addition, the catalyst demonstrated high Faradic efficiency and long-term durability due to its fast bubble detachment ability that diminishes the structure aggregation and metal leaching from the current collector.

The bubble accumulation around the active sites causes the severe bubble shielding effect, which will block the exposed areas, hinder the electrolyte transport to the underlying support, decreases the desorption kinetics of produced gases, increase the internal resistance of the catalyst and high activation barrier is needed for O-O coupling. Therefore, rational design of electrode architecture to assist the electrolyte diffusion decreases the adhesion forces of gases with surface and reduces the internal resistance (within pores) of catalyst are needed to ensure the practical viability of anode materials. Jiang's and Sun's group investigated that super hydrophilicity and aerophobicity could be achieved by regulating the catalyst's micro/nanostructure and surface composition [204–206]. Sun group synthesized CoS_x-Ni_3S_2 nanosheet array via hydrothermal process, where nanosheet structure provides the aerophobic, hydrophilic surface assisted the electrolyte penetration and provides short diffusion channels for gases desorption (Fig. 13A-L) [207]. The authors monitored the contact angle of 0°, 113.2° and 131.5° for nickel foam (NF), Ni_3S_2/NF, and CoS_x-Ni_3S_2/NF, respectively, demonstrating that hetro nanostructure facilitates the electrolyte penetration and sustained high mechanical and structural durability during OER (Fig. 13M-S). In addition, Li et al. reported a top-down method to fabricate the oxide/sulfide heterostructure (N-$NiMoO_4$/NiS_2) to catalyze the OER efficiently [208]. The nanowire/nanosheets have an abundant epitaxial heterogenous interface with super hydrophilic and aerophobic characteristics promoting the charge and transfer rate and increasing active sites' intrinsic reactivity and durability. The characterization results unveiled that the electronic cloud migrated from N-$NiMoO_4$ to NiS_2 via the epitaxial heterogeneous diffusion route and enhanced the support resistance against passivation in strongly alkaline conditions. Furthermore, the free-standing 3D aerophobic electrode decorated with 2D nanosheets possessed high specificity and ECSA, increased the material's corrosion resistance, and suppressed the metal leaching at a high anodic potential. Piao and coworkers modulated catalyst wettability and interfacial engineering by designing the Sn_4P_3/Co_2P stalk"-"cap"-typed nanoarrays supported over Ni foam with super hydrophilicity and aerophobicity and demonstrated the following merits concurrently [209]. (1) The heterojunction optimizes the d-band position relative to the Fermi level and increases the charge transfer rate at the electrode-electrolyte interface. (2) The nano-arrayed structure ensured the maximum exposure of active sites with high structural and mechanical durability. (3) The grafted cap on the top of the nanostructure enhanced the hydrophilicity and aerophobicity of active components, preventing the bubble accumulations and sustaining the high current density without noticeable degradation. Based on contact angle measurement, authors concluded that rough caps implantation increases the hydrophilicity of the electrode surface (Fig. 14A). Furthermore, the optimal capturing indicated that gas bubbles with large diameter block the active sites, impose resistance for mass diffusion, and increase the overpotential for specific current densities. The heterostructure decreased the bubble diameter, and adhesion forces between active and gas bubbles enabled the catalyst to sustain the high geometric activity (Fig. 14B-I). It has been found that porous frameworks in carbon-based material coated with active components have unique features of aerophobicity and hydrophilicity, impart ohmic resistance-free path for electron migration, facilitate the gases desorption rate and lessen the dead area of the electrode surface. Gosh, the group synthesized the

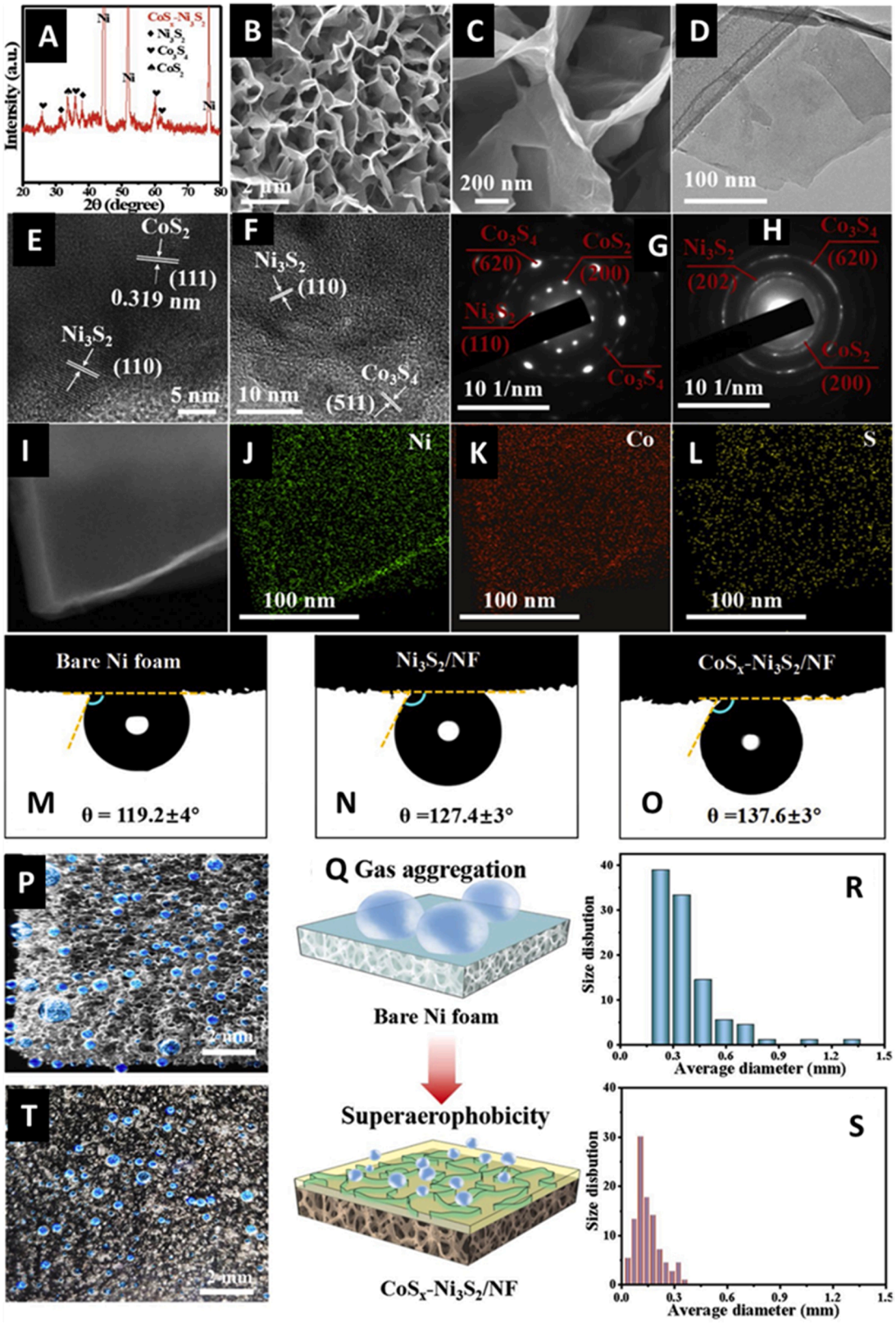

Fig. 13. Morphology and Chemical composition of the CoS_x-Ni_3S_2 catalyst. (A) XRD pattern. (B,C) SEM images. (D,E,F) High and low-magnification TEM images of a CoS_x-Ni_3S_2 nanosheet. (G,H) Selected area electron diffraction (SAED) spectra of CoS_x-Ni_3S_2. (I-L) EDS element mapping images for Ni, Co and S. (M, N,O) Bubble contact angles under water (P,T) Optical photographs for the bubble evolution process of various electrodes at specified current density (Q) Pictorial presentation of bubble evolution process on CoS_x-Ni_3S_2/NF and NF (R,S) Bubble diameter statistics of CoS_x-Ni_3S_2/NF and bare NF composites.
Reproduced with permission from ref [207]. Copyright 2020, Elsevier.

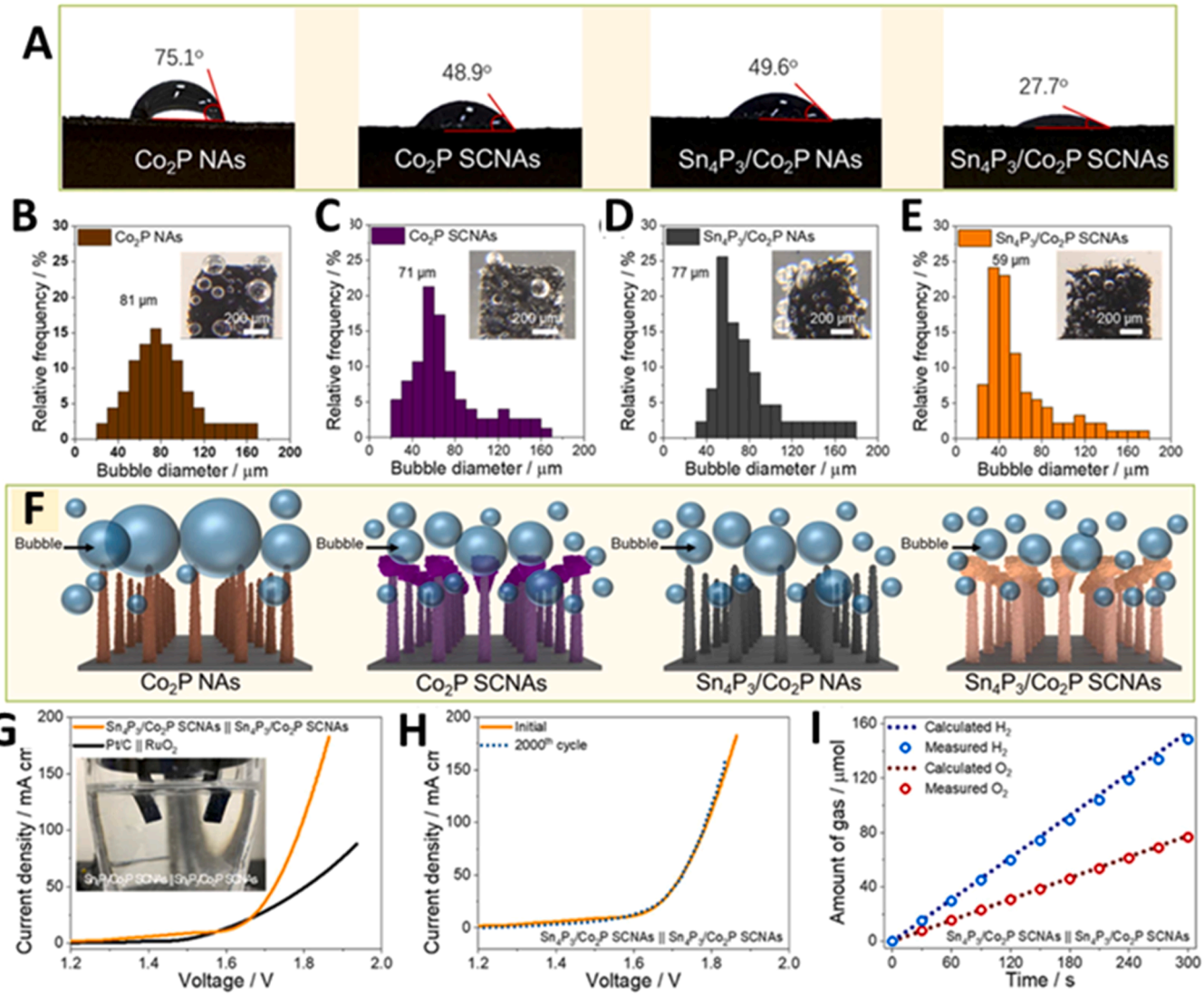

Fig. 14. (A) Analysis of contact angle Co_2P NAs, Sn_4P_3/Co_2P SCNAs, Sn_4P_3/Co_2P NAs, and Co_2P SCNAs the generation of a gas bubble with an average diameter on (B) Co_2P NAs, (C) Co_2P SCNAs, (D) Sn_4P_3/Co_2P NAs, and (E) Sn_4P_3/Co_2P SCNAs, and (F) Schematic presentation of bubble size release from various catalysts. Overall water splitting performance of Sn_4P_3/Co_2P SCNAs-built two-electrode cell. (G) LSV curves of Sn_4P_3/Co_2P SCNAs-built cell and Pt/C||RuO_2-based cell, inset: the digital photo of Sn_4P_3/Co_2P SCNAs-built cell, (H) LSV polarization curves of the Sn_4P_3/Co_2P SCNAs-built cell before and after 2000 cycles, (I) Theoretical and experimental amounts of O_2 and H_2 during water electrolysis.
Reproduced with permission from ref [209]. Copyright 2021, Elsevier.

bimetallic heterostructure containing Ni_2P-Cu_2P active sites grown over NF graphene carbon nanotubes (Ni-Gr-CNTs) with super aerophobicity revealed high structural, chemical, mechanical durability and corrosion resistance [210]. The high sustainability of the electrode was attributed to the super hydrophilic and aerophobic architectures that boost the adhesion of the electrocatalyst towards the electrolyte and lessen the bonding towards the produced gases. The contact angle measurement demonstrated that bimetallic heterojunction decoration over Ni-Gr-CNTs drastically increases the hydrophilicity of active sites and decreases the bubble diameter. The authors concluded that introducing a porous carbon-based backbone offered short diffusion channels for mass migration that are highly needed for support durability. The CNTs and graphene over Ni foam provide the additional surface area to anchor the nanostructure on its surface and mitigate the probability of accumulation, one of the major causes of the catalyst activity deterioration. The 3-D structure of the electrode with flower-like morphology provides highly dense edges with optimum d band position, reduces the activation energy for OER, and increases the catalyst's corrosion resistance. The same group has reported leaf like $Sn4P_3$ nano architecture with hydrophilic features on a highly conducting collector of Ni–Gr–CNTs developed through thermal chemical vapor deposition followed by a solvothermal process [211]. The heterostructure revealed high catalytic performance for OER in terms of low input voltage, high TOF, Faradic efficiency, low charge transfer resistance, and long-term operational durability in an alkaline medium. The admirable activity and robustness of the catalyst were attributed to the following merits: (1) The Sn_4P_3 nano structure anchored on Ni–Gr–CNTs offered reactive sites with optimum chemisorption energy, decreased the required activation barrier and enhanced the chemical stability of active sites, (2) The 3D porous structure offered short diffusion channels for mass transportation and suppress the nanostructure aggregation, (3) The sharp edges and conducting support provides enough contact portion between electrode and electrolyte and decrease the probability of support passivation due to the growth of non-conducting oxide layer. (4) High number of DOS near to fermi level and higher atomic radii of Sn promote the electronic conduction, reduce the ohmic resistance at the electrode-electrolyte interface, within electrode pores, and active sites-current collector boundary, and increase the intrinsic reactivity of active sites.

Young equation and theoretical model are used to interpret the hydrophilicity/hydrophobicity and hydrophilicity/aerophobicity of materials as expressed in the following equations (Eq. 16 &17).

$$\Upsilon_{SV} = \Upsilon_{SL} + \Upsilon_{LV} Cos\theta \quad (16)$$

$$\Upsilon_{SL} = \Upsilon_{SV} + \Upsilon_{LV} Cos\alpha \quad (17)$$

Here γSV, γSL, γLV are the interface tension of solid-liquid, solid-gas, and liquid gas, respectively, while α and θ are the intrinsic contact angles of the materials. Based on these, Cassie and Wenzel investigate surface architecture's impact on achieving super hydrophilicity and aerophobicity. Furthermore, the investigation revealed that micro/nanostructured surfaces with suitable chemical composition are the key to controlling the proper wettability of active sites [212]. Shan et al. have prepared a hierarchical amorphous structure $CoMoS_x$ with super hydrophilicity-aerophobicity characteristics, showing great activity and durability for OER in an alkaline environment [197]. The catalyst revealed impressive durability for 100 h without noticeable degradation and was attributed to the proper wettability of the electrode surface, which accelerated the electrolyte penetration and bubbles detachment. The hierarchical surface with the tunable Co composition favored the discontinuous state of 3 phase bubble contact line that reduces the adhesion forces at the solid-gas boundary and increases the chemical, mechanical and structural robustness of active sites. The electrocatalyst wettability can be optimized by optimizing the morphological features, facets, engineering defects, and strains. The distortion of surface structure alters the electronic system, increases the electrochemically accessible surface area, and promotes fast electronic movement with abundant active sites [167]. The exposed defects at the interface boundary benefit the interaction and activation of intermediates in the interface, which is favorable for intermediates' optimum adsorption and desorption [213]. The flexible disorder structure provides enough space for the electrolyte for diffusion and increases the ASF. The flexible disorders in the regular system can be created by changing the atomic pattern and induced through many approaches, i.e., strain, vacancy, substitution, and surface roughness [214]. T ul Haq et al. have recently reported that amorphous S-substituted Cu_2O-CuO nanoneedles are directly grown on Cu substrate through an anodization approach. The S substitution creates the disorders that provide abundant active sites with high intrinsic activity, and its hydrophilic features ensure the fast bubble detachment from the active sites. In addition, the nanoneedles have firm contact with metallic Cu and reveal high durability and corrosion resistance even in aggressive seawater oxidation [215]. In another report, $Ni_xCo_{3-x}S_4$ decorated Ni_3S_2 nanosheet arrays supported on nickel foam were synthesized through a cation exchange reaction between Ni_3S_2 supported over Ni foam and Co^{2+} ions. It was noted that the catalyst retains its morphology and intrinsic activity after the long-term OER process with a slight positive shift in the B.E. The exposed $Ni_xCo_{3-x}S_4$ was oxidized to the corresponding oxide/hydroxide, but the underlying Ni_3S_2 nanosheet retains its chemical structure. The thin film of the corresponding oxide is electrically connected to the underlying Ni_3S_2 nanosheet and triggers the charge transfer at the interface. Although the exposed material is oxidized, the underlying conductive layer assists in the accessibility of active sites during water oxidation [216].

It is worth mentioning that organic ligand plays a vital role in altering the electronic state of metals and facilitating the desorption of gases and molecules. Recently, Wei Chen and his coworker investigated that a higher density of electronic cloud facilitates the desorption of oxygen molecules, which is promising for OER. However, they found that the complete removal of the organic ligand from the surface of Pd NCs deteriorates its performance for OER [217]. Similarly, Shaoqi Zhan et al. demonstrated that carboxylate ligands provide an intramolecular O_2 and facilitate the O-O bond formation and remote the electrochemically active center to facilitate the OH nucleophilic attack [218]. We also experimentally observed that the partial and complete removal of ligands from the surface of NCs showed different electrochemical behavior for OER. The partial removal of ligands enhances the OER performance, but the catalytic activity for OER drastically decreases after its complete removal. These observations demonstrate that the presence of an optimum electronic cloud favored the desorption of oxygen molecules, and surface ligands play a vital role in regulating electronic states.

8. Strong catalyst support interactions

The catalyst support interfacial interaction defines the surface free energy, unsaturation, steric environment, chemical structure, and dangling of active components, thus leading to a different external geometric effect (particles surface, dimensions, defects) and internal electronic system (coordination between active sites and underlying support, and charge transfer kinetics at the interface) [219]. Immobilizing nanostructures on support is crucial for improving their stability and managing their homogenous dispersion [220]. The underlying support stabilized the guest materials and provided additional active sites for the electrochemical process [221]. The catalyst support interactions, therefore, have a substantial impact on the nanostructure's reactivity, selectivity, and durability [169,222]. The interfacial metal support interactions can reshuffle the electronic distribution of both guest and host, and this effect is more paramount to a couple of atomic layers at the interface. The different outer band center positions of the catalyst and support altered the chemical environment of metals after coupling and characterized the position of antibonding states and the population of an electron in it [223]. The difference between the Fermi level of catalyst and support defines the direction and magnitude of charge transfer. The support reducibility, conductivity, morphology, the volume of defects, and exposed crystal planes are essential metrics to accelerate the charge transfer resistance and enhance the sustainability of active components [224].

Zhang group investigated the impact of different substrates, including conductive metal oxides (FTO, ITO), glassy carbon, and metal foils, i.e., Pd, Au, Cu, Ti, and Co on the electrochemical performance of Ni-Fe LDH for OER [225]. The experimental findings revealed that Ni-Fe LDH has considerably distinguished OER performance on the different substrates depending on the electronic structure of Ni active sites during redox reaction just before water oxidation. Compared to conventional inert conductive supports like FTO, ITO, and glassy carbon, the use of Co as non-noble metal support dramatically enhances the activity of Ni-Fe-LDH by a factor of 10 (Fig. 15A,B). In-depth investigation using XPS, AFM, and TEM analysis showed that Co was added to Ni-Fe-LDH during OER, creating a porous Ni-Fe-Co-OxHy layer. The more significant oxidative and OER catalytically active Ni (Fe) atoms with shorter Ni (Fe)-O bond lengths and lower coordination numbers were only seen in the presence of the Co support, according to in situ XAS experiments, demonstrating a strong synergetic effect among Ni, Fe, and Co. The strong interfacial interaction between Ni-Fe guest and Co-host due to comparable orbital configuration modulates the chemisorption energy, provides additional Co active sites, and increases active sites' structural, chemical, and mechanical durability (Fig. 15C-I). Similarly, Greeley and coworkers reported that active site interaction with the underlying support is crucial to diminishing the metal leaching and structural transformation to the inactive phase [226]. In-situ characterization tools and DFT modeling have been utilized to interrogate the origin of the stability of transition metal-based ultrathin hydroxide films. The geometric structure and valance state of metals are stabilized by tuning the elemental nature of the substrate. The findings demonstrated that the magnitude of sustainability of active components has a linear relationship with the adhesion energy between the catalyst and support. The active sites' adhesion with the current collector not only increases the durability, but provides additional edges and facets to remarkably reduce the activation barrier for O-O coupling. In his report, Jaramillo

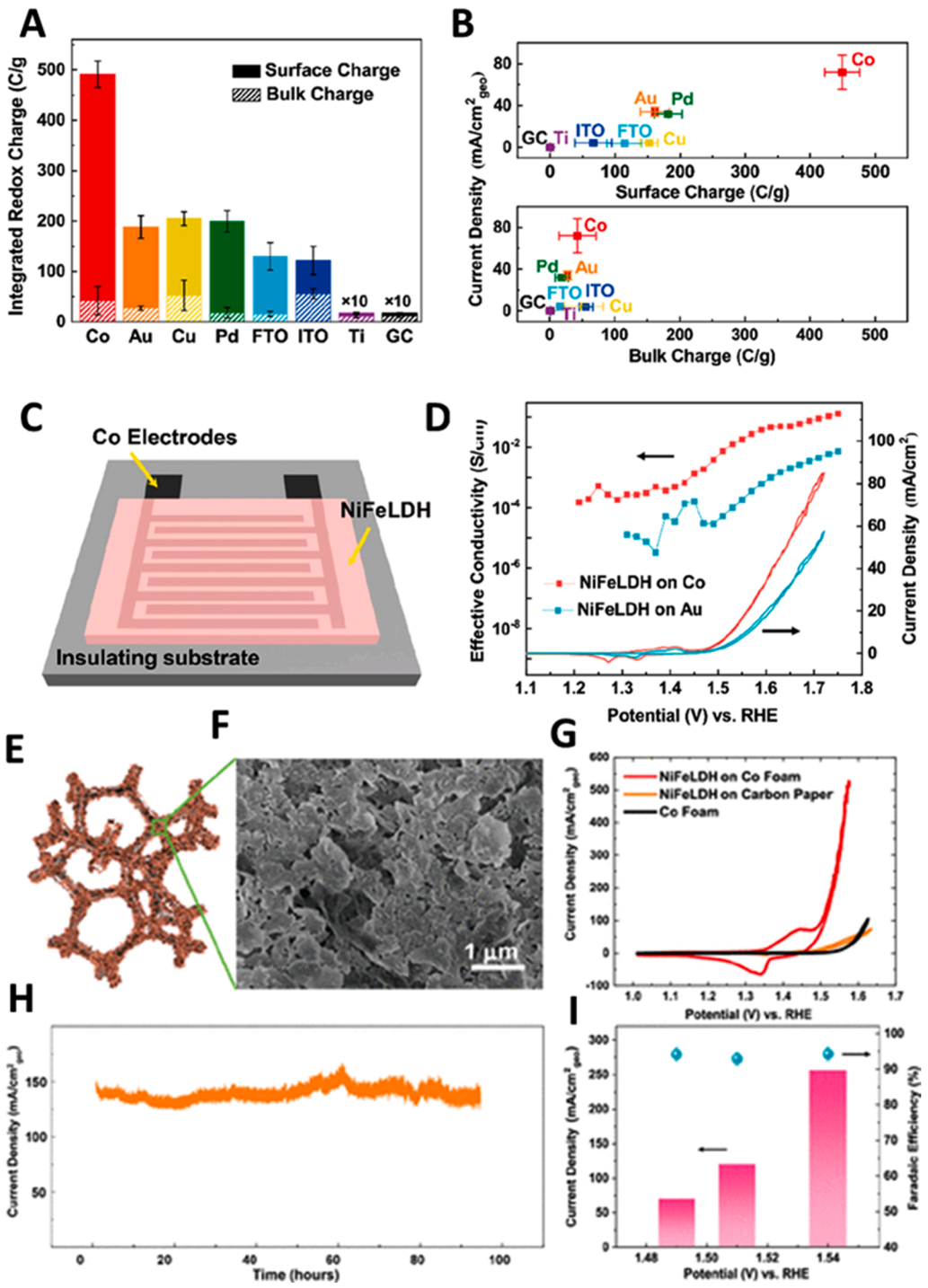

Fig. 15. Sustainable redo chemistry of Ni^{2+}/Ni^{3+} with high catalytic activity. (A) Faradic current from the integrated oxidation peak of NiFeLDH on various supports, spectacles the charge distribution in the bulk (hatched) and on the surface (solid) of the catalyst, respectively. (B) j correlation of NiFeLDH at $\eta = 350$ mV and the integrated surface (top panel) and bulk (bottom panel) charge of the forward redox wave on different supports in 1 M KOH electrolytes. (C) pictorial diagram for the interdigital dual-working electro-catalyst coated electrode. (D) The conductivity of NiFeLDH on an interdigitated array of Au (blue) and Co (red) electrodes as a function of applied potential in an O_2 saturated 1 M KOH. CV curves with a sweeping rate of 10 mV s^{-1} are overlaid. (E,F) Schematic illustration and SEM image of NiFeLDH/Co foam. (G) Anodic CV of NiFeLDH @Co foam, bare Co foam, and NiFeLDH@ carbon paper. (H) Constant potential electrolysis for NiFeLDH@Co foam at 1.52 V vs RHE. (I) j and Faradaic efficiency from GC measurement of evolved O_2 at different applied potentials.
Reproduced with permission from ref [225]. Copyright 2020, American Chemical Society.

and coworkers investigated the impact of two different flat substrates, i.e., glassy carbon (GC) and Au, on the intrinsic reactivity, geometric response, and sustainability of Ni-OOH, Ni-Ce-OOH, and Ni-Fe-OOH catalyst [227]. The experimental results revealed that Ni-based catalyst loaded over Au substrate attained higher intrinsic activity than GC in 1 M KOH electrolyte. The authors used different characterization tools, including ICP-OES, EIS, in-situ X-ray absorption spectroscopy, cross-sectional TEM, and Ni redox peak integration to inspect the origin of high activity and sustainability due to Au substrate. The catalyst with the same mass loading over Au substrate demonstrated 6-time higher efficiency compared to the GC, and this outstanding performance was attributed to the following unique features of Au substrate; (1) A high mass of catalyst electronically connected and physically adhered to the current collector, suppress the formation of nonconductive oxide layer formation and responsible for the mechanical durability of catalyst and support. (2) Au film has much higher electrical conductivity than GC, facilitates intermediate adsorption and desorption, and triggers the reaction kinetics at low overpotential. (3) The catalyst has strong interfacial interaction with the Au substrate due to the relativistic effect, offers conductive channels for charge transfer, and enhances the chemical and structural durability of Ni-based active sites. In our recent report, we have fabricated Gd-doped CoB amorphous nanosheets on Au-coated glass slide via electrodeposition [97]. The magnitude of applied potential and metal stoichiometry was used to control the

nucleation and growth of the nanostructure, followed by treatment with $NaBH_4$ to create oxygen vacancies. The oxygen vacancies modulated the electronic structure of Co and ameliorated the catalytic process. As a result, the hybrid catalyst possessed faster reaction kinetics, high conductivity, high TOF, small charge transfer resistance, and long-term operational durability at high current density. We have attributed this outstanding intrinsic activity and sustainability from the electrochemical results to the firm intimate contact between Gd-CoB active sites and Au underlying support. The microscopic and spectroscopic analysis demonstrated that Au film controls the nanostructure's homogeneous growth and modifies the nanosheets' electronic and surface structure. The SEM, XPS, and ICP-OES studies were carried out after long-term durability experiments in alkaline electrolytes, suggesting structural, chemical, and mechanical durability. The strong interfacial interaction of the gold-based current collector with the active sites enhanced the performance of thin film catalysts due to the electronic structure modification of active sites. To investigate the impact of the Au substrate, we have cathodically deposited the same material on Ti and Cu foil in identical conditions. However, the material's morphology and nature were reproducible but very smooth in the case of Au substrate with a high roughness factor. From the electrochemical experiments, the high onset potential and high resistance (charge transfer resistance) while using Ti and Cu foil validate the promising role of Au substrate. Being an excellent current collector, Au could consequently tune the inherent properties of overall hybrid material and enhance the sustainability of active component.

Conventional nanomaterials need polymeric binders to be cast on the current collectors, which unavoidably block the active sites, impede the mass transfer, and increase the resistance for electronic conduction [228]. The hybridization of nanocarbon to increase the electrical conductivity of transition metal-based catalysts suffers from the etching and self-oxidation at high anodic potential, deteriorating the sustainability of active sites. The week's intimate contact between the substrate and active phase offers low mass loading with a limited number of active sites. The coated catalyst triggered nonconductive oxide layer formation at high positive potential and suffered from metal leaching and support passivation [71]. Recent findings demonstrated that the development of free-standing electrodes by directly growing the active sites on a current collector has unique merits compared to conventional powder materials; (1) The direct fabrication of active phase on a current collector without any conductive additive and polymeric binder simplifies the electrode assembling process and lessen the capital expense in the synthesis process [229]. (2) The strong adhesive forces due to metal-metal orbital compatibility in self-supported catalysts offer high mass loading with abundant exposed active sites [178]. (3) Free-standing electrodes have more practical viability and easily modulate the electronic and surface structure of the catalyst to increase the intrinsic activity, selectivity, and corrosion resistance [230]. It's also easy to realize the proper wettability with super hydrophilic and aerophobic features in a self-supported catalyst to accelerate the charge, mass transfer, and bubbles detachment. The firm intimate contact ensured active sites' structural, chemical, and mechanical durability at a high current density where immense gases are produced [231].

Chen et al. have synthesized free-standing Ru-doped Ni-CoP flowers on 3D NF due to their high conductivity and interconnected open channels, facilitated electron, and mass migration, and accelerated the bubble's detachment [232]. The self-supported electrode revealed low charge transfer resistance due to strong interfacial interaction between active sites and 3D NF current collector and sustained the high geometric activity at low input voltage for a long time. The authors have credited the high intrinsic activity and durability to the following aspects: (1) Ru introduction modulates the electronic structure of metals, enhanced the DOS near to Fermi level, and conductivity of the catalyst facilitated the charger transfer reaction at the electrode-electrolyte interface (Fig. 16A-E). (2) The tight mechanical adhesion between the active phase and high surface area NF promoted the electrolyte penetration and gas desorption and ensured the catalyst's high structural and mechanical durability [233]. The direct growth of the active phase on the current collector without any binder offered maximum exposure of active sites and facilitated the redox reaction with high metal redox recyclability (Fig. 16F-I). The transition metals (Fe, Co, and Ni) efficiency and sustainability can be enhanced by modulating the electronic structure either via direct modification of the local chemical system or through the interfacial interaction between active sites and substrate [234,235]. Recent investigations revealed that the strong interfacial interaction enhanced the intrinsic activity by providing resistance-free diffusion channels and avoiding structural or mechanical damages at a high anodic potential. These characteristics suggested that the strong interfacial interaction is a practical way to enhance the activity and durability of active sites on a commercial scale [236,237]. It has been reported that the electronic structure of Fe-OOH could be favorably modified by creating a strong interfacial interaction with Ni-Fe LDH, and the inter adhesion forces have an inverse relation with the average particle size [89]. Ni-Fe LDH stabilized the ultra-small magnetic Fe-OOH NPs and showed high OER performance in an alkaline medium (Fig. 17A-S). The spectroscopic investigations, i.e., EXAFS, XANES, large amplitude Fourier Transformed A.C. voltammetry, and D. C. voltammetry, were performed to investigate the mechanistic pathway, and the results unveiled that Fe was present in its high valance state (Fe^{3+}) with a shorter bond (Fe^{3+}-O) and its interaction with the Ni substrate manipulated the local electronic structure increased the intrinsic activity of active sites and stabilized the OER intermediates. A durable and cost-effective OER electrocatalyst requires a rational design of substrate and active sites to create strong interfacial interactions. The morphology and chemical composition of both the active phase and current collector defines the adhesion energy. It has been found that TiO_2 growth in nanotubular form with high surface area and chemical alterations by introducing the nitrogen in TiO_2 lattice enhanced its interaction ability with the 3d or 4d metals. The ultralow doze of Ir NPs was anchored on titanium oxynitride (Ti-ON), which shows high catalytic activity and corrosion resistance during water oxidation [238]. The in-depth investigations demonstrated that the surface structure modification of the TiO_2 substrate and its passivation with the nitridation process enhanced the structural and electronic interaction with the Ir NPs, modified the Ir electronic structure, and enhanced the ASF. Charge transfer resistance is critical in defining the intrinsic activity and durability of catalysts for redox reactions. The direct growth of nanostructures on a conductive substrate with a high surface area is crucial to sustainably catalyze the reactions at low input voltage with a high reaction rate. Zhang's group developed a free-standing electrode by growing the $NiSe_2$ on NF, demonstrating high catalytic activity and robustness [239]. NF is highly conductive, and the direct growth of $NiSe_2$ nanostructure provides firm electric and structural contact between the active component and current collector offered exposed active sites with short diffusion channels. The EIS results demonstrated that the direct growth of nanostructure o substrate has low charge transfer resistance, destabilizes the water molecule, and favors the sustainable O-O coupling. The porous structure of the catalyst and substrate accelerated the electrolyte penetration and bubbles detachment and enhanced the ASF [240]. Wang et al. have developed free-standing Ni-V-LDH, Ni-V-Ir-LDH, and Ni-V-Ru-LDH direct on conductive NF and compared their electrochemical performance for water electrolysis [241]. The experimental results revealed that the synergistic electronic and atomic structure modulation by creating the intermetallic interaction of Ru and Ir with the Ni-V-LDH and current collector boost the catalytic performance (Fig. 18A-D). The Ru and Ir presence affected the sheet's size and decreased the charge transfer resistance. Raman and XRD analysis showed that the Ru or Ir introduction distorted the lattice structure of Ni-V-LDH, and the creation of V vacancies enhanced the electronic intermetallic interaction between the active phase and the current collector validated by EXAFS analysis. The strong interfacial interaction of disordered structures enhanced the TOF, exchanged

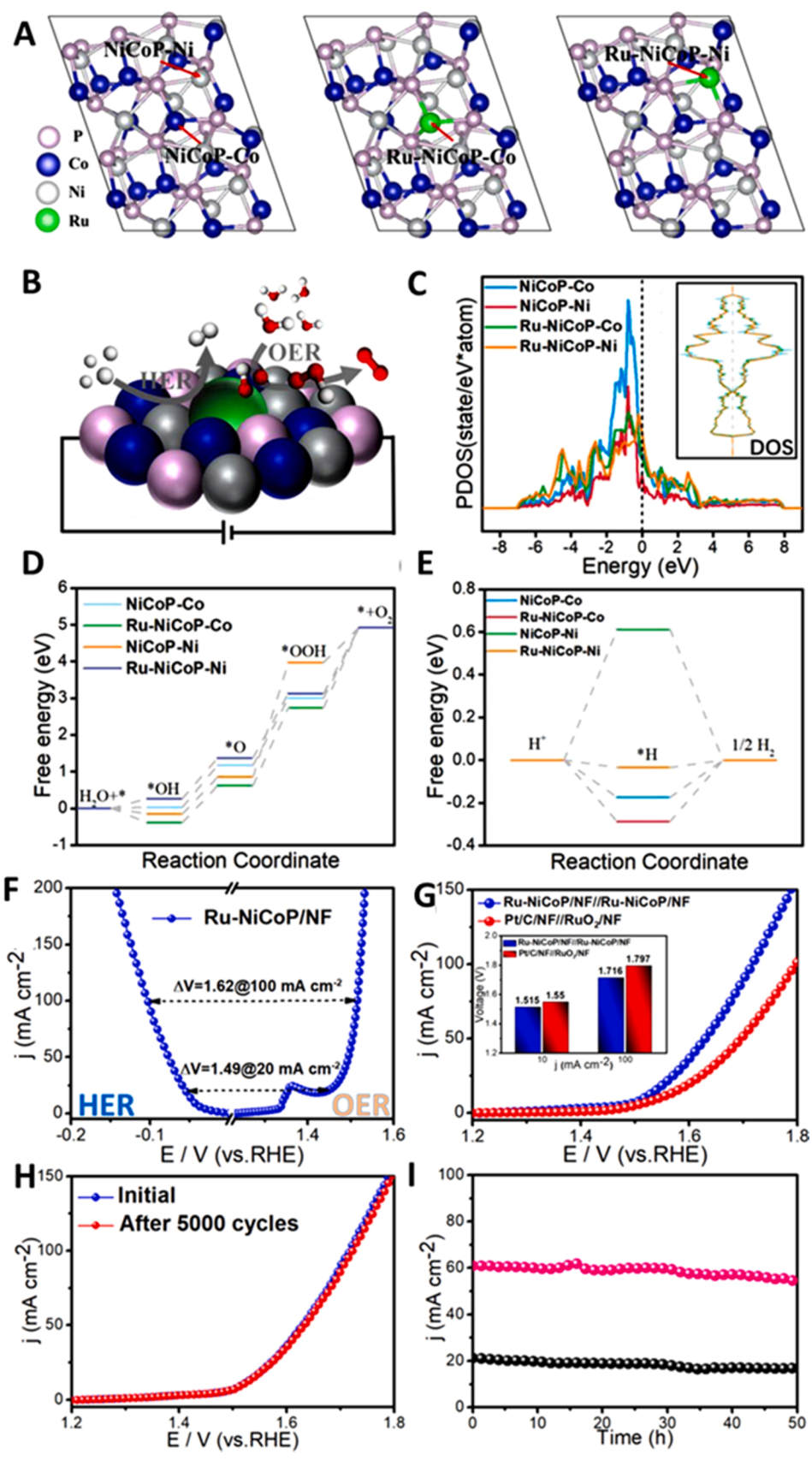

Fig. 16. (A) Ru-NiCoP and NiCoP top views after optimization, where substitution of Ni and Co atoms done by Ru atoms at Ru-NiCoP model (B) OER and HER mechanism on Ru single-site. Green, Grey, light pink and blue, and balls represent the Ru, P, Ni and Co atoms. (C) Calculated PDOS of special single-site on numerous catalysts, where Fermi energy level are shown by vertical dotted line and inset illustrates DOS of overall catalysts.(D) Free energy diagrams on single-sites of NiCoP and Ru-NiCoP for OER (E) and HER (F) Polarization curves of Ru-NiCoP/NF in for OER and HER in 1 M KOH (G) Polarization curves of Ru-NiCoP/NF= |Ru-NiCoP/NF and Pt/C/NF= |RuO_2/NF for overall water electrolysis; Inset consistent of voltages at j = 10 and 100 mA cm^{-2}. (H) Corresponding polarization curves before and after 5000 CV cycles of Ru-NiCoP/NF= |Ru-NiCoP/NF. (I) Time-dependent current density curves for Ru-NiCoP/NF= |Ru-NiCoP/NF for 50 h at constant potentials.
Reproduced with permission from ref [232]. Copyright 2020, Elsevier.

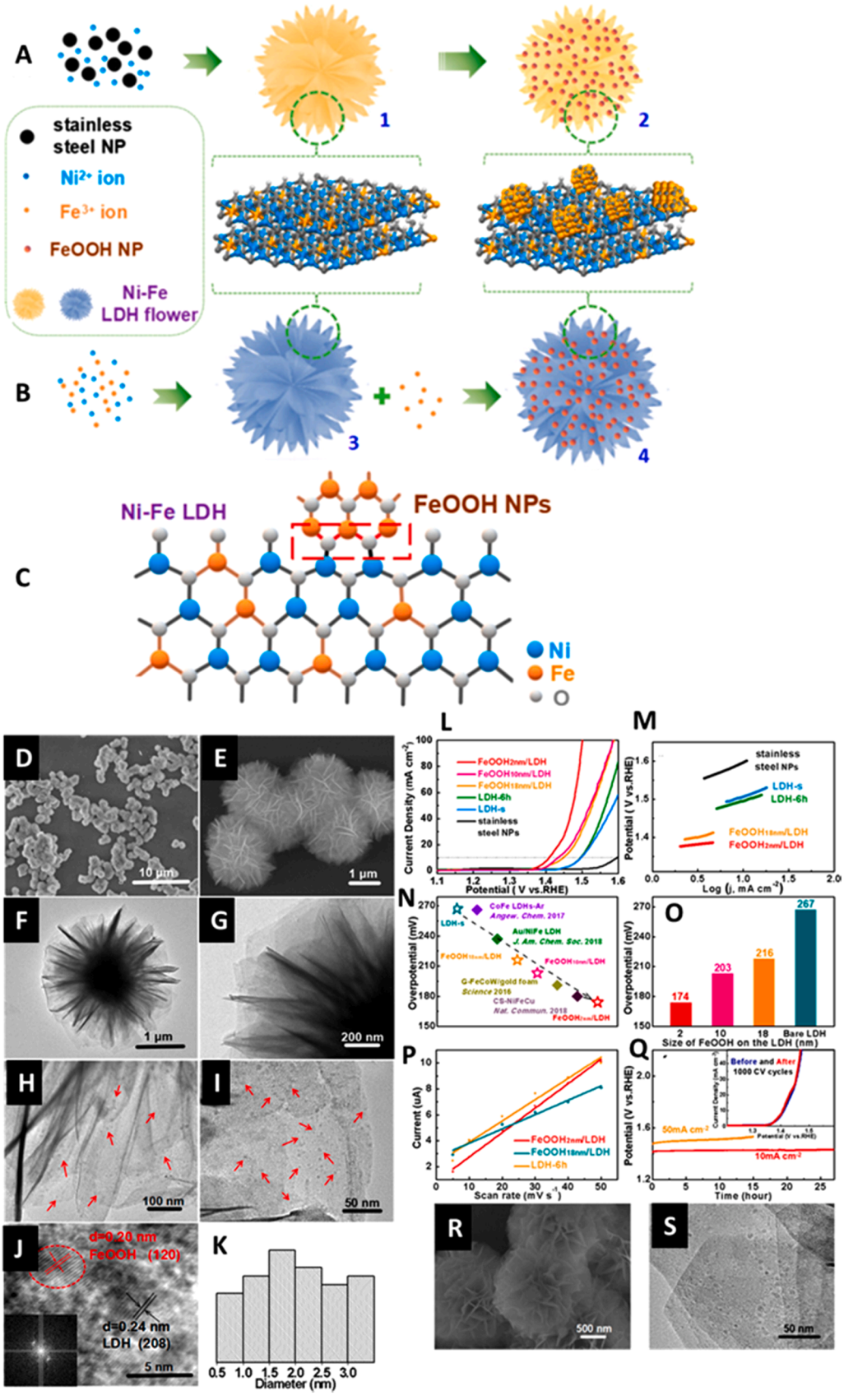

Fig. 17. (A) One-Pot Synthesis where (1) Early stage formation of Intermediate LDH Flower, where deposition of FeOOH NPs occur to form (2) the $FeOOH_{2\ nm}$/LDH Composite; (B) Stepwise Synthetic route where (3) the utilization of preformed LDH as a supported material for preferential FeOOH NPs deposition with numerous average sizes to form (4) FeOOH/LDH (C) Schematic illustration of Interfacial Interaction through oxygen bridges formation (e.g., $Fe^{(3+\delta)+}$–O–Ni^{2+}) (D,E) SEM, (F–I) TEM and (J) HRTEM images of the $FeOOH_{2\ nm}$/LDH, inset in (J) is the FFT pattern of a FeOOH NP. (K) Size distribution of FeOOH NPs (L) LSV curves and (M) Tafel plots (N) OER overpotential comparison at 10 mA cm^{-2} with reported transition metal-based catalysts. (O) Overpotentials comparison (P) Linear plots of cathodic charging currents Vs scan rate. (Q) Galvanostatic polarization curves of $FeOOH_{2\ nm}$/LDH, insert in (Q) is LSV curves of $FeOOH_{2\ nm}$/LDH before and after 1000 CV cycles. (R) SEM and (S) TEM images $FeOOH_{2\ nm}$/LDH after 1000 CV cycles.
Reproduced with permission from ref [89]. Copyright 2018, American Chemical Society.

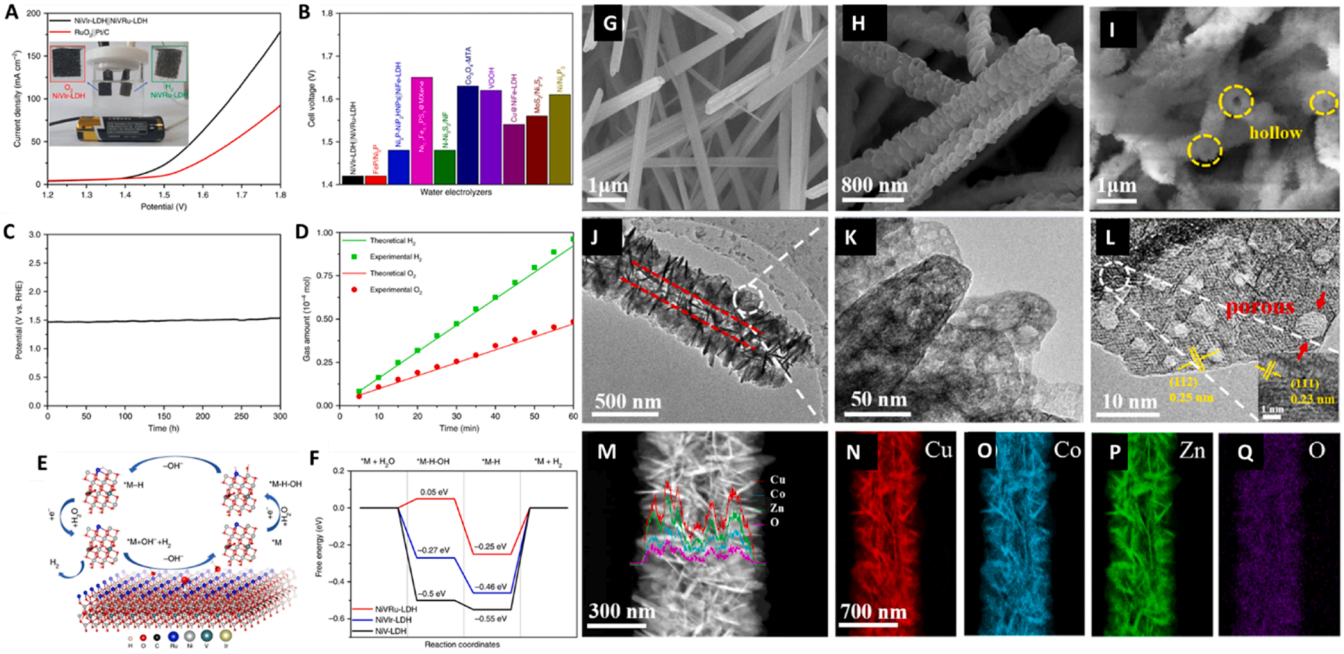

Fig. 18. . (A) The polarization curves of NiVIr-LDH||NiVRu-LDH and RuO_2||Pt/C for overall water electrolysis. The inset is of single-cell AAA battery (B)Voltage comparison at 10 mA cm^{-2} current density for the NiVIr-LDH||NiVRu-LDH with state-of-art electrodes (C) The chronopotentiometric curve of NiVIr-LDH||NiVRu-LDH for overall water electrolysis at a constant 10 mA cm^{-2} current density (D) Faradic efficiency plot for both OER and HER for NiVRu-LDH and NiVIr-LDH (E) NiVRu-LDH atomic model and HER mechanism (F) HER free energy diagram on NiV-LDH, NiVIr-LDH and NiVRu-LDH catalysts. Copyright 2019, Nature Publishing Group. Structural characterizations including SEM images of (G) $Cu(OH)_2$/CF, (H) $Cu(OH)_2$ @ZIF/CF(Co:Zn = 6:4) and (I) CuO@CoZn-LDH/CF. (J) TEM images with Low magnification, (K) TEM images of high magnification, (L) lattice image, (M) HAADF image and EDS line scanning and (N-Q) Elemental mapping of CuO@CoZn-LDH/CF. Copyright 2021, Elsevier.
(a) Reproduced with permission from ref [241]. (b) Reproduced with permission from ref [243].

current density, and exhibited high corrosion resistance. The experimental findings and DFT calculation suggested that the lattice distortion and strong interfacial interaction decrease the free energy of four elementary steps in OER, suppress the catalyst, support passivation, and enhance the ASF (Fig. 18E,F). To avoid the immobilization of active sites on the current collector with a polymeric binder, a self-supported electrode ensured the high exposure of active sites with a fast rate for electron and mass transportation. It has been investigated that compared to pristine metal foil/foam, the nanostructured substrate provides additional active sites with high intrinsic activity and specific surface area to provide the nucleation sites for the growth of guest materials and enhance the structural stability of the catalyst. For the sustainable electrode, assembling a space-confined hierarchical structure-based electrocatalyst is a selective choice [242]. Li's group proposed a facile strategy for developing a self-supported catalyst using LDH-supported $Cu(OH)_2$ nanowires as a precursor [243]. The obtained CuO @Co-Zn-LDH has a highly ordered hollow structure with a defect-rich porous surface, providing an efficient way for electrolyte penetration and gas desorption (Fig. 18 G-Q). The strong interfacial interaction between active sites and substrate and porous surface structure ensures the high structural durability of the catalyst at a high anodic potential. Du's group proposed an anion intercalation electrodeposition strategy for developing Co_4N-CeO_2 hybrid 2-D nanosheets decorated over graphite plates [244]. The self-supported electrode revealed high intrinsic activity and superior stability at the high geometric activity of 500 $mAcm^{-2}$ to meet the industrial demand. Based on in-depth findings, the authors have credited this remarkable performance to the following features of hybrid material: (1) The self-supported monolithic electrode maintained a stable working state and high efficiency due to hydrophilic surface structure and strong catalyst support interaction that ensured the easy penetration of electrolyte, facilitate the electronic conduction from the conductive support to the active phase and acerate the bubbles detachment. (2) The strong interfacial interaction between the CeO_2 and Co_4N increases a water molecule's polarizability and enhances the dissociation rate at low input voltage. (3) The strong electronic interaction between active sites and support decreases the energy barrier for O-O coupling and offered resistance-free channels for electron movement [237,245]. The microwave-assisted hydrothermal method has been recognized as an effective method to create firm contact between the substrate and active component, reducing the electrical resistance and enhancing the structural and chemical resistance of the catalyst against transformation to inactive phase. The Ni-Fe Prussian blue analog has been fabricated directly over Ni-P-O rods, ensuring strong adhesion between the conductive substrate and catalyst layer [246]. The catalyst possessed abundant active sites, which catalyzed the water oxidation reaction at low overpotential. The post-characterization results endorsed the structural and mechanical robustness of the catalyst layer. The exceptional 100 h of catalyst stability in 2 electrode configuration was attributed to the following factors: (1) The Ni-Fe-P layer chemical derived from the Ni-Fe Prussian blue analog offered high specific activity optimized chemisorption energy to stabilize the OER intermediates. (2) The hierarchical structure ensured the substrate's resistance-free interface and high conductivity to accelerate the reaction rate. (3) The rod-like structure grown over Ni foam enhanced the corrosion resistance and prevented the delamination and structural degradation caused by gas bubbles during continuous electrolysis. Surface and interface engineering have been considered power tools to tune active sites' activity, selectivity, and durability. Surface structure engineering can optimize surface wettability, electrolyte penetration, and gas desorption, tailor the electronic structure of the catalyst, and enhance the catalyst performance. In contrast, interface engineering can modulate the stability and intrinsic activity from inner boundaries at the catalyst-support interface. Interface engineering in free-standing electrode materials can efficiently decrease the aggregation of active sites and enhance the structural durability of the catalyst. Bing Li group

reported that self-supported flexible 3-D ordered macroporous (3DOM) $Co(OH)_2$/Ni-Mo@ carbon cloth with tuned surface and interface exhibited good catalytic performance for OER [247]. The surface and interface of the hybrid material were optimized by developing the core-shell structure comprised of 3DOM $Co(OH)_2$ encapsulated Ni-Mo alloys directly grown over a flexible CC current collector using polystyrene as the template. The catalyst has a porous structure, ensuring the maximum contact portion between the electrolyte and water molecule accelerates the mass transfer at the interface boundary and avoids metal leaching. The strong catalyst support interaction offered a smooth pathway for the electronic conduction and enhanced the durability of the active component. The DFT calculations demonstrated that the synergistic intermetallic interactions become stronger at the heterogeneous interface responsible for the high intrinsic activity. The firm anchoring of $Co(OH)_2$ cavities to the Ni-Mo alloys in a homogenous way provides abundant active sites with high intrinsic activity (Figures). The free energy profile revealed that the energy barrier for the potential determining step reduces drastically after heterogeneous interactions due to the electronic density transfer from self-oxidized Co-OOH to Ni-Mo alloy. This electron redistribution at the interface triggers the formation of active phases on the catalyst's surface and accelerates the reaction kinetics. The OH* and O* intermediates preferably adsorb on the Ni-Mo surface while kinetically sluggish OOH* intermediate adsorb on the Co-OOH d band center. The strong interfacial interaction provides dual sites for the electrochemical reaction and decreases the energy barrier for O-O coupling and shortens the diffusion channels for ions and mass migration and boost the robustness of active components. The recent finding demonstrates that the interface structure between two active sites with different chemisorption energy can be used as a channel for electron transportation through various intermediates [248]. The physical and chemical properties of catalysts can be controlled by controlling the surface and structure of different catalysts at interface boundaries [249]. The size alteration of a component at the interface modulates electronic structure for optimizing proton and electron transfer and balancing the intermediate adsorption-desorption with an optimum on the surface and interface of the catalyst [250]. The size reduction at the interface provides a way to tune the chemisorption behaviors to affect the reactant reactivity. The decrease in particle size at the interface creates a strong interfacial interaction and promotes the electronic conductivity, changes the B.E for the intermediate, and improves the catalytic activity, stability, and selectivity of the electrocatalyst [251].

Recently, we have proposed a novel strategy for developing Au NCs anchored on Gd- Co2B nanoflakes, which were grown on both sides of conductive r-TiO_2 nanosheet (NS) arrays, offered high-density active sites and large surface area for selective seawater electrolysis [252]. Because ultrasmall Au NCs have low surface energy and work function, it is highly challenging to create a strong interfacial interaction between the current collector and decorated Au NCs. We have experimentally observed that due to weak interaction, the catalyst deactivated after a few cycles due to sintering and metal leaching from the catalyst surface. We tackled this challenge by creating s strong interaction between different components of hybrid materials via microwave-assisted heating in ethylene glycol (EG) solvent. The EG has a high loss tangent value ($\tan \delta = 1.350$), is considered a good microwave absorbent, and facilitates efficient heating due to the rotational motion of molecules having permanent dipole moment. Interestingly, compared to the conventional heating process, we did not observe the considerable impact of microwave heating on the surface structure of the catalyst. The synthesized catalyst simultaneously demonstrated the following benefits: (I) The high surface area, outstanding corrosion resistance, a strong skeleton of the r-TiO_2 NS, and the robust armor of the Gd-Co_2B nanoflakes work in concert to provide good stability against the aggressive seawater. (2) The OOH formation is stabilized by the partial oxidation of Co through Au doping, which increases the OER selectivity. (3) Due to the high conductivity of Co_2B and Au, efficient charge transfer between the catalyst surface and seawater was observed, which would increase the water splitting kinetics at a low overpotential. Additionally, the unfilled 4 f orbitals of Gd's electrons could remain in the hyper 5d orbitals and transform into valance electrons, which supports electronic conduction. (4) The effective MW heating created strong interfacial interactions between the different catalyst components, especially at the catalyst-support interface, and indorsed the mechanical and structural durability due to synergistic promotions.

We used various characterization tools to investigate the compositional changes and surface structural modification of post-catalyst after the long-term electrolysis process. TEM images recorded after the catalysis process demonstrate that NCs retained their morphology. The redox states of the metals have been determined with XPS before and after catalysis. From the comparative analysis, it is evident that Au^0 is present before and after catalysis. However, after electrolysis, the Au^0 peak slightly shifts to the higher BE with increased intensity. Meanwhile, no reduction in the peak intensity for Au^0 was observed, indicating retaining the original composition and periodic reshuffling of an electronic configuration for the sustained electrode process. However, without microwave treatment increase in the overpotential and a decrease in the peak intensity for Au in the XPS spectrum was observed that might be due to the structural/morphological rearrangements and leaching of highly soluble $Au^{1+,3+}$ towards the electrolyte and thus reducing the numbers of accessible catalytic sites [253]. This observation was further strengthened by observing the decrease in the intensity of the Au^0 peak and the change in the color of the electrolyte due to the dissolution of Au. The persistent Au 4 F XPS intensity, the color of the electrolyte, and the absence of Au content in the electrolyte analyzed with ICP-OES for microwave-treated sample validate our hypothesis that microwave treatment creates a strong interaction between nanosized Au and Gd-Co_2B @TiO_2 sheets. Furthermore, there is a probability that metal oxide derivatives sometimes dissolve in the electrolyte's high anodic potential due to the high polar index value. For further justification, we also recorded inductively coupled plasma optical emission spectroscopic (ICP-OES) measurements of alkaline seawater electrolytes after 20 h continuous electrolysis. The results demonstrate that boron species is not present in the electrolyte solution, suggesting that boron species retain as the inherent part of hybrid material and act as an active phase rather than dissolving in the electrolyte as observed for other non-oxide-based catalysts [110,254].

9. Seawater electrolysis

Fresh and purified water feedstock is currently used in electrolysis, but its limited resources across the globe suppressed its commercial interest. The other process associated with water purification, e.g., desalination, imposes significant economic restraints, including land investment, plantation, maintenance, and transportation. These constraints motivated the researchers to use unpurified seawater because seawater and ocean represented 97% of total earth water, taking away the pretreatment system and simplifying the electrolyzer engineering [255]. It is also facile to power direct seawater electrolyzers with intermittent renewable technology, e.g., photovoltaic system and wind turbine in the coastal zone. However, the following bottlenecks severely hamper the natural seawater electrolysis viability for green hydrogen production. The 1st challenge is the anode selectivity for OER intermediate in the presence of immense Cl^- ions. Although chloride anion Cl^- oxidation generates valuable products, e.g., hypochlorous acid, hypochlorite, and Cl_2 gas, it changes the electrolyte chemistry and severely erodes the electrode surface. The Cl-related product complicates the electrode chemistry, causes gas purity issues, and possibly depends on the electrolyte pH, operating temperature, and applied anodic and cathodic potential. Strasser and coworkers computed the kinetic and thermodynamic favorability of different Cl-related products in different pH. According to their findings, hypochlorite is the primary product in an alkaline environment, while chlorine gas evolution is

thermodynamically favorable in acidic conditions (Eqs. 18–19) [256].

$$2Cl^- \rightarrow Cl_2 + 2e^- (pH = 0, E^0 = +1.36V_{SHE} \quad (18)$$

$$Cl^- + 2OH^- \rightarrow ClO^- + H_2O + 2e^- (pH = 14, E^0 = +0.89V_{SHE} \quad (19)$$

The standard equilibrium potential of CER ($+1.36V_{SHE}$) is slightly higher than the water oxidation ($+1.23V_{SHE}$), demonstrating the thermodynamic favorability of OER; however, OER is a multistep multielectron process where CER kinetics is each feasible compared to the OER. The thermodynamic potential difference between the anodic competition reactions increases with the pH of the electrolyte, and an alkaline environment offers a large kinetic potential window for OER compared to a neutral or acidic medium. The equilibrium potential of OER in an alkaline medium is 0.48 V, smaller than the hypochlorite formation. The 2nd challenge is the anode durability issue, where different microbes, bacteria, and other non-innocent ions in natural seawater severely hamper the anode sustainability. For example, the soluble bicarbonate ions in seawater decomposed to carbonate ions in the presence of hydroxyl ions which hydrolyze to the insoluble Ca and Mg hydroxide (Fig. 20) [18,257]. These sediments block the catalyst surface and cause ion and mass transport limitations (Eq. 18) [258,259].

$$MgCO_3 + 2OH^- \rightarrow Mg(OH)_2 + CO_2 \quad (20)$$

The excessive chloride ions in natural seawater severely erode the active center and substrate via absorption, dissolution, and hydroxide formation [260]. In addition, the high anodic potential accelerates the chloride ion's diffusion from the bulk to the electrode surface due to the lowest unoccupied molecular orbital of the anode, where Cl- ions are oxidized by transferring the electron from its HUMO to the anode LUMO. These absorbed ions coordinate with the surrounding chloride anions and cause dissolution, ultimately leading to hydroxide formation in the presence of hydroxide ions (Eqs. 21–23) [261].

$$\text{Absorption}: M + Cl^- \rightarrow MCl_{ads} + e^- \quad (21)$$

$$\text{Dissolution}: MCl_{ads} + Cl^- \rightarrow MCl_x^- \quad (22)$$

$$\text{Hydroxide formation}: MCl_x^- + OH^- \rightarrow M(OH)_x + Cl^- \quad (23)$$

An ideal anode should have the following features for sustainable hydrogen production from immense feedstock, i.e., natural seawater. (1)

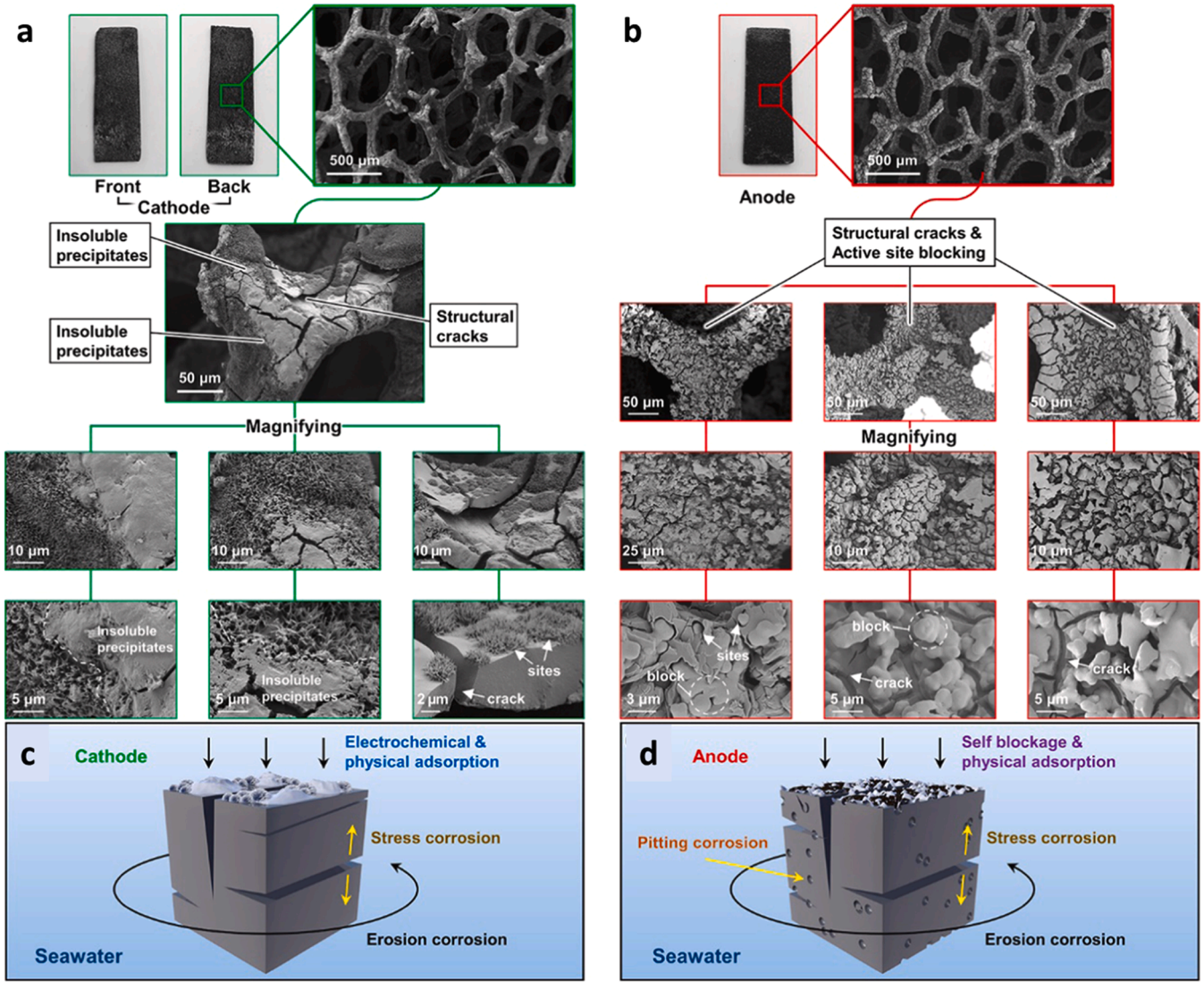

Fig. 19. Surface structure evaluation of Ni/Co-doped defect-rich Cu-based sulfides and oxides after continuous cyclic operations in natural seawater. (a-b) The active site blockage due to the accumulation of sediments and structural cracks on the anode and cathode surface is visible in SEM images. (c-d) The systematic model for the cathode and anode reveals the stress and erosion-corrosion mechanism.
Reproduced with permission. 257. Copyright 2021, Elsevier.

abundant active sites with high intrinsic activity and selectivity for OER intermediates. (2) high structural, chemical, and mechanical durability with high corrosion resistance (3) short diffusion channels for ions and mass conduction at the interface [262]. Considering these factors, we have recently proposed different strategies to enhance the activity, selectivity, and corrosion resistance of anode working in direct seawater electrolysis. (1) Electronic modulation to optimize the binding energy of active centers so it will preferably coordinate with the OER intermediates in the presence of chloride ions. (2) Surface oxygen vacancies optimization depends on the p-type and n-type transition metal oxide, which favor the active phase generation and OER sluggish reaction kinetics. (3) Surface structure modulation by creating the porosity and amorphousness in the catalyst that offers abundant active sites with super hydrophilic and aerophobic character and provides short diffusion channels for mass and ions transportation. (4) Strong catalyst support interaction to enhance the structural and mechanical durability of active sites and to reduce the metal leaching probability under the influence of high anodic potential. (5) passive layer next to the OER active phase to prevent the chloride ions diffusion and adsorption and enhance the corrosion resistance. The electronic and structural modification and strong catalyst support interaction strategy to enhance the anode's durability are discussed in the above sections. In this section, we will focus on the protective layer development on the anode to prevent it from stress and pitting corrosion. (Fig. 19).

Even with a high-performance anode material and suitable electrolyte, seawater's aggressive Cl^- anions can erode the catalyst surface via the M-Cl-OH production pathway. This corrosion weakens the substrate structure, obstructs active sites, slows reaction kinetics, and lowers product purity. Therefore, researchers employed a protective layer close to the OER actual functional sites to boost the selectivity and stability of anode material in seawater electrolysis. Ma et al. reported that the optimum concentration of sulfate anions in the electrolyte significantly enhanced the selectivity of active centers for OER intermediates and the corrosion resistance [263]. The theoretical and experimental results demonstrated that sulfate anions selectively adsorbed on the positively polarized anode surface and impeded the Cl^- ions adsorption through electrostatic repulsion. These repulsive forces work well for mono and multi-metals catalyst. The molecular dynamic simulations demonstrated that in the absence of this anion additive, Cl^- anions diffuse towards the anode surface, enhance the metal dissolution rate linearly with the applied potential and cause stress and pitting corrosion. However, the mass diffusion rate of sulfate anions (1.070×10^{-9} m^2 s^{-1}) is much higher than the chloride anion (2.030×10^{-9} m^2 s^{-1}), preferably coordinated with the polarized anode. It creates a negative electric field that repels the chloride anion from the vicinity of the anode surface. However, these anions also increase the potential barrier for OH^- attacks and the potential barrier for O-O coupling. Therefore, the optimum ratio of these anions concerning the active centers is crucial to enhance the corrosion resistance without considerable reduction in the catalytic efficiency.

A recent investigation revealed that nonmetal coordination with metal optimizes the adsorption energy and oxidizes to N-O passive layer (N- nonmetals, e.g., N, P, S, B, etc.) that repel the Cl^- ions electrostatically and prevent the metal dissolution. Chang et al. probed P's impact in Fe-doped $NiSe_2$ anode for aggressive direct seawater electrolysis [264]. The insightful investigations demonstrated that P content up to a certain level enhanced the electronic conduction at the electrode-electrolyte interface, served as P-O passive layer that masks the Se and Ni, Fe from dissolution, and enhanced the selectivity and corrosion resistance. Metal phosphides erode in the presence of strong oxidizing agents and operate well in alkaline seawater with high chemical and mechanical durability. The following characteristics of metal sulfide are responsible for its high corrosion resistance.

1. The metal coordination with phosphorus 2 p orbital and its electronic linkage with underlying support decreases the metal dissolution.
2. The P content modulates the electrode's surface structure, shields the core of the active site from Cl^- attack, and prevents the metal from leaching into aggressive seawater.

The P-O layer adsorbed at the electrolyte-electrode junction, increasing the diffusion barrier for metal dissolution. The M-P bond enhanced the water destabilization due to one electron-proton equilibrium between M^{3+}-OH and M^{4+}-O while phosphate ion act as soft base abstract the soft acid, i.e., H+ ions, reducing the activation barrier for O-O coupling and enhanced the selectivity and durability of the anode [265]. Wu et al. have designed the core-shell structure of CoP-FeOOH, revealing high resistance against the structural and chemical transformation to inactive phases [266]. The catalyst was immersed in natural seawater for a long time, and no structural degradation or stress and corrosion pits were visible on the electrode surface, demonstrating the synthesized electrode's structural stability and corrosion resistance. The experimental results show that the CoP core decreases the charge transfer resistance for intermediate adsorption and minimizes the Cl^- adsorption due to electrostatic repulsion forces. In addition, the electronic linkage between transition metals and P nonmetals enhanced the entropy of the system, decreased the system free energy, reduced the metal leaching probability due to Cl^- ions adsorption, and overall improved the ASF of the anode material for alkaline water electrolysis. The anion incorporation also accelerates the metal oxidation to a higher valance state, generate additional active centers, and increases the activity and durability of active sites. Ni foam-supported 3D hetero-lateral Ni_3S_2/Co_3S_4 (Ni-Co-S) nanosheets revealed excellent selectivity and durability for seawater oxidation [267]. The spectroscopic results indicated that the M-S bond chemically transforms to M-OH/M-OOH, core the active metal center, impede the chloride ions diffusion and the formation of a nonconductive layer, and enhance the support stability. In addition, the electrochemically generated passive layer and core-shell feature of the designed electrode ensure structural integrity during seawater oxidation. Li et al. have designed Ni_3S_2 coated MoS_2 layer and evaluated its performance for unpurified seawater electrolysis [268]. The polyanionic Ni-S layer protects the MoS layer and repels the Cl^- ions, enhancing the material's corrosion resistance. At high anodic potential, Mo has an affinity for chloride ions due to its electronic configuration (s^1d^5), but the passive layer doesn't permit the diffusion of chloride ions and prevents the adsorption-dissolution and hydroxide formation. The Ni-S layer also provides additional active sites, enhances the intrinsic activity of active sites, offers short diffusion channels for electron movement at the electrode-electrolyte interface, and enhances the structural and chemical durability of the catalyst.

10. Sustainability in practical devises for alkaline water electrolysis

The practical water electrolysis powered by intermittent renewable energy resources (e.g., wind turbine, photovoltaic cell the repeated incoming power disruption unavoidably depolarized the electrode and reversed the potential on the electrode surface, potentially leading to the degradation in electrocatalyst performance due to the corrosion of active sites [269,270]. Therefore, it is highly demandable to design bifunctional electrocatalysts with high reversibility and corrosion resistance. The strong electronic linkage between the active sites and the current collector with super hydrophilic aerophobic characters are the key features to enhance the durability of bifunctional catalysts. Recently, the Piao group has developed an Sn_4P_3/Co_2P "stalk"-"cap"--typed nanostructure, demonstrating outstanding activity and sustainability under the influence of reversed applied potential for overall water electrolysis (Fig. 20 A-E) [209]. The heterointerface construction modulates the surface and electronic structure of the catalyst, which enhances the intrinsic activity of active sites, facilitates e the charge and mass transfer at low input voltage, and ultimately enhances the sustainability of active sites at a higher geometric activity. The catalyst

sustained 100 mAcm-2 during water electrolysis for 24 h without any noticeable hysteresis. The authors have attributed the sustainability of fabricated electrodes to the following points. (1) The heterointerface remarkably tuned the surface and electronic structure of the active site, induced the rapid charge transfer, and minimized the support passivation. (2) The unique needle-like nanotexture offered short diffusion channels for ions and mass migration, enhanced the effective contact portion at the electrode and electrolyte interface, and precluded the nonconducting layer formation. The rough surface of Ni foam offered a strong electronic linkage between the support and active sites. It improved the mechanical and structural durability of the active sites at high input voltage. The excessive interlinkage of active sites without polymeric binder increases the electronic conduction and minimizes the un-demandable mass/volume dead portion. The implanted cap on the catalyst surface increases the roughness factor, improves the wettability of active sites and gas desorption rate, and enhances the overall stability of the catalyst. Zhao and coworkers revealed that asymmetry introduction into the electrocatalyst created strong interfacial interaction and offered an unprecedented synergistic promotion for water dissociation [271]. Furthermore, the oxidation and reduction reaction on the active centers with the same electronic and surface structure offered high corrosion resistance, especially for the electrochemical devices integrated with an intermittent energy source, and sustained the activity under interrupted applied potential.

Similarly, in another report, NiMoS/ NiMoOx nanoarray was assembled as anode and cathode in two electrode configurations needing only a small input voltage of 1.82 V to deliver a current density of 1 A/cm^2 in 1 M KOH [272]. The heterointerface offered a super-aerophobic surface that enhanced the gas desorption rate, impeded the surface blockage due to the bubbles accumulation, and enhanced the structural durability of the device. The catalyst sustained the high geometric activity of 500 mAcm^{-2} for more than 500 h in industrial conditions without considerable degradation (Fig. 20**F,G**). The spectroscopic results demonstrated the formation of a passive hydroxide layer on the electrode surface that prevented the metal dissolution and enhanced the ASF. The catalyst preserved the surface structure during water electrolysis and presented industrial hope. This remarkable performance was assigned to the different factors including 3-D hierarchical heterostructures offering a synergistic effect of the redox-induced surface reconstruction and enhanced the self-healing property of active sites. Furthermore, the defective species at the heterointerface enhanced the specific activity of the catalyst with low charge transfer resistance, promoting the water dissociation and stability of active sites.

The interconnected structure with exposed grain boundaries demonstrated super hydrophilic and aerophobic characteristics that are highly beneficial for sustainable water electrolysis. It has been investigated that the electrochemical conversion of TMO nanostructure to small nanoparticles via a Li-induced conversion reaction offered strongly interconnected boundaries that serve as an active center for intermediate adsorption and stable mechanical and structural features in the harsh electrolyte [273]. The Li-induced Ni-Fe-O_x nanostructure sustained the geometric activity of 10 mAcm^{-2} in 2 electrode configurations for more than 200 h without noticeable degradation. The electronically interconnected structure facilitates the redox process at reactive boundaries, enhancing the self-healing property of active sites during water electrolysis. Tang et al. have found that Mn doping modulates Co carbonate hydroxide nanosheets' electronic and surface structure [274]. The favorable interaction of the intermediate with the active center in overall water electrolysis enhanced the activity and sustainability of active sites. Based on the theoretical and experimental analysis, the authors have attributed the sustainable behaviors of catalysts to the following features. (1) Mn doping in the Co nanostructure modified the metallic bonding in the structure, decreased the surface energy of uncoordinated active sites, and stabilized the vertically oriented nanosheets; (2) The Mn introduction into the Co lattice optimized the electronic structure of active center that needed small input voltage for intermediate adsorption and suppressed the support passivation during overall water electrolysis. (3) The unique surface structure of the synthesized electrode offered a short diffusion channel for mass and ions conduction that minimized the metal dissolution rate and enhanced the overall ASF.

Recently many integrated devices, including electrocatalyst electrolytes and perovskite solar cells, have been reported for commercial interest (Fig. 20H-J) [275]. Although these integrated devices revealed promising conversion efficiency, certain bottlenecks impeded their commercial viability. (1) Moisture can easily break the lattice structure of perovskite materials; therefore, it's impossible to immerse these materials directly in an aqueous solution. To minimize the perovskite layer degradation, researchers have designed the device by keeping the perovskite materials outside the electrolyte cell connected with an electrocatalyst through an electronic circuit [276]. However, these external circuits enhanced the ohmic losses due to inefficient electrical connection and increased the complexity of the device. (2) The catalyst in this integrated system should possess the bifunctional behavior to catalyze both half-cell reactions simultaneously. However, most current research focused on a single electrode, i.e., cathode or anode. (3) Mostly, traditional state-of-the-art perovskite solar cells are employed in this integrated system due to high efficiency and open circuit voltage constraining the device's economic viability. Therefore, to design a valuable and sustainable integrated device, it is essential to fabricate a compact wireless design with an efficient catalyst manufactured from low-cost materials via a scalable route [277]. (Table 1).

11. Conclusion and future perspective

The dissolution, agglomerations, and detachment of active sites are the crucial factors accountable for the instability of the catalyst. Electrocatalyst dissolution is generally related to the catalyst's physical properties and chemical environment. At the same time, detachment and accumulation of active sites are associated with the interactions between the catalyst and underlying support. In this review, we have summarized recent inspiring progress in developing stable OER electrocatalysts with high intrinsic activity and proposed design strategies to address the stability challenges. In addition, we have spotlighted several strategies, including cations, anions, and heteroatom doping, to optimize the electronic structure and to prevent metal dissolution, defects engineering, and morphology optimization to tune the surface structure for maximum atom usage with enhanced structural stability and strong catalyst support interactions with super hydrophilic-aerophobic characteristics to prevent dissolution and agglomeration of active sites.

It should be noted that these strategies should be fitted into one electrocatalyst to fulfill the anode's chemical, structural and mechanical durability at high geometric activity. Although the primary focus of the review article is on the OER catalyst, the design strategies also adopt to construct a durable catalyst for HER. Despite the remarkable achievements and progress summarized in this review, designing a scalable and stable anode with high ASF remains an urgent challenge. The following critical issues need to be considered for future research in water electrolysis.

11.1. Intrinsic activity and sustainability marker

In general, the current response is reported in terms of geometric current density, which does not reflect the actual activity because the selected electrode area is never the same as the truly projected area because of the high surface area and roughness factor of the nanostructured based electrocatalyst. Consequently, geometrical area normalization exaggerates the activity of nearly every reported electrocatalyst [296]. Frequently, mass activity and specific activity are employed to address this issue. Mass activity indicates the current response normalized by the amount of catalyst loaded and has the unit A/g^1. Even though it seems reasonable compared to activity normalized

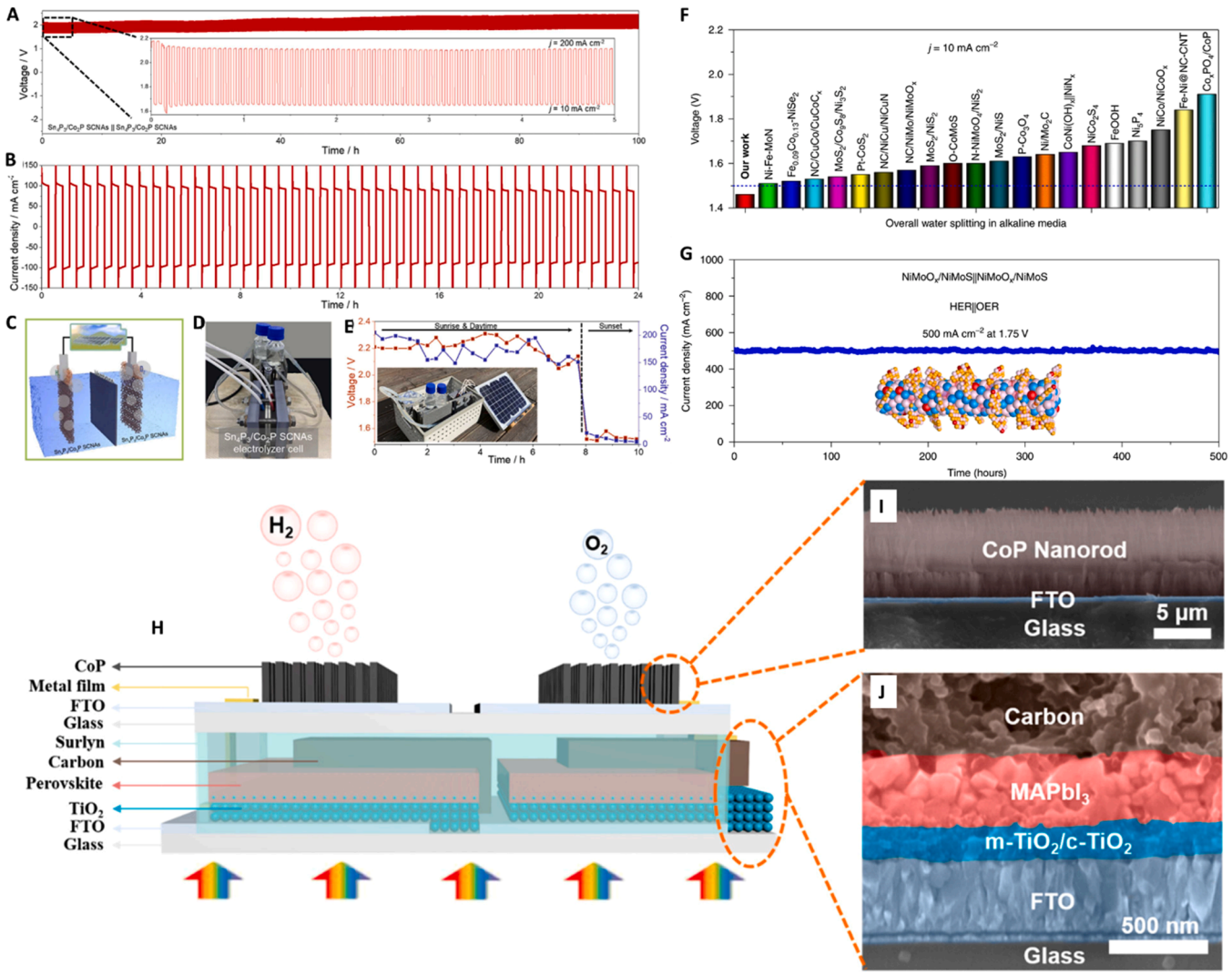

Fig. 20. Overall water splitting performance of a two-electrode cell made with Sn_4P_3/Co_2P SCNAs. (A) 100-hour Chronopotentiometric curve at 10 and 200 mAcm^2. (B) for 24 h, the chronoamperometric curve of a Sn_4P_3/Co_2P SCNAs-built cell with an applied potential of 1.8 V and a polarity switch interval of 1000 s, (C) schematic representation of the two-electrode electrolyzer, (D) digital photo of the completed electrolyzer, (E) voltage and current response of the solar-powered Sn_4P_3/Co2P SCNAs-cell for water electrolysis. Reproduced with permission. 209 Copyright 2022, Elsevier. (F) Cell voltage for different electrocatalysts at geometric activity of 10 mA cm^{-2}. (G) Chronoamperometric test for NiMoS/ NiMoOx at 1.75 V in 1.0 M KOH at 25 °C. Reproduced with permission. 272 Copyright 2020, Nature. (H) Integrated device schematic structure with two CoP electrodes/Surly/two series-connected PSCs. Cross-sectional SEM images of (I) a CoP electrode with a glass/FTO/CoP nanorod structure and (J) a PSC with a glass/FTO/TiO_2/perovskite/carbon structure. Reproduced with permission. 275 Copyright 2020, American chemical Society.

by geometric area, the problem is that only some active sites in the loaded catalyst are exposed to the electrolyte and participate in the reaction. Therefore, only the active sites exposed directly to the electrolyte solution are accountable for the recorded current response. In addition, catalyst loss throughout the reaction reduces the catalyst's actual mass. This indicates that current response normalization by the loading assessed before the reaction can be highly deceptive [297]. As a result, adjusting the current response by catalyst mass loaded is not an optimal method for determining the intrinsic activity.

Furthermore, when samples of the same amount of the same material but with varying particle sizes and shapes (such that the exposed area is different) are examined under the same conditions, this can lead to significant differences in results. On the other hand, the specific activity is a more exact method for evaluating an electrocatalyst's (intrinsic) activity, wherein the actual surface area of the catalyst normalizes the current response. However, determining an electrocatalyst's active/real surface area is challenging. There is no precise and controlled method to determine the active site density and surface area, including the double-layer capacitance (*C*dl) method. To estimate the electrochemical active surface area, a ratio of C_{dl} and specific capacitance (C_s) of material is considered from the literature. The C_{dl} value varies considerably and strongly depends on catalyst lifetime, electrolyte composition, and electrode-electrolyte exposure time [75]. Similarly, the specific surface area calculation using Brunauer–Emmett–Teller (BET) isotherms also has limitations. The surface area from adsorption-desorption isotherms corresponds to the area of gas, and all these sorption sites are not electrochemically active. Moreover, this method is not viable for supported electrocatalysts that require scratching and sonication, which considerably change the actual surface area. This pre-experiment physical process accelerates the aggregation of catalyst nuclei and masks the significant portion of active sites [298]. Therefore, overpotentials calculated with mass, specific, or geometric activity only represent the apparent activity of the whole interface (i.e., electrolyte-catalyst-substrate) and never demonstrate the intrinsic activity of an electrocatalyst.

Unlike other parameters, e.g., overpotential at benchmarking

Table 1
Anode durability in alkaline water electrolysis.

No	Catalyst	Substrate	Stability	References
1	Ni-Fe-LDH @NiCoP	NF	100 h	[278]
2	$Ni_xCo_{3-x}S4$ @Ni_3S_2	NF	200 h	[216]
3	Ru-Fe–$Ni(OH)_2$	NF	680 h	[279]
4	Ni_3Se_2	NF	500 h	[280]
5	$W_{0.5}Co_{0.4}Fe_{0.1}$	NF	500 h	[281]
6	NiFeP-MoO_2	NF	100 h	[282]
7	Ni_5Co_3Mo–OH	NF	100 h	[283]
8	$La_{0.5}Sr_{0.5}CoO_{3-\delta}$ @$MoSe_2$	NM	1000 h	[284]
9	$Pb_2Ru_2O_{6.5}$, $Bi_{2.4}Ru_{1.6}O_7$	GC	200 h	[285]
10	$NiCo_2O_4$	GC	1000 h	[286]
11	Ni-P	CP	180 h	[109]
12	**Co_3Se_4**	CoF	3500 h	[287]
13	Ni-Fe LDH	IF	6000 h	[288]
14	$Ni(OH)_2$/FeOOH@Ni_xFe_y	SS	1000 h	[289]
15	Ni–Fe-OOH@NiFe alloy	GC	120 h	[290]
16	S-substituted Ni_3Se_4	CP	100 h	[291]
17	Au-$GdCoB_2$	TiO_2	200 h	[252]
18	NiO_x-FeO_x	g-C_3N_4	100 h	[292]
19	FeS_2/CoS_2	NF	10,000 Cycles	[170]
20	Fe_2O_3 @CuO	CF	5000 Cycles	[293]
21	TaO_2F	GrC	20,000 Cycles	[294]
22	Co_3Fe_7	CS	4000 Cycles	[295]

NF= Nickel Foam, NM= Nickel Mesh, GC=Glassy carbon, CP= carbon paper, CF= Cupper Foam, CoF= Cobalt Foam, IF= Iron Foam, SS= Stainless steel, GrF= Graphitized carbon, CS= Carbon sheet

geometric activity, turnover frequency demonstrated the direct information on the rate of desired product formation or reactant consumption in electrochemical energy conversion reaction. TOF reflects the intrinsic activity of active sites, and for this, TOF is an impeccable option [299]. Because all the other activity parameters revealed the apparent activity of active sites due to unavoidable capacitive currents and kinetically and thermodynamically competing reactions, we strongly recommend that the reviewer must report the TOF of their catalyst before and after catalysis in a proper way and compare the intrinsic activity and stability of active sites with other reported work.

11.2. Suggested Characterization tools to understand instability issue

To evaluate the durability of the catalyst, constant current or potential electrolysis is often performed for a few hours on the catalyst with high mass loading, and if no alteration in the current or potential is observed, it is claimed to be durable [75,258]. However, these testing protocols are insufficient to probe the real stability of the catalyst and only applicable up to the extent of preliminary evaluation. The catalyst with high mass loading eroded and improved its performance over time as its roughness factor increased and then deteriorated completely after complete corrosion. Therefore, it is highly recommended to use very low mass loading (sub-monolayers) for stability testing and analyze the electrolyte with an ICP-OES analysis after long-term continuous operations for interrogating the catalyst's dissolution.

Although, in the last few years, the in-depth understanding of the fundamental process of water electrolysis has advanced quickly, there is no consensus on the actual mechanism of catalyst deactivation because of the chemical transformation of the catalyst during electrocatalysis. Therefore, it is highly needed to use theoretical simulations and advanced in-situ characterization tools to clarify the deactivation mechanism at the molecular level. A thorough characterization of the catalyst's electronic, crystal, and surface structure using operando tools such as Raman spectroscopy, TEM, AFM, XRD, XPS, XRF, XANES, electron paramagnetic resonance (EPR) would provide the actual deactivation mechanism conducive to the design of advanced electrocatalyst. Suppose these advanced operando tools are not available in the lab. In that case, researchers are highly encouraged to use ex-situ characterization tools before and after catalysis, i.e., XPS, XRF, ICP-MS, EDS for chemical structure and composition alteration, SEM, TEM, AFM for structural stability, and XRD to probe the possible appearance of new phases during water oxidation [300]. The active site dissolution and redeposition process need to be considered in a future study to get insights into catalyst surface reconstruction. The findings of how metal ions dissolute and redeposited under anodic potential and how different underlying support provide nucleation sites for the segregation of active metal components need to be interpreted next. As the deposition rate mainly depends on the ions concentration in electrolyte and deposition potential, tuning the dynamic OER stability can be considered [300].

11.3. Outlook for the synthesis of sustainable anode

Developing scalable electrodes is crucial to bridge the gap between lab and industrial-scale performance. Although numerous methods for creating efficient OER catalysts with low mass have been developed, the yield and quality of these catalysts are insufficient to satisfy industrial and commercial requirements because synthetic processes are time-consuming and expensive [301,302]. To enhance the commercial viability of electrocatalysts, the synthesis process should qualify for these unique figures of merits. (1) Large area electrode with low cost per unit geometric area [303]. (2) Controlled nucleation and growth structure on the diverse current collector [304]. (3) Low structural variability and high yield, (4) Strong electronic interaction of active components with underlying support [305]. Electrical conductivity and material stability are improved by the direct growth of active sites on conducting support without using any polymeric binder and conducting agents. In addition, the catalyst's physical stability on the supporting material may be improved by the Ohmic contact between the electrode and catalyst, which may lessen electron losses between the interface and overpotentials [306]. Although stability experiments on catalysts made with highly durable supporting materials like metal oxides (e.g., NiO, TiO_2) and carbon-based materials (e.g., graphene, CNT) revealed the long-term structural stability, in-depth knowledge of the relationship between strong contact and particle behaviors under the anodic potentials is lacking [307–310]. It is crucial to create a firm contact between the catalyst and the support because NP's mobility during catalysis would lead to NPs aggregation and catalyst deterioration.

Pre-treatment, such as acid treatment, plasma etches, and doping on supporting materials to develop functional groups on their surface and to enhance the surface area is suggested to achieve catalyst-support solid contact [311–314]. However, the pre-treatment could decrease the current collector's electrical conductivity and improve the charge transfer resistance at the electrode-electrolyte interface. Additionally, deterioration of supporting materials (such as carbon oxidation) at a high electrical potential area is a problem that will always exist, especially for OER [315,316].

11.4. Development of selective interfaces to enhance the ASF

For the development of selective catalysts with high intrinsic activity and durability, researchers should focus on the development of distinctive interface structures in heterostructure materials for the design of their nanoscale morphology because the synergistic effect, electrical interaction, and strain impact created by heterostructure materials' have a significant effect on enhanced catalytic performance [317–319]. For the development of selective interface by chemical doping, the following guiding principles should be considered: The chosen elements, including Fe, Co, Ni, and other first-row transition metals, have some level of catalytic activity to boost the number of active sites, so it is highly recommended that the dopant material should be in nanometric size with high surface area [320]. Additionally, non-3d high-charged metals like W and Mo are effective dopants because they have a strong ability to reduce the Gibbs free energy required to generate the electrocatalytic intermediate [321–324].' Similarly, nonmetallic elements like B, N, S, Se, and P can potentially optimize the

chemisorption energy of active sites and improve the aerophobic characteristics of transition metals [325–328]. To prevent seriously altering or destroying the structure of the materials, it is also essential to control the number of doped elements (typically 10% of the total elements). The synthesis approach for chemical doping has a critical role in developing the distinctive interface, and the template approach, electrodeposition method, hydro/solvent thermal method, and ion exchange method are the most popular and valuable among the several doping techniques.

11.5. Chemical doping to increases the intrinsic reactivity of anode with high durability

Chemical doping, the most popular technique, is an effective way to control the electronic and surface structure of materials and to enhance chemical sustainability, but the number of dopants should be kept to a minimum to prevent the formation of new crystal phases that could disrupt the original structure, block the active sites, and increases the activation barrier for O-O coupling [329,330]. Additionally, due to uncertainty in the crystalline structure and atomic arrangement, chemical doping of the multielement will make it challenging to comprehend the actual active sites and reaction mechanisms accurately and clearly [331]. Numerous delicate or complicated structures that provide short diffusion channels for ions and mass migration and optimize the surface structure for the absorption/desorption of gases can be created using nano heterostructure engineering [83,32]. However, structural anisotropy is typically present in 1D and 2D materials, impeding ineffective electron transport and mass diffusion, resulting in limited cycling reversibility [333,334]. The extensive preparation route and difficulty in morphology reproducibility are the additional factors that limit the commercial interest in complex nanostructures. Compared to chemical doping and nanostructure engineering, the straightforward production of hybrids, such as an active component grown on a conductive substrate, has the advantages of easy synthesis and good controllability [335,336]. However, some heterostructure-based hybrid bulks may contain saturated active interfaces, limiting their electrochemical performance [337,338]. So, choosing different methods and combining them to create heterostructures is promising for developing sustainable anode.

11.6. Development of hollow structure to enhance the aerophilic character of anode

Another field that can be anticipated to grow significantly is that of the creation of hollow catalysts with several, spatially segregated catalytic functions [339]. This is due to the advanced and still developing synthesis capabilities and their inherent adaptability. It is also anticipated that improvements in electron microscopy and nano spectroscopy techniques with nanometer spatial resolution will aid in the creation and improvement of synthesis techniques that allow the precise, regioselective assembly of various catalytic functionalities within single hollow nanoparticles [340]. To comprehend the multifunctionality of such catalysts and to clarify the significance of the spatial intimacy between various catalytic functions coexisting within single nanoparticles as opposed to the case where single-function nanoparticles are concurrently added to the reaction media, detailed kinetic studies should be carried out. In other words, the kinetic relevance of the residence time for reaction intermediates between various active sites should be explored. The rational development of hollow catalyst materials in the fields of electro- and photocatalysis in the area of sustainable energy systems will likely require a more systematic evaluation of those effects brought about strictly by their hollow particle morphology versus those resulting from, for example, nanosizing, the creation of structural defects, etc [341,342]. A general inverse relationship between total porosity and mechanical strength exists for porous materials of interest as catalysts or catalyst supports, which must be considered in the fabrication of heterointerface hybrid materials [343]. The typical ratios of shell thickness to particle diameter for hollow (nano)materials are in the range of 10–30%, which translates into intraparticle void volume fractions surpassing 30% and places them in the porosity domain sensitive to demonstrating inferior mechanical properties. However, it has recently been demonstrated that these materials' mechanical properties may exceed those predicted for analog materials with equivalent, traditional porosity, particularly for well-developed, highly symmetric hollow spherical particles [344,345].

Declaration of Competing Interest

The authors declare that they have no known competing financial interests or personal relationships that could have appeared to influence the work reported in this paper.

Data Availability

Data will be made available on request.

References

[1] P. Lianos, Review of recent trends in photoelectrocatalytic conversion of solar energy to electricity and hydrogen, Appl. Catal. B Environ. (2017), https://doi.org/10.1016/j.apcatb.2017.03.067.
[2] S.O. Ganiyu, C.A. Martínez-Huitle, M.A. Rodrigo, Renewable energies driven electrochemical wastewater/soil decontamination technologies: a critical review of fundamental concepts and applications, Appl. Catal. B Environ. (2020), https://doi.org/10.1016/j.apcatb.2020.118857.
[3] L. Li, B. Wang, G. Zhang, G. Yang, T. Yang, S. Yang, S. Yang, Electrochemically modifying the electronic structure of IrO2 nanoparticles for overall electrochemical water splitting with extensive adaptability, Adv. Energy Mater. 10 (2020), https://doi.org/10.1002/aenm.202001600.
[4] T. Longden, F.J. Beck, F. Jotzo, R. Andrews, M. Prasad, 'Clean' hydrogen? – comparing the emissions and costs of fossil fuel versus renewable electricity based hydrogen, Appl. Energy 306 (2022), 118145, https://doi.org/10.1016/j.apenergy.2021.118145.
[5] H. Sun, J.M. Yang, J.G. Li, Z. Li, X. Ao, Y.Z. Liu, Y. Zhang, Y. Li, C. Wang, J. Tang, Synergistic coupling of NiTe nanoarrays with RuO2 and NiFe-LDH layers for high-efficiency electrochemical-/photovoltage-driven overall water splitting, Appl. Catal. B Environ. (2020), https://doi.org/10.1016/j.apcatb.2020.118988.
[6] Y. Jiang, J. Huang, B. Mao, T. An, J. Wang, M. Cao, Inside solid-liquid interfaces: understanding the influence of the electrical double layer on alkaline hydrogen evolution reaction, Appl. Catal. B Environ. (2021), https://doi.org/10.1016/j.apcatb.2021.120220.
[7] F. Sun, J. Qin, Z. Wang, M. Yu, X. Wu, X. Sun, J. Qiu, Energy-saving hydrogen production by chlorine-free hybrid seawater splitting coupling hydrazine degradation, Nat. Commun. (2021), https://doi.org/10.1038/s41467-021-24529-3.
[8] Y. Liu, S. Jiang, S. Li, L. Zhou, Z. Li, J. Li, M. Shao, Interface engineering of (Ni, Fe)S2@MoS2 heterostructures for synergetic electrochemical water splitting, Appl. Catal. B Environ. (2019), https://doi.org/10.1016/j.apcatb.2019.01.094.
[9] C. Sun, J.A. Alonso, J. Bian, Recent advances in perovskite-type oxides for energy conversion and storage applications, Adv. Energy Mater. (2021), https://doi.org/10.1002/aenm.202000459.
[10] H. Zhang, Y. Lv, C. Chen, C. Lv, X. Wu, J. Guo, D. Jia, Inter-doped ruthenium–nickel oxide heterostructure nanosheets with dual active centers for electrochemical-/solar-driven overall water splitting, Appl. Catal. B Environ. (2021), https://doi.org/10.1016/j.apcatb.2021.120611.
[11] L. Tao, M. Huang, S. Guo, Q. Wang, M. Li, X. Xiao, G. Cao, Y. Shao, Y. Shen, Y. Fu, M. Wang, Surface modification of NiCo2Te4 nanoclusters: a highly efficient electrocatalyst for overall water-splitting in neutral solution, Appl. Catal. B Environ. (2019), https://doi.org/10.1016/j.apcatb.2019.05.010.
[12] L. Sun, V. Reddu, X. Wang, Chem. Soc. Rev. Multi-At. Clust. Catal. Effic. Electro (2022), https://doi.org/10.1039/d2cs00233g.
[13] Q. Liu, M. Ranocchiari, J.A.Van Bokhoven, Catalyst overcoating engineering towards high-performance electrocatalysis, Chem. Soc. Rev. (2022), https://doi.org/10.1039/d1cs00270h.
[14] J. Zhu, L. Hu, P. Zhao, L.Y.S. Lee, K.Y. Wong, Recent advances in electrocatalytic hydrogen evolution using nanoparticles, Chem. Rev. (2019), https://doi.org/10.1021/acs.chemrev.9b00248.
[15] Y. Sun, Y. Wang, J.Y.C. Chen, K. Fujisawa, C.F. Holder, J.T. Miller, V.H. Crespi, M. Terrones, R.E. Schaak, Interface-mediated noble metal deposition on transition metal dichalcogenide nanostructures, Nat. Chem. 12 (2020) 284–293, https://doi.org/10.1038/s41557-020-0418-3.
[16] Q. Yao, B. Huang, Y. Xu, L. Li, Q. Shao, X. Huang, A chemical etching strategy to improve and stabilize RuO2-based nanoassemblies for acidic oxygen evolution, Nano Energy 84 (2021), 105909, https://doi.org/10.1016/j.nanoen.2021.105909.

[17] P.F. Liu, H. Yin, H.Q. Fu, M.Y. Zu, H.G. Yang, H. Zhao, Activation strategies of water-splitting electrocatalysts, J. Mater. Chem. A. (2020), https://doi.org/10.1039/d0ta01680b.
[18] S. Khatun, H. Hirani, P. Roy, Seawater electrocatalysis: activity and selectivity, J. Mater. Chem. A. 9 (2021) 74–86, https://doi.org/10.1039/d0ta08709b.
[19] W. Yang, Z. Wang, W. Zhang, S. Guo, Electronic-structure tuning of water-splitting nanocatalysts, Trends Chem. (2019), https://doi.org/10.1016/j.trechm.2019.03.006.
[20] Q. Sun, Y. Tong, P. Chen, B. Zhou, X. Dong, Universal strategy of bimetal heterostructures as superior bifunctional catalysts for electrochemical water splitting, ACS Sustain. Chem. Eng. (2021), https://doi.org/10.1021/acssuschemeng.1c00037.
[21] H. Sun, X. Xu, Y. Song, W. Zhou, Z. Shao, Designing high-valence metal sites for electrochemical water splitting, Adv. Funct. Mater. (2021), https://doi.org/10.1002/adfm.202009779.
[22] G. Huang, Z. Xiao, R. Chen, S. Wang, Defect engineering of cobalt-based materials for electrocatalytic water splitting, ACS Sustain. Chem. Eng. (2018), https://doi.org/10.1021/acssuschemeng.8b04397.
[23] L. Zhang, H. Zhu, J. Hao, C. Wang, Y. Wen, H. Li, S. Lu, F. Duan, M. Du, Integrating the cationic engineering and hollow structure engineering into perovskites oxides for efficient and stable electrocatalytic oxygen evolution, Electrochim. Acta (2019), https://doi.org/10.1016/j.electacta.2019.135033.
[24] Y.Z. Wang, M. Yang, Y.M. Ding, N.W. Li, L. Yu, Recent advances in complex hollow electrocatalysts for water splitting, Adv. Funct. Mater. (2022), https://doi.org/10.1002/adfm.202108681.
[25] Y. Luo, Z. Zhang, M. Chhowalla, B. Liu, Recent advances in design of electrocatalysts for high-current-density water splitting, Adv. Mater. (2022), https://doi.org/10.1002/adma.202108133.
[26] Y. Li, B. Huang, Y. Sun, M. Luo, Y. Yang, Y. Qin, L. Wang, C. Li, F. Lv, W. Zhang, S. Guo, Multimetal borides nanochains as efficient electrocatalysts for overall water splitting, Small (2019), https://doi.org/10.1002/smll.201804212.
[27] Q. Xu, J. Zhang, H. Zhang, L. Zhang, L. Chen, Y. Hu, H. Jiang, C. Li, Atomic heterointerface engineering overcomes the activity limitation of electrocatalysts and promises highly-efficient alkaline water splitting, Energy Environ. Sci. (2021), https://doi.org/10.1039/d1ee02105b.
[28] C. Wang, H. Shang, H. Xu, Y. Du, Nanoboxes endow non-noble-metal-based electrocatalysts with high efficiency for overall water splitting, J. Mater. Chem. A. (2021), https://doi.org/10.1039/d0ta10596a.
[29] Q. Wen, Y. Zhao, Y. Liu, H. Li, T. Zhai, Ultrahigh-current-density and long-term-durability electrocatalysts for water splitting, Small (2022), https://doi.org/10.1002/smll.202104513.
[30] X. Liu, M. Gong, S. Deng, T. Zhao, T. Shen, J. Zhang, D. Wang, Transforming damage into benefit: corrosion engineering enabled electrocatalysts for water splitting, Adv. Funct. Mater. (2021), https://doi.org/10.1002/adfm.202009032.
[31] J. Zhang, C. Liu, B. Zhang, Insights into single-atom metal–support interactions in electrocatalytic water splitting, Small Methods 3 (2019) 1–15, https://doi.org/10.1002/smtd.201800481.
[32] A.R. Zeradjanin, P. Narangoda, I. Spanos, J. Masa, R. Schlögl, How to minimise destabilising effect of gas bubbles on water splitting electrocatalysts? Curr. Opin. Electrochem. (2021) https://doi.org/10.1016/j.coelec.2021.100797.
[33] J. Zhang, Q. Zhang, X. Feng, Support and interface effects in water-splitting electrocatalysts, Adv. Mater. 31 (2019) 1–19, https://doi.org/10.1002/adma.201808167.
[34] M. Görlin, P. Chernev, J.F. De Araújo, T. Reier, S. Dresp, B. Paul, R. Krähnert, H. Dau, P. Strasser, Oxygen evolution reaction dynamics, faradaic charge efficiency, and the active metal redox states of Ni-Fe oxide water splitting electrocatalysts, J. Am. Chem. Soc. (2016), https://doi.org/10.1021/jacs.6b00332.
[35] J.S. Yoo, X. Rong, Y. Liu, A.M. Kolpak, Role of lattice oxygen participation in understanding trends in the oxygen evolution reaction on perovskites, ACS Catal. (2018), https://doi.org/10.1021/acscatal.8b00612.
[36] E. Fabbri, M. Nachtegaal, T. Binninger, X. Cheng, B.J. Kim, J. Durst, F. Bozza, T. Graule, R. Schäublin, L. Wiles, M. Pertoso, N. Danilovic, K.E. Ayers, T. J. Schmidt, Dynamic surface self-reconstruction is the key of highly active perovskite nano-electrocatalysts for water splitting, Nat. Mater. (2017), https://doi.org/10.1038/nmat4938.
[37] H. Liu, M. Jin, D. Zhan, J. Wang, X. Cai, Y. Qiu, L. Lai, Stacking faults triggered strain engineering of ZIF-67 derived Ni-Co bimetal phosphide for enhanced overall water splitting, Appl. Catal. B Environ. (2020), https://doi.org/10.1016/j.apcatb.2020.118951.
[38] G. Chen, Z. Hu, Y. Zhu, B. Gu, Y. Zhong, H.J. Lin, C. Te Chen, W. Zhou, Z. Shao, A universal strategy to design superior water-splitting electrocatalysts based on fast in situ reconstruction of amorphous nanofilm precursors, Adv. Mater. 30 (2018) 1–8, https://doi.org/10.1002/adma.201804333.
[39] F. Te Tsai, Y.Y. Chuang, H.H. Hsieh, Y.H. Chen, C.W. Pao, J.L. Chen, C.Y. Lu, C. K. Hao, W.F. Liaw, Morphological and electronic optimization of nanostructured FeCoNi-based electrocatalysts by Al dopants for neutral/alkaline water splitting, ACS Appl. Energy Mater. (2022), https://doi.org/10.1021/acsaem.2c00238.
[40] J. Yin, J. Jin, H. Lin, Z. Yin, J. Li, M. Lu, L. Guo, P. Xi, Y. Tang, C.H. Yan, Optimized metal chalcogenides for boosting water splitting, Adv. Sci. (2020), https://doi.org/10.1002/advs.201903070.
[41] X. Du, J. Huang, J. Zhang, Y. Yan, C. Wu, Y. Hu, C. Yan, T. Lei, W. Chen, C. Fan, J. Xiong, Modulating electronic structures of inorganic nanomaterials for efficient electrocatalytic water splitting, Angew. Chem. - Int. Ed. (2019), https://doi.org/10.1002/anie.201810104.
[42] Y. Guo, X. Zhou, J. Tang, S. Tanaka, Y.V. Kaneti, J. Na, B. Jiang, Y. Yamauchi, Y. Bando, Y. Sugahara, Multiscale structural optimization: Highly efficient hollow iron-doped metal sulfide heterostructures as bifunctional electrocatalysts for water splitting, Nano Energy (2020), https://doi.org/10.1016/j.nanoen.2020.104913.
[43] M. Gu, X. Deng, M. Lin, H. Wang, A. Gao, X. Huang, X. Zhang, Ultrathin NiCo bimetallic molybdate nanosheets coated CuOx nanotubes: heterostructure and bimetallic synergistic optimization of the active site for highly efficient overall water splitting, Adv. Energy Mater. (2021), https://doi.org/10.1002/aenm.202102361.
[44] T. Ul Haq, S. Mansour, Y. Haik, Electronic and structural modification of Mn3O4nanosheets for selective and sustained seawater oxidation, ACS Appl. Mater. Interfaces (2021), https://doi.org/10.1021/acsami.1c24304.
[45] L. Huang, Z. Li, S. Sun, G. Sun, Y. Li, S. Han, J. Lian, Nis/Mos2 complex grown on carbon paper as bifunctional electrocatalyst for full water splitting, SSRN Electron. J. (2022), https://doi.org/10.2139/ssrn.4047630.
[46] D. Liu, Z. Song, S. Cheng, Y. Wang, A. Saad, S. Deng, J. Shen, X. Huang, X. Cai, P. Tsiakaras, Mesoporous IrNiTa metal glass ribbon as a superior self-standing bifunctional catalyst for water electrolysis, Chem. Eng. J. (2022), https://doi.org/10.1016/j.cej.2021.134210.
[47] H. Liu, C. Xi, J. Xin, G. Zhang, S. Zhang, Z. Zhang, Q. Huang, J. Li, H. Liu, J. Kang, Free-standing nanoporous NiMnFeMo alloy: An efficient non-precious metal electrocatalyst for water splitting, Chem. Eng. J. (2021), https://doi.org/10.1016/j.cej.2020.126530.
[48] A. Majeed, P.X. Hou, F. Zhang, H. Tabassum, X. Li, G.X. Li, C. Liu, H.M. Cheng, A. Freestanding Single-Wall, Carbon nanotube film decorated with N-doped carbon-encapsulated Ni nanoparticles as a bifunctional electrocatalyst for overall water splitting, Adv. Sci. (2019), https://doi.org/10.1002/advs.201802177.
[49] S. Anantharaj, S. Kundu, Do the evaluation parameters reflect intrinsic activity of electrocatalysts in electrochemical water splitting? ACS Energy Lett. (2019) https://doi.org/10.1021/acsenergylett.9b00686.
[50] F. Luo, L. Guo, Y. Xie, J. Xu, K. Qu, Z. Yang, Iridium nanorods as a robust and stable bifunctional electrocatalyst for pH-universal water splitting, Appl. Catal. B Environ. (2020), https://doi.org/10.1016/j.apcatb.2020.119394.
[51] W. Liu, D. Cao, D. Cheng, Review on synthesis and catalytic coupling mechanism of highly active electrocatalysts for water splitting, Energy Technol. (2021), https://doi.org/10.1002/ente.202000855.
[52] S.B. Karki, A.N. Andriotis, M. Menon, F. Ramezanipour, Bifunctional water-splitting electrocatalysis achieved by defect order in LaA2Fe3O8(A = Ca, Sr), ACS Appl. Energy Mater. (2021), https://doi.org/10.1021/acsaem.1c02028.
[53] A. Indra, P.W. Menezes, I. Zaharieva, H. Dau, M. Driess, Detecting structural transformation of cobalt phosphonate to active bifunctional catalysts for electrochemical water-splitting, J. Mater. Chem. A. (2020), https://doi.org/10.1039/c9ta09775a.
[54] Z. Wang, N. Heng, X. Wang, J. He, Y. Zhao, Surface and morphology structure evolution of metal phosphide for designing overall water splitting electrocatalyst, J. Catal. (2019), https://doi.org/10.1016/j.jcat.2019.04.016.
[55] H. Li, S. Chen, X. Jia, B. Xu, H. Lin, H. Yang, L. Song, X. Wang, Amorphous nickel-cobalt complexes hybridized with 1T-phase molybdenum disulfide via hydrazine-induced phase transformation for water splitting, Nat. Commun. (2017), https://doi.org/10.1038/ncomms15377.
[56] C. Jin, P. Zhai, Y. Wei, Q. Chen, X. Wang, W. Yang, J. Xiao, Q. He, Q. Liu, Y. Gong, Ni(OH)2 templated synthesis of ultrathin Ni3S2 Nanosheets as bifunctional electrocatalyst for overall water splitting, Small (2021), https://doi.org/10.1002/smll.202102097.
[57] Y. Kim, P.P. Lopes, S. Park, A. Lee, J. Lim, H. Lee, S. Back, Y. Jung, N. Danilovic, V. Stamenkovic, J. Erlebacher, J. Snyder, N.M. Markovic, oxygen evolution catalysts, Nat. Commun. (n.d.) 1–8. ⟨doi:10.1038/s41467–017-01734–7⟩.
[58] J. Knöppel, M. Möckl, D. Escalera-López, K. Stojanovski, M. Bierling, T. Böhm, S. Thiele, M. Rzepka, S. Cherevko, On the limitations in assessing stability of oxygen evolution catalysts using aqueous model electrochemical cells, Nat. Commun. (2021), https://doi.org/10.1038/s41467-021-22296-9.
[59] W.H. Lee, M.H. Han, Y.J. Ko, B.K. Min, K.H. Chae, H.S. Oh, Electrode reconstruction strategy for oxygen evolution reaction: maintaining Fe-CoOOH phase with intermediate-spin state during electrolysis, Nat. Commun. (2022), https://doi.org/10.1038/s41467-022-28260-5.
[60] T. Binninger, R. Mohamed, K. Waltar, E. Fabbri, P. Levecque, R. Kötz, T. J. Schmidt, Thermodynamic explanation of the universal correlation between oxygen evolution activity and corrosion of oxide catalysts, Sci. Rep. (2015), https://doi.org/10.1038/srep12167.
[61] A.E. Thorarinsdottir, S.S. Veroneau, D.G. Nocera, Self-healing oxygen evolution catalysts, Nat. Commun. (2022), https://doi.org/10.1038/s41467-022-28723-9.
[62] C. Feng, F. Wang, Z. Liu, M. Nakabayashi, Y. Xiao, Q. Zeng, J. Fu, Q. Wu, C. Cui, Y. Han, N. Shibata, K. Domen, I.D. Sharp, Y. Li, A self-healing catalyst for electrocatalytic and photoelectrochemical oxygen evolution in highly alkaline conditions, Nat. Commun. (2021), https://doi.org/10.1038/s41467-021-26281-0.
[63] Y. Surendranath, D.G. Nocera, Oxygen evolution reaction chemistry of oxide-based electrodes, Prog. Inorg. Chem. (2011), https://doi.org/10.1002/9781118148235.ch9.
[64] J. Li, C.A. Triana, W. Wan, D.P. Adiyeri Saseendran, Y. Zhao, S.E. Balaghi, S. Heidari, G.R. Patzke, Molecular and heterogeneous water oxidation catalysts: recent progress and joint perspectives, Chem. Soc. Rev. (2021), https://doi.org/10.1039/d0cs00978d.

[65] C. Hu, L. Zhang, J. Gong, Recent progress made in the mechanism comprehension and design of electrocatalysts for alkaline water splitting, Energy Environ. Sci. (2019), https://doi.org/10.1039/c9ee01202h.
[66] D. Cao, H. Xu, D. Cheng, Branch-leaf-shaped CuNi@NiFeCu nanodendrites as highly efficient electrocatalysts for overall water splitting, Appl. Catal. B Environ. (2021), https://doi.org/10.1016/j.apcatb.2021.120600.
[67] P.S.Camillo Spöri, Jason Tai Hong Kwan, Arman Bonakdarpour, David P. Wilkinson, Chemie, Angew. Chem. Int. Ed. Engl. (n.d.) doi:10.1002/anie.201608601.
[68] J. Shan, C. Ye, S. Chen, T. Sun, Y. Jiao, L. Liu, C. Zhu, L. Song, Y. Han, M. Jaroniec, Y. Zhu, Y. Zheng, S.Z. Qiao, Short-range ordered iridium single atoms integrated into cobalt oxide spinel structure for highly efficient electrocatalytic water oxidation, J. Am. Chem. Soc. (2021), https://doi.org/10.1021/jacs.1c01525.
[69] X. Tang, S. Wang, L. Qian, M. Ren, P. Sun, Y. Li, J.Q. Yang, Corrosion properties of candidate materials in supercritical water oxidation process, J. Adv. Oxid. Technol. (2016), https://doi.org/10.1515/jaots-2016-0119.
[70] S. Cherevko, A.R. Zeradjanin, A.A. Topalov, N. Kulyk, I. Katsounaros, K.J. J. Mayrhofer, Dissolution of noble metals during oxygen evolution in acidic media, ChemCatChem (2014), https://doi.org/10.1002/cctc.201402194.
[71] N.T. Suen, S.F. Hung, Q. Quan, N. Zhang, Y.J. Xu, H.M. Chen, Electrocatalysis for the oxygen evolution reaction: recent development and future perspectives, Chem. Soc. Rev. 46 (2017) 337–365, https://doi.org/10.1039/c6cs00328a.
[72] F. Luo, H. Hu, X. Zhao, Z. Yang, Q. Zhang, J. Xu, T. Kaneko, Y. Yoshida, C. Zhu, W. Cai, Robust and stable acidic overall water splitting on ir single atoms, Nano Lett. (2020), https://doi.org/10.1021/acs.nanolett.0c00127.
[73] C.H.M. Van Oversteeg, H.Q. Doan, F.M.F. De Groot, T. Cuk, In situ X-ray absorption spectroscopy of transition metal based water oxidation catalysts, Chem. Soc. Rev. (2017), https://doi.org/10.1039/c6cs00230g.
[74] D.Y. Chung, P.P. Lopes, P. Farinazzo Bergamo Dias Martins, H. He, T. Kawaguchi, P. Zapol, H. You, D. Tripkovic, D. Strmcnik, Y. Zhu, S. Seifert, S. Lee, V. R. Stamenkovic, N.M. Markovic, Dynamic stability of active sites in hydr(oxy) oxides for the oxygen evolution reaction, Nat. Energy 5 (2020) 222–230, https://doi.org/10.1038/s41560-020-0576-y.
[75] C.C.L. McCrory, S. Jung, J.C. Peters, T.F. Jaramillo, Benchmarking heterogeneous electrocatalysts for the oxygen evolution reaction, J. Am. Chem. Soc. 135 (2013) 16977–16987, https://doi.org/10.1021/ja407115p.
[76] X. Xie, L. Du, L. Yan, S. Park, Y. Qiu, J. Sokolowski, W. Wang, Y. Shao, Oxygen evolution reaction in alkaline environment: material challenges and solutions, Adv. Funct. Mater. (2022), https://doi.org/10.1002/adfm.202110036.
[77] H. Dau, C. Limberg, T. Reier, M. Risch, S. Roggan, P. Strasser, The mechanism of water oxidation: from electrolysis via homogeneous to biological catalysis, ChemCatChem 2 (2010) 724–761, https://doi.org/10.1002/cctc.201000126.
[78] A. Zagalskaya, V. Alexandrov, Role of defects in the interplay between adsorbate evolving and lattice oxygen mechanisms of the oxygen evolution reaction in RuO2 and IrO2, ACS Catal. (2020), https://doi.org/10.1021/acscatal.9b05544.
[79] A. Grimaud, O. Diaz-Morales, B. Han, W.T. Hong, Y.L. Lee, L. Giordano, K. A. Stoerzinger, M.T.M. Koper, Y. Shao-Horn, Activating lattice oxygen redox reactions in metal oxides to catalyse oxygen evolution, Nat. Chem. (2017), https://doi.org/10.1038/nchem.2695.
[80] Z.F. Huang, J. Song, Y. Du, S. Xi, S. Dou, J.M.V. Nsanzimana, C. Wang, Z.J. Xu, X. Wang, Chemical and structural origin of lattice oxygen oxidation in Co–Zn oxyhydroxide oxygen evolution electrocatalysts, Nat. Energy 4 (2019) 329–338, https://doi.org/10.1038/s41560-019-0355-9.
[81] A. Moysiadou, S. Lee, C.S. Hsu, H.M. Chen, X. Hu, Mechanism of oxygen evolution catalyzed by cobalt oxyhydroxide: cobalt superoxide species as a key intermediate and dioxygen release as a rate-determining step, J. Am. Chem. Soc. (2020), https://doi.org/10.1021/jacs.0c04867.
[82] M.J. Craig, G. Coulter, E. Dolan, J. Soriano-López, E. Mates-Torres, W. Schmitt, M. García-Melchor, Universal scaling relations for the rational design of molecular water oxidation catalysts with near-zero overpotential, Nat. Commun. (2019), https://doi.org/10.1038/s41467-019-12994-w.
[83] M.T.M. Koper, Thermodynamic theory of multi-electron transfer reactions: Implications for electrocatalysis, J. Electroanal. Chem. (2011), https://doi.org/10.1016/j.jelechem.2010.10.004.
[84] X. Cui, P. Ren, C. Ma, J. Zhao, R. Chen, S. Chen, N.P. Rajan, H. Li, L. Yu, Z. Tian, D. Deng, Robust interface Ru centers for high-performance acidic oxygen evolution, Adv. Mater. (2020), https://doi.org/10.1002/adma.201908126.
[85] A.J. Medford, A. Vojvodic, J.S. Hummelshøj, J. Voss, F. Abild-Pedersen, F. Studt, T. Bligaard, A. Nilsson, J.K. Nørskov, From the Sabatier principle to a predictive theory of transition-metal heterogeneous catalysis, J. Catal. (2015), https://doi.org/10.1016/j.jcat.2014.12.033.
[86] O. Diaz-Morales, I. Ledezma-Yanez, M.T.M. Koper, F. Calle-Vallejo, Guidelines for the rational design of Ni-based double hydroxide electrocatalysts for the oxygen evolution reaction, ACS Catal. (2015), https://doi.org/10.1021/acscatal.5b01638.
[87] T. Ling, D.Y. Yan, Y. Jiao, H. Wang, Y. Zheng, X. Zheng, J. Mao, X.W. Du, Z. Hu, M. Jaroniec, S.Z. Qiao, Engineering surface atomic structure of single-crystal cobalt (II) oxide nanorods for superior electrocatalysis, Nat. Commun. (2016), https://doi.org/10.1038/ncomms12876.
[88] J.R. Petrie, V.R. Cooper, J.W. Freeland, T.L. Meyer, Z. Zhang, D.A. Lutterman, H. N. Lee, Enhanced bifunctional oxygen catalysis in strained LaNiO3 perovskites, J. Am. Chem. Soc. (2016), https://doi.org/10.1021/jacs.5b11713.
[89] J. Chen, F. Zheng, S.J. Zhang, A. Fisher, Y. Zhou, Z. Wang, Y. Li, B. Bin Xu, J.T. Li, S.G. Sun, Interfacial Interaction between FeOOH and Ni-Fe LDH to Modulate the Local Electronic Structure for Enhanced OER Electrocatalysis, ACS Catal. (2018), https://doi.org/10.1021/acscatal.8b03489.
[90] P.P. Lopes, D.Y. Chung, X. Rui, H. Zheng, H. He, P. Farinazzo Bergamo Dias Martins, D. Strmcnik, V.R. Stamenkovic, P. Zapol, J.F. Mitchell, R.F. Klie, N. M. Markovic, Dynamically stable active sites from surface evolution of perovskite materials during the oxygen evolution reaction, J. Am. Chem. Soc. (2021), https://doi.org/10.1021/jacs.0c08959.
[91] Y. Liu, Q. Li, R. Si, G.D. Li, W. Li, D.P. Liu, D. Wang, L. Sun, Y. Zhang, X. Zou, Coupling sub-nanometric copper clusters with quasi-amorphous cobalt sulfide yields efficient and robust electrocatalysts for water splitting reaction, Adv. Mater. (2017), https://doi.org/10.1002/adma.201606200.
[92] B. Chakraborty, R. Beltrán-Suito, J.N. Hausmann, S. Garai, M. Driess, P. W. Menezes, Enabling iron-based highly effective electrochemical water-splitting and selective oxygenation of organic substrates through in situ surface modification of intermetallic iron stannide precatalyst, Adv. Energy Mater. (2020), https://doi.org/10.1002/aenm.202001377.
[93] T.U. Haq, Y. Haik, I. Hussain, H.U. Rehman, T.A. Al-Ansari, Gd-doped Ni-oxychloride nanoclusters: new nanoscale electrocatalysts for high-performance water oxidation through surface and structural modification, ACS Appl. Mater. Interfaces 13 (2021) 468–479, https://doi.org/10.1021/acsami.0c17216.
[94] X.J. Chua, J. Luxa, A.Y.S. Eng, S.M. Tan, Z. Sofer, M. Pumera, Negative electrocatalytic effects of p-doping niobium and tantalum on MoS2 and WS2 for the hydrogen evolution reaction and oxygen reduction reaction, ACS Catal. 6 (2016) 5724–5734, https://doi.org/10.1021/acscatal.6b01593.
[95] S. Zhou, X. Miao, X. Zhao, C. Ma, Y. Qiu, Z. Hu, J. Zhao, L. Shi, J. Zeng, Engineering electrocatalytic activity in nanosized perovskite cobaltite through surface spin-state transition, Nat. Commun. 7 (2016) 1–7, https://doi.org/10.1038/ncomms11510.
[96] J.W.D. Ng, M. García-Melchor, M. Bajdich, P. Chakthranont, C. Kirk, A. Vojvodic, T.F. Jaramillo, Gold-supported cerium-doped NiO x catalysts for water oxidation, Nat. Energy 1 (2016) 1–8, https://doi.org/10.1038/nenergy.2016.53.
[97] T. ul Haq, S.A. Mansour, A. Munir, Y. Haik, Gold-supported gadolinium doped CoB amorphous sheet: a new benchmark electrocatalyst for water oxidation with high turnover frequency, Adv. Funct. Mater. 1910309 (2020) 1–11, https://doi.org/10.1002/adfm.201910309.
[98] L. Li, Z. Hu, L. Tao, J. Xu, J.C. Yu, Efficient electronic transport in partially disordered Co3O4 nanosheets for electrocatalytic oxygen evolution reaction, ACS Appl. Energy Mater. (2020), https://doi.org/10.1021/acsaem.0c00190.
[99] J.A.D. del Rosario, G. Li, M.F.M. Labata, J.D. Ocon, P.Y.A. Chuang, Unravelling the roles of alkali-metal cations for the enhanced oxygen evolution reaction in alkaline media, Appl. Catal. B Environ. 288 (2021), 119981, https://doi.org/10.1016/j.apcatb.2021.119981.
[100] Y. Sun, T. Zhang, C. Li, K. Xu, Y. Li, Compositional engineering of sulfides, phosphides, carbides, nitrides, oxides, and hydroxides for water splitting, J. Mater. Chem. A. 8 (2020) 13415–13436, https://doi.org/10.1039/d0ta05038e.
[101] P. Chen, T. Zhou, M. Zhang, Y. Tong, C. Zhong, N. Zhang, L. Zhang, C. Wu, Y. Xie, 3D nitrogen-anion-decorated nickel sulfides for highly efficient overall water splitting, Adv. Mater. (2017), https://doi.org/10.1002/adma.201701584.
[102] B. Zhang, F. Yang, X. Liu, N. Wu, S. Che, Y. Li, Phosphorus doped nickel-molybdenum aerogel for efficient overall water splitting, Appl. Catal. B Environ. 298 (2021), https://doi.org/10.1016/j.apcatb.2021.120494.
[103] J. Wang, J. Hu, C. Liang, L. Chang, Y. Du, X. Han, J. Sun, P. Xu, Surface reconstruction of phosphorus-doped cobalt molybdate microarrays in electrochemical water splitting, Chem. Eng. J. 446 (2022), 137094, https://doi.org/10.1016/j.cej.2022.137094.
[104] C. Liu, D. Jia, Q. Hao, X. Zheng, Y. Li, C. Tang, H. Liu, J. Zhang, X. Zheng, P-doped iron-nickel sulfide nanosheet arrays for highly efficient overall water splitting, ACS Appl. Mater. Interfaces (2019), https://doi.org/10.1021/acsami.9b04528.
[105] S. Li, L. Wang, H. Su, A.N. Hong, Y. Wang, H. Yang, L. Ge, W. Song, J. Liu, T. Ma, X. Bu, P. Feng, Electron redistributed s-doped nickel iron phosphides derived from one-step phosphatization of MOFs for significantly boosting electrochemical water splitting, Adv. Funct. Mater. (2022), https://doi.org/10.1002/adfm.202200733.
[106] M.A.R. Anjum, M.S. Okyay, M. Kim, M.H. Lee, N. Park, J.S. Lee, Bifunctional sulfur-doped cobalt phosphide electrocatalyst outperforms all-noble-metal electrocatalysts in alkaline electrolyzer for overall water splitting, Nano Energy (2018), https://doi.org/10.1016/j.nanoen.2018.08.064.
[107] T. ul Haq, Y. Haik, S doped Cu2O-CuO nanoneedles array: Free standing oxygen evolution electrode with high efficiency and corrosion resistance for seawater splitting, Catal. Today (2021), https://doi.org/10.1016/j.cattod.2021.09.015.
[108] W.K. Jo, S. Moru, S. Tonda, Cobalt-coordinated sulfur-doped graphitic carbon nitride on reduced graphene oxide: an efficient metal-(n,s)-c-class bifunctional electrocatalyst for overall water splitting in alkaline media, ACS Sustain. Chem. Eng. (2019), https://doi.org/10.1021/acssuschemeng.9b02705.
[109] X. Wang, W. Li, D. Xiong, D.Y. Petrovykh, L. Liu, Bifunctional nickel phosphide nanocatalysts supported on carbon fiber paper for highly efficient and stable overall water splitting, Adv. Funct. Mater. 26 (2016) 4067–4077, https://doi.org/10.1002/adfm.201505509.
[110] C. Tang, N. Cheng, Z. Pu, W. Xing, X. Sun, NiSe nanowire film supported on nickel foam: an efficient and stable 3d bifunctional electrode for full water splitting, Angew. Chem. - Int. Ed. 54 (2015) 9351–9355, https://doi.org/10.1002/anie.201503407.
[111] X. Chen, Z. Qiu, H. Xing, S. Fei, J. Li, L. Ma, Y. Li, D. Liu, Sulfur-doping/leaching induced structural transformation toward boosting electrocatalytic water splitting, Appl. Catal. B Environ. (2022), https://doi.org/10.1016/j.apcatb.2021.121030.

[112] S. Niu, W.J. Jiang, Z. Wei, T. Tang, J. Ma, J.S. Hu, L.J. Wan, Se-doping activates FeOOH for cost-effective and efficient electrochemical water oxidation, J. Am. Chem. Soc. 141 (2019) 7005–7013, https://doi.org/10.1021/jacs.9b01214.
[113] J. Zhu, M. Sun, S. Liu, X. Liu, K. Hu, L. Wang, Study of active sites on Se-MnS/NiS heterojunctions as highly efficient bifunctional electrocatalysts for overall water splitting, J. Mater. Chem. A. (2019), https://doi.org/10.1039/c9ta10860b.
[114] X. Du, Y. Ding, X. Zhang, Selectively Se-doped Co3O4@CeO2 nanoparticle-dotted nanoneedle arrays for high-efficiency overall water splitting, Appl. Surf. Sci. (2021), https://doi.org/10.1016/j.apsusc.2021.150227.
[115] H. Jin, X. Liu, S. Chen, A. Vasileff, L. Li, Y. Jiao, L. Song, Y. Zheng, S.Z. Qiao, Heteroatom-doped transition metal electrocatalysts for hydrogen evolution reaction, ACS Energy Lett. 4 (2019) 805–810, https://doi.org/10.1021/acsenergylett.9b00348.
[116] K. Liang, L. Guo, K. Marcus, S. Zhang, Z. Yang, D.E. Perea, L. Zhou, Y. Du, Y. Yang, Overall water splitting with room-temperature synthesized NiFe oxyfluoride nanoporous films, ACS Catal. 7 (2017) 8406–8412, https://doi.org/10.1021/acscatal.7b02991.
[117] H. Han, J. Woo, Y.R. Hong, Y.C. Chung, S. Mhin, Polarized electronic configuration in transition metal-fluoride oxide hollow nanoprism for highly efficient and robust water splitting, ACS Appl. Energy Mater. (2019), https://doi.org/10.1021/acsaem.9b00449.
[118] H. Jiang, Q. He, X. Li, X. Su, Y. Zhang, S. Chen, S. Zhang, G. Zhang, J. Jiang, Y. Luo, P.M. Ajayan, L. Song, Tracking structural self-reconstruction and identifying true active sites toward cobalt oxychloride precatalyst of oxygen evolution reaction, Adv. Mater. 31 (2019) 1–8, https://doi.org/10.1002/adma.201805127.
[119] Z. Xiao, Y. Wang, Y.C. Huang, Z. Wei, C.L. Dong, J. Ma, S. Shen, Y. Li, S. Wang, Filling the oxygen vacancies in Co3O4 with phosphorus: an ultra-efficient electrocatalyst for overall water splitting, Energy Environ. Sci. (2017), https://doi.org/10.1039/c7ee01917c.
[120] Y. Tang, C. Yang, X. Xu, Y. Kang, J. Henzie, W. Que, Y. Yamauchi, MXene nanoarchitectonics: defect-engineered 2D MXenes towards enhanced electrochemical water splitting, Adv. Energy Mater. (2022), https://doi.org/10.1002/aenm.202103867.
[121] T.I. Singh, G. Rajeshkhanna, U.N. Pan, T. Kshetri, H. Lin, N.H. Kim, J.H. Lee, Alkaline water splitting enhancement by MOF-derived Fe–Co–Oxide/Co@NC-mNS heterostructure: boosting OER and HER through defect engineering and in situ oxidation, Small (2021), https://doi.org/10.1002/smll.202101312.
[122] S. Huang, Z. Jin, P. Ning, C. Gao, Y. Wu, X. Liu, P. Xin, Z. Chen, Y. Jiang, Z. Hu, Z. Chen, Synergistically modulating electronic structure of NiS2 hierarchical architectures by phosphorus doping and sulfur-vacancies defect engineering enables efficient electrocatalytic water splitting, Chem. Eng. J. (2021), https://doi.org/10.1016/j.cej.2020.127630.
[123] L. Wang, C. Peng, H. Lin, B. Zhao, Unraveling the role of defects in electrocatalysts for water splitting: recent advances and perspectives, Energy Fuels (2022), https://doi.org/10.1021/acs.energyfuels.2c02017.
[124] W. Lei, Y. Yu, H. Zhang, Q. Jia, S. Zhang, Defect engineering of nanostructures: Insights into photoelectrochemical water splitting, Mater. Today (2022), https://doi.org/10.1016/j.mattod.2021.10.028.
[125] J. Zhang, H. Zhou, Y. Liu, J. Zhang, Y. Cui, J. Li, J. Lian, G. Wang, Q. Jiang, Interface engineering of CoP3/Ni2P for boosting the wide pH range water-splitting activity, ACS Appl. Mater. Interfaces (2021), https://doi.org/10.1021/acsami.1c14685.
[126] P. Zhai, M. Xia, Y. Wu, G. Zhang, J. Gao, B. Zhang, S. Cao, Y. Zhang, Z. Li, Z. Fan, C. Wang, X. Zhang, J.T. Miller, L. Sun, J. Hou, Engineering single-atomic ruthenium catalytic sites on defective nickel-iron layered double hydroxide for overall water splitting, Nat. Commun. (2021), https://doi.org/10.1038/s41467-021-24828-9.
[127] H. Li, S. Wu, Z.D. Hood, J. Sun, B. Hu, C. Liang, S. Yang, Y. Xu, B. Jiang, Atomic defects in ultra-thin mesoporous TiO2 enhance photocatalytic hydrogen evolution from water splitting, Appl. Surf. Sci. (2020), https://doi.org/10.1016/j.apsusc.2020.145723.
[128] H. Liu, Q. He, H. Jiang, Y. Lin, Y. Zhang, M. Habib, S. Chen, L. Song, Electronic Structure Reconfiguration toward Pyrite NiS2 via Engineered Heteroatom Defect Boosting Overall Water Splitting, ACS Nano (2017), https://doi.org/10.1021/acsnano.7b06501.
[129] W. Li, H. Zhang, M. Hong, L. Zhang, X. Feng, M. Shi, W. Hu, S. Mu, Defective RuO2/TiO2 nano-heterostructure advances hydrogen production by electrochemical water splitting, Chem. Eng. J. (2022), https://doi.org/10.1016/j.cej.2021.134072.
[130] Y. Wu, R. Yao, Q. Zhao, J. Li, G. Liu, La-RuO2 nanocrystals with efficient electrocatalytic activity for overall water splitting in acidic media: Synergistic effect of La doping and oxygen vacancy, Chem. Eng. J. (2022), https://doi.org/10.1016/j.cej.2022.135699.
[131] W. Yang, J. Zeng, Y. Hua, C. Xu, S.S. Siwal, Q. Zhang, Defect engineering of cobalt microspheres by S doping and electrochemical oxidation as efficient bifunctional and durable electrocatalysts for water splitting at high current densities, J. Power Sources (2019), https://doi.org/10.1016/j.jpowsour.2019.226887.
[132] L. Wang, Y. Hao, L. Deng, F. Hu, S. Zhao, L. Li, S. Peng, Rapid complete reconfiguration induced actual active species for industrial hydrogen evolution reaction, Nat. Commun. 13 (2022), https://doi.org/10.1038/s41467-022-33590-5.
[133] J. Zhang, Q. Xu, J. Wang, Y. Li, H. Jiang, C. Li, Dual-defective Co3O4 nanoarrays enrich target intermediates and promise high-efficient overall water splitting, Chem. Eng. J. (2021), https://doi.org/10.1016/j.cej.2021.130328.
[134] D. Liu, H. Ai, J. Li, M. Fang, M. Chen, D. Liu, X. Du, P. Zhou, F. Li, K.H. Lo, Y. Tang, S. Chen, L. Wang, G. Xing, H. Pan, Surface reconstruction and phase transition on vanadium–cobalt–iron trimetal nitrides to form active oxyhydroxide for enhanced electrocatalytic water oxidation, Adv. Energy Mater. (2020), https://doi.org/10.1002/aenm.202002464.
[135] X. Liu, R. Guo, K. Ni, F. Xia, C. Niu, B. Wen, J. Meng, P. Wu, J. Wu, X. Wu, L. Mai, Reconstruction-determined alkaline water electrolysis at industrial temperatures, Adv. Mater. (2020), https://doi.org/10.1002/adma.202001136.
[136] F. Polo-Garzon, Z. Bao, X. Zhang, W. Huang, Z. Wu, Surface reconstructions of metal oxides and the consequences on catalytic chemistry, ACS Catal. (2019), https://doi.org/10.1021/acscatal.9b01097.
[137] S. Park, M. Shviro, H. Hartmann, A. Besmehn, J. Mayer, D. Stolten, M. Carmo, Nickel structures as a template strategy to create shaped iridium electrocatalysts for electrochemical water splitting, ACS Appl. Mater. Interfaces (2021), https://doi.org/10.1021/acsami.0c23026.
[138] B.N. Khiarak, A.A. Zahraei, K. nazarzade, H.R.A. Hasanjani, H. Mohammadzadeh, Shape-controlled synthesis of thorn-like 1D phosphorized Co supported by Ni foam electrocatalysts for overall water splitting, J. Mater. Sci. Mater. Electron. (2021), https://doi.org/10.1007/s10854-021-06379-3.
[139] N. Zhang, Q. Shao, Y. Pi, J. Guo, X. Huang, Solvent-mediated shape tuning of well-defined rhodium nanocrystals for efficient electrochemical water splitting, Chem. Mater. (2017), https://doi.org/10.1021/acs.chemmater.7b01588.
[140] B. You, M.T. Tang, C. Tsai, F. Abild-Pedersen, X. Zheng, H. Li, Enhancing electrocatalytic water splitting by strain engineering, Adv. Mater. (2019), https://doi.org/10.1002/adma.201807001.
[141] M. Li, Z. Zhao, Z. Xia, M. Luo, Q. Zhang, Y. Qin, L. Tao, K. Yin, Y. Chao, L. Gu, W. Yang, Y. Yu, G. Lu, S. Guo, Exclusive strain effect boosts overall water splitting in PdCu/Ir core/shell nanocrystals, Angew. Chem. - Int. Ed. (2021), https://doi.org/10.1002/anie.202016199.
[142] J. Masa, P. Weide, D. Peeters, I. Sinev, W. Xia, Z. Sun, C. Somsen, M. Muhler, W. Schuhmann, Amorphous cobalt boride (Co2B) as a highly efficient nonprecious catalyst for electrochemical water splitting: oxygen and hydrogen evolution, Adv. Energy Mater. (2016), https://doi.org/10.1002/aenm.201600980.
[143] Y. Wang, X. Li, M. Zhang, Y. Zhou, D. Rao, C. Zhong, J. Zhang, X. Han, W. Hu, Y. Zhang, K. Zaghib, Y. Wang, Y. Deng, Lattice-strain engineering of homogeneous NiS0.5Se0.5 core–shell nanostructure as a highly efficient and robust electrocatalyst for overall water splitting, Adv. Mater. (2020), https://doi.org/10.1002/adma.202000231.
[144] C. Li, S. Yan, J. Fang, Construction of lattice strain in bimetallic nanostructures and its effectiveness in electrochemical applications, Small (2021), https://doi.org/10.1002/smll.202102244.
[145] W. Sun, Z. Zhou, W.Q. Zaman, L.M. Cao, J. Yang, Rational manipulation of IrO2 lattice strain on α-MnO2 nanorods as a highly efficient water-splitting catalyst, ACS Appl. Mater. Interfaces (2017), https://doi.org/10.1021/acsami.7b12775.
[146] M. Li, Z. Zhao, Z. Xia, M. Luo, Q. Zhang, Y. Qin, L. Tao, K. Yin, Y. Chao, L. Gu, W. Yang, Y. Yu, G. Lu, S. Guo, Exclusive strain effect boosts overall water splitting in PdCu/Ir Core/shell nanocrystals, Angew. Chem. (2021), https://doi.org/10.1002/ange.202016199.
[147] X. Gao, Y. Zhou, Y. Tan, S. Liu, Z. Cheng, Z. Shen, Strain effects on Co,N co-decorated graphyne catalysts for overall water splitting electrocatalysis, Phys. Chem. Chem. Phys. (2020), https://doi.org/10.1039/c9cp05548g.
[148] H.N. Nong, H.S. Oh, T. Reier, E. Willinger, M.G. Willinger, V. Petkov, D. Teschner, P. Strasser, Oxide-supported IrNiOx core-shell particles as efficient, cost-effective, and stable catalysts for electrochemical water splitting, Angew. Chem. - Int. Ed. (2015), https://doi.org/10.1002/anie.201411072.
[149] D. Thanh Tran, T. Kshetri, N. Dinh Chuong, J. Gautam, H. Van Hien, L. Huu Tuan, N.H. Kim, J.H. Lee, Emerging core-shell nanostructured catalysts of transition metal encapsulated by two-dimensional carbon materials for electrochemical applications, Nano Today (2018), https://doi.org/10.1016/j.nantod.2018.08.006.
[150] X. Yin, L. Yang, Q. Gao, Core-shell nanostructured electrocatalysts for water splitting, Nanoscale (2020), https://doi.org/10.1039/d0nr03719b.
[151] C. Gao, F. Lyu, Y. Yin, Encapsulated metal nanoparticles for catalysis, Chem. Rev. (2021), https://doi.org/10.1021/acs.chemrev.0c00237.
[152] A. Shafiee, N. Rabiee, S. Ahmadi, M. Baneshi, M. Khatami, S. Iravani, R.S. Varma, Core–shell nanophotocatalysts: review of materials and applications, ACS Appl. Nano Mater. (2022), https://doi.org/10.1021/acsanm.1c03714.
[153] W. Zhu, W. Chen, H. Yu, Y. Zeng, F. Ming, H. Liang, Z. Wang, NiCo/NiCo–OH and NiFe/NiFe–OH core shell nanostructures for water splitting electrocatalysis at large currents, Appl. Catal. B Environ. (2020), https://doi.org/10.1016/j.apcatb.2020.119326.
[154] H. Wang, Z.N. Chen, D. Wu, M. Cao, F. Sun, H. Zhang, H. You, W. Zhuang, R. Cao, Significantly enhanced overall water splitting performance by partial oxidation of Ir through Au modification in core-shell alloy structure, J. Am. Chem. Soc. 143 (2021) 4639–4645, https://doi.org/10.1021/jacs.0c12740.
[155] F. Yang, T. Xiong, P. Huang, S. Zhou, Q. Tan, H. Yang, Y. Huang, M.S. Jie, T. Balogun, Nanostructured transition metal compounds coated 3D porous core-shell carbon fiber as monolith water splitting electrocatalysts: a general strategy, Chem. Eng. J. (2021), https://doi.org/10.1016/j.cej.2021.130279.
[156] L. Yu, H. Zhou, J. Sun, F. Qin, D. Luo, L. Xie, F. Yu, J. Bao, Y. Li, Y. Yu, S. Chen, Z. Ren, Hierarchical Cu@CoFe layered double hydroxide core-shell nanoarchitectures as bifunctional electrocatalysts for efficient overall water splitting, Nano Energy (2017), https://doi.org/10.1016/j.nanoen.2017.09.045.
[157] S.J. Patil, N.R. Chodankar, S.K. Hwang, P.A. Shinde, G. Seeta Rama Raju, K. Shanmugam Ranjith, Y.S. Huh, Y.K. Han, Co-metal–organic framework derived

CoSe2@MoSe2 core–shell structure on carbon cloth as an efficient bifunctional catalyst for overall water splitting, Chem. Eng. J. (2022), https://doi.org/10.1016/j.cej.2021.132379.
[158] Y. Yang, B. Zhu, P.F. Guo, W.J. Wang, W.T. Wang, K. Wang, Z.H. He, Z.T. Liu, Core-shell trimetallic NiFeV disulfides and amorphous high-valance NiFe hydroxide nanosheets enhancing oxygen evolution reaction, Chem. Eng. J. (2022), https://doi.org/10.1016/j.cej.2021.133047.
[159] L. Tian, Z. Li, M. Song, J. Li, Recent progress in water-splitting electrocatalysis mediated by 2D noble metal materials, Nanoscale (2021), https://doi.org/10.1039/d1nr02232f.
[160] L. Li, P. Wang, Q. Shao, X. Huang, Metallic nanostructures with low dimensionality for electrochemical water splitting, Chem. Soc. Rev. (2020), https://doi.org/10.1039/d0cs00013b.
[161] H. Liang, L. Li, F. Meng, L. Dang, J. Zhuo, A. Forticaux, Z. Wang, S. Jin, Porous two-dimensional nanosheets converted from layered double hydroxides and their applications in electrocatalytic water splitting, Chem. Mater. (2015), https://doi.org/10.1021/acs.chemmater.5b02177.
[162] Z. Kou, K. Wang, Z. Liu, L. Zeng, Z. Li, B. Yang, L. Lei, C. Yuan, Y. Hou, Recent advances in manifold exfoliated synthesis of two-dimensional non-precious metal-based nanosheet electrocatalysts for water splitting, Small Struct. (2022), https://doi.org/10.1002/sstr.202100153.
[163] J. Hou, S. Cao, Y. Sun, Y. Wu, F. Liang, Z. Lin, L. Sun, Atomically thin mesoporous In2O3–x/In2S3 lateral heterostructures enabling robust broadband-light photoelectrochemical water splitting, Adv. Energy Mater. (2018), https://doi.org/10.1002/aenm.201701114.
[164] F. Zheng, W. Zhang, X. Zhang, Y. Zhang, W. Chen, Sub-2 nm ultrathin and robust 2D FeNi layered double hydroxide nanosheets packed with 1D FeNi-MOFs for enhanced oxygen evolution electrocatalysis, Adv. Funct. Mater. (2021), https://doi.org/10.1002/adfm.202103318.
[165] L. Li, L. Bu, B. Huang, P. Wang, C. Shen, S. Bai, T.S. Chan, Q. Shao, Z. Hu, X. Huang, Compensating electronic effect enables fast site-to-site electron transfer over ultrathin rumn nanosheet branches toward highly electroactive and stable water splitting, Adv. Mater. (2021), https://doi.org/10.1002/adma.202105308.
[166] W. Zhang, X. Jiang, Z. Dong, J. Wang, N. Zhang, J. Liu, G.R. Xu, L. Wang, Porous Pd/NiFeOx nanosheets enhance the pH-universal overall water splitting, Adv. Funct. Mater. (2021), https://doi.org/10.1002/adfm.202107181.
[167] F. Hu, D. Yu, M. Ye, H. Wang, Y. Hao, L. Wang, L. Li, X. Han, S. Peng, Lattice-matching formed mesoporous transition metal oxide heterostructures advance water splitting by active Fe–O–Cu bridges, Adv. Energy Mater. 12 (2022) 1–10, https://doi.org/10.1002/aenm.202200067.
[168] G. Zhou, M. Li, Y. Li, H. Dong, D. Sun, X. Liu, L. Xu, Z. Tian, Y. Tang, Regulating the electronic structure of CoP nanosheets by O incorporation for high-efficiency electrochemical overall water splitting, Adv. Funct. Mater. (2020), https://doi.org/10.1002/adfm.201905252.
[169] Y. Sun, K. Xu, Z. Wei, H. Li, T. Zhang, X. Li, W. Cai, J. Ma, H.J. Fan, Y. Li, Strong electronic interaction in dual-cation-incorporated NiSe2 nanosheets with lattice distortion for highly efficient overall water splitting, Adv. Mater. (2018), https://doi.org/10.1002/adma.201802121.
[170] Y. Li, J. Yin, L. An, M. Lu, K. Sun, Y.Q. Zhao, D. Gao, F. Cheng, P. Xi, FeS2/CoS2 interface nanosheets as efficient bifunctional electrocatalyst for overall water splitting, Small (2018), https://doi.org/10.1002/smll.201801070.
[171] L. Yang, Z. Guo, J. Huang, Y. Xi, R. Gao, G. Su, W. Wang, L. Cao, B. Dong, Vertical growth of 2D amorphous FePO4 nanosheet on Ni Foam: outer and inner structural design for superior water splitting, Adv. Mater. (2017), https://doi.org/10.1002/adma.201704574.
[172] H. Guo, Z. Fang, H. Li, D. Fernandez, G. Henkelman, S.M. Humphrey, G. Yu, Rational design of rhodium-iridium alloy nanoparticles as highly active catalysts for acidic oxygen evolution, ACS Nano (2019), https://doi.org/10.1021/acsnano.9b06244.
[173] Z. Fang, L. Peng, H. Lv, Y. Zhu, C. Yan, S. Wang, P. Kalyani, X. Wu, G. Yu, Metallic transition metal selenide holey nanosheets for efficient oxygen evolution electrocatalysis, ACS Nano (2017), https://doi.org/10.1021/acsnano.7b05481.
[174] M. Qu, Y. Jiang, M. Yang, S. Liu, Q. Guo, W. Shen, M. Li, R. He, Regulating electron density of NiFe-P nanosheets electrocatalysts by a trifle of Ru for high-efficient overall water splitting, Appl. Catal. B Environ. (2020), https://doi.org/10.1016/j.apcatb.2019.118324.
[175] K. Wang, H. Du, S. He, L. Liu, K. Yang, J. Sun, Y. Liu, Z. Du, L. Xie, W. Ai, W. Huang, Kinetically controlled, scalable synthesis of γ-FeOOH nanosheet arrays on nickel foam toward efficient oxygen evolution: the key role of in-situ-generated γ-NiOOH, Adv. Mater. 33 (2021) 1–10, https://doi.org/10.1002/adma.202005587.
[176] M.S. Islam, M. Kim, X. Jin, S.M. Oh, N.S. Lee, H. Kim, S.J. Hwang, Bifunctional 2D superlattice electrocatalysts of layered double hydroxide-transition metal dichalcogenide active for overall water splitting, ACS Energy Lett. (2018), https://doi.org/10.1021/acsenergylett.8b00134.
[177] B. Liu, H.Q. Peng, C.N. Ho, H. Xue, S. Wu, T.W. Ng, C.S. Lee, W. Zhang, Mesoporous nanosheet networked hybrids of cobalt oxide and cobalt phosphate for efficient electrochemical and photoelectrochemical oxygen evolution, Small (2017), https://doi.org/10.1002/smll.201701875.
[178] H.B. Tao, L. Fang, J. Chen, H. Bin Yang, J. Gao, J. Miao, S. Chen, B. Liu, Identification of surface reactivity descriptor for transition metal oxides in oxygen evolution reaction, J. Am. Chem. Soc. (2016), https://doi.org/10.1021/jacs.6b05398.
[179] M. Fang, G. Dong, R. Wei, J.C. Ho, Hierarchical nanostructures: design for sustainable water splitting, Adv. Energy Mater. (2017), https://doi.org/10.1002/aenm.201700559.
[180] D. Kong, Y. Wang, S. Huang, Y. Von Lim, M. Wang, T. Xu, J. Zang, X. Li, H. Y. Yang, Defect-Engineered 3D hierarchical NiMo3S4 nanoflowers as bifunctional electrocatalyst for overall water splitting, J. Colloid Interface Sci. (2022), https://doi.org/10.1016/j.jcis.2021.10.020.
[181] Y. Hou, M. Qiu, G. Nam, M.G. Kim, T. Zhang, K. Liu, X. Zhuang, J. Cho, C. Yuan, X. Feng, Integrated hierarchical cobalt sulfide/nickel selenide hybrid nanosheets as an efficient three-dimensional electrode for electrochemical and photoelectrochemical water splitting, Nano Lett. (2017), https://doi.org/10.1021/acs.nanolett.7b01030.
[182] L. Yang, L. Zhang, N-enriched porous carbon encapsulated bimetallic phosphides with hierarchical structure derived from controlled electrodepositing multilayer ZIFs for electrochemical overall water splitting, Appl. Catal. B Environ. (2019), https://doi.org/10.1016/j.apcatb.2019.118053.
[183] A. Tahir, T. Haq, F. Aftab, M. Zaheer, H. Duran, K. Kirchhoff, I. Lieberwirth, S.N. Arshad, Aleena Tahir, Tanveer ul Haq, Faryal Aftab, Muhammad Zaheer, Hatice Duran, Katrin Kirchhoff, Ingo Lieberwirth, and Salman N. Arshad *, 2023 2–11. ⟨doi:10.1021/acsanm.2c04344⟩.
[184] M. Singh, T.T. Nguyen, J. Balamurugan, N.H. Kim, J.H. Lee, Rational manipulation of 3D hierarchical oxygenated nickel tungsten selenide nanosheet as the efficient bifunctional electrocatalyst for overall water splitting, Chem. Eng. J. (2022), https://doi.org/10.1016/j.cej.2021.132888.
[185] S.Q. Liu, M.R. Gao, S. Liu, J.L. Luo, Hierarchically assembling cobalt/nickel carbonate hydroxide on copper nitride nanowires for highly efficient water splitting, Appl. Catal. B Environ. (2021), https://doi.org/10.1016/j.apcatb.2021.120148.
[186] A. Peugeot, C.E. Creissen, D. Karapinar, H.N. Tran, M. Schreiber, M. Fontecave, Benchmarking of oxygen evolution catalysts on porous nickel supports, Joule (2021), https://doi.org/10.1016/j.joule.2021.03.022.
[187] D. Yu, Y. Hao, S. Han, S. Zhao, Q. Zhou, C.H. Kuo, F. Hu, L. Li, H.Y. Chen, J. Ren, S. Peng, Ultrafast combustion synthesis of robust and efficient electrocatalysts for high-current-density water oxidation, ACS Nano (2022), https://doi.org/10.1021/acsnano.2c11939.
[188] Y. Yao, J. He, L. Ma, J. Wang, L. Peng, X. Zhu, K. Li, M. Qu, Self-supported Co9S8-Ni3S2-CNTs/NF electrode with superwetting multistage micro-nano structure for efficient bifunctional overall water splitting, J. Colloid Interface Sci. (2022), https://doi.org/10.1016/j.jcis.2022.02.071.
[189] Z. Wu, Y. Zhao, H. Wu, Y. Gao, Z. Chen, W. Jin, J. Wang, T. Ma, L. Wang, Corrosion engineering on iron foam toward efficiently electrocatalytic overall water splitting powered by sustainable energy, Adv. Funct. Mater. (2021), https://doi.org/10.1002/adfm.202010437.
[190] A. Kong, M. Peng, H. Gu, S. Zhao, Y. Lv, M. Liu, Y. Sun, S. Dai, Y. Fu, J. Zhang, W. Li, Synergetic control of Ru/MXene 3D electrode with superhydrophilicity and superaerophobicity for overall water splitting, Chem. Eng. J. (2021), https://doi.org/10.1016/j.cej.2021.131234.
[191] B.K. Kim, M.J. Kim, J.J. Kim, Impact of surface hydrophilicity on electrochemical water splitting, ACS Appl. Mater. Interfaces (2021), https://doi.org/10.1021/acsami.0c22409.
[192] G. Wosiak, J. da Silva, S.S. Sena, R.N. de Andrade, E. Pereira, CFD simulation and experimental comparison of bubble-induced convection during electrochemical water splitting, Chem. Eng. J. (2022), https://doi.org/10.1016/j.cej.2021.133194.
[193] K. Obata, F.F. Abdi, Bubble-induced convection stabilizes the local pH during solar water splitting in neutral pH electrolytes, Sustain. Energy Fuels. (2021), https://doi.org/10.1039/d1se00679g.
[194] T. Kou, S. Wang, Y. Li, Perspective on high-rate alkaline water splitting, ACS Mater. Lett. (2021), https://doi.org/10.1021/acsmaterialslett.0c00536.
[195] Y.K. Li, G. Zhang, W.T. Lu, F.F. Cao, Amorphous Ni–Fe–Mo suboxides coupled with ni network as porous nanoplate array on nickel foam: a highly efficient and durable bifunctional electrode for overall water splitting, Adv. Sci. (2020), https://doi.org/10.1002/advs.201902034.
[196] X. Zhang, J. Hu, X. Cheng, K.A. Nartey, L. Zhang, Double metal–organic frameworks derived Fe–Co–Ni phosphides nanosheets as high-performance electrocatalyst for alkaline electrochemical water splitting, Electrochim. Acta (2021), https://doi.org/10.1016/j.electacta.2020.137536.
[197] X. Shan, J. Liu, H. Mu, Y. Xiao, B. Mei, W. Liu, G. Lin, Z. Jiang, L. Wen, L. Jiang, An engineered superhydrophilic/superaerophobic electrocatalyst composed of the supported CoMoSx chalcogel for overall water splitting, Angew. Chem. - Int. Ed. 59 (2020) 1659–1665, https://doi.org/10.1002/anie.201911617.
[198] W. Xu, Z. Lu, X. Sun, L. Jiang, X. Duan, Superwetting electrodes for gas-involving electrocatalysis, Acc. Chem. Res. (2018), https://doi.org/10.1021/acs.accounts.8b00070.
[199] T. Fujimura, W. Hikima, Y. Fukunaka, T. Homma, Analysis of the effect of surface wettability on hydrogen evolution reaction in water electrolysis using micro-patterned electrodes, Electrochem. Commun. (2019), https://doi.org/10.1016/j.elecom.2019.02.018.
[200] J. Chen, L. Guo, Size effect of one-dimensional nanostructures on bubble nucleation in water splitting, Appl. Phys. Lett. (2019), https://doi.org/10.1063/1.5115977.
[201] G. Sakuma, Y. Fukunaka, H. Matsushima, Nucleation and growth of electrolytic gas bubbles under microgravity, Int. J. Hydrog. Energy (2014), https://doi.org/10.1016/j.ijhydene.2014.03.059.
[202] S.H. Ahn, I. Choi, H.Y. Park, S.J. Hwang, S.J. Yoo, E. Cho, H.J. Kim, D. Henkensmeier, S.W. Nam, S.K. Kim, J.H. Jang, Effect of morphology of electrodeposited Ni catalysts on the behavior of bubbles generated during the oxygen evolution reaction in alkaline water electrolysis, Chem. Commun. (2013), https://doi.org/10.1039/c3cc44891f.

[203] J. Shen, J. Li, B. Li, Y. Zheng, X. Bao, J. Guo, Y. Guo, C. Lai, W. Lei, S. Wang, H. Shao, Ambient fast synthesis of superaerophobic/superhydrophilic electrode for superior electrocatalytic water oxidation, Energy Environ. Mater. (2022) 0–3, https://doi.org/10.1002/eem2.12462.
[204] Z. Lu, W. Xu, J. Ma, Y. Li, X. Sun, L. Jiang, Superaerophilic carbon-nanotube-array electrode for high-performance oxygen reduction reaction, Adv. Mater. (2016), https://doi.org/10.1002/adma.201504652.
[205] S. Wang, K. Liu, X. Yao, L. Jiang, Bioinspired surfaces with superwettability: new insight on theory, design, and applications, Chem. Rev. (2015), https://doi.org/10.1021/cr400083y.
[206] Q. Zhang, P. Li, D. Zhou, Z. Chang, Y. Kuang, X. Sun, Superaerophobic ultrathin Ni–Mo alloy nanosheet array from in situ topotactic reduction for hydrogen evolution reaction, Small (2017), https://doi.org/10.1002/smll.201701648.
[207] L. Jiang, N. Yang, C. Yang, X. Zhu, Y. Jiang, X. Shen, C. Li, Q. Sun, Surface wettability engineering: CoSx-Ni3S2 nanoarray electrode for improving overall water splitting, Appl. Catal. B Environ. (2020), https://doi.org/10.1016/j.apcatb.2020.118780.
[208] L. An, J. Feng, Y. Zhang, R. Wang, H. Liu, G.C. Wang, F. Cheng, P. Xi, Epitaxial heterogeneous interfaces on N-NiMoO4/NiS2 nanowires/nanosheets to boost hydrogen and oxygen production for overall water splitting, Adv. Funct. Mater. (2019), https://doi.org/10.1002/adfm.201805298.
[209] X. Qin, B. Yan, D. Kim, Z. Teng, T. Chen, J. Choi, L. Xu, Y. Piao, Interfacial engineering and hydrophilic/aerophobic tuning of Sn4P3/Co2P heterojunction nanoarrays for high-efficiency fully reversible water electrolysis, Appl. Catal. B Environ. (2022), https://doi.org/10.1016/j.apcatb.2021.120923.
[210] S. Riyajuddin, K. Azmi, M. Pahuja, S. Kumar, T. Maruyama, C. Bera, K. Ghosh, Super-hydrophilic hierarchical Ni-foam-graphene-carbon nanotubes-Ni2p-cup2Nano-architecture as efficient electrocatalyst for overall water splitting, ACS Nano 15 (2021) 5586–5599, https://doi.org/10.1021/acsnano.1c00647.
[211] S. Riyajuddin, M. Pahuja, P.K. Sachdeva, K. Azmi, S. Kumar, M. Afshan, F. Ali, J. Sultana, T. Maruyama, C. Bera, K. Ghosh, Super-hydrophilic leaflike Sn4P3on the porous seamless graphene-carbon nanotube heterostructure as an efficient electrocatalyst for solar-driven overall water splitting, ACS Nano (2022), https://doi.org/10.1021/acsnano.2c00466.
[212] P. Wang, B. Wang, Designing self-supported electrocatalysts for electrochemical water splitting: surface/interface engineering toward enhanced electrocatalytic performance, ACS Appl. Mater. Interfaces (2021), https://doi.org/10.1021/acsami.1c17448.
[213] L. Zou, J. Li, D. Zakharov, E.A. Stach, G. Zhou, In situ atomic-scale imaging of the metal/oxide interfacial transformation, Nat. Commun. (2017), https://doi.org/10.1038/s41467-017-00371-4.
[214] X. Yu, Z.Y. Yu, X.L. Zhang, P. Li, B. Sun, X. Gao, K. Yan, H. Liu, Y. Duan, M.R. Gao, G. Wang, S.H. Yu, Highly disordered cobalt oxide nanostructure induced by sulfur incorporation for efficient overall water splitting, Nano Energy 71 (2020), 104652, https://doi.org/10.1016/j.nanoen.2020.104652.
[215] T. ul Haq, Y. Haik, S doped Cu2O-CuO nanoneedles array: free standing oxygen evolution electrode with high efficiency and corrosion resistance for sea water splitting, Catal. Today (2021), https://doi.org/10.1016/j.cattod.2021.09.015.
[216] Y. Wu, Y. Liu, G.D. Li, X. Zou, X. Lian, D. Wang, L. Sun, T. Asefa, X. Zou, Efficient electrocatalysis of overall water splitting by ultrasmall NixCo3−xS4 coupled Ni3S2 nanosheet arrays, Nano Energy (2017), https://doi.org/10.1016/j.nanoen.2017.03.024.
[217] X. Gao, W. Chen, Highly stable and efficient Pd6(SR)12 cluster catalysts for the hydrogen and oxygen evolution reactions, Chem. Commun. (2017), https://doi.org/10.1039/c7cc04787h.
[218] S. Zhan, J.A. De Gracia Triviño, M.S.G. Ahlquist, The carboxylate ligand as an oxide relay in catalytic water oxidation, J. Am. Chem. Soc. 141 (2019) 10247–10252, https://doi.org/10.1021/jacs.9b02585.
[219] L. Zhou, S. Lu, S. Guo, Recent progress on precious metal single atom materials for water splitting catalysis, SusMat (2021), https://doi.org/10.1002/sus2.15.
[220] J.E. Lee, K.J. Jeon, P.L. Show, I.H. Lee, S.C. Jung, Y.J. Choi, G.H. Rhee, K.Y.A. Lin, Y.K. Park, Mini review on H2 production from electrochemical water splitting according to special nanostructured morphology of electrocatalysts, Fuel (2022), https://doi.org/10.1016/j.fuel.2021.122048.
[221] H. Zhang, W. Cheng, D. Luan, X.W. Lou, Atomically dispersed reactive centers for electrocatalytic CO_2 reduction and water splitting, Angew. Chem. - Int. Ed. (2021), https://doi.org/10.1002/anie.202014112.
[222] W. Liu, H. Zhang, C. Li, X. Wang, J. Liu, X. Zhang, Non-noble metal single-atom catalysts prepared by wet chemical method and their applications in electrochemical water splitting, J. Energy Chem. (2020), https://doi.org/10.1016/j.jechem.2020.02.020.
[223] F. Davodi, E. Mühlhausen, M. Tavakkoli, J. Sainio, H. Jiang, B. Gökce, G. Marzun, T. Kallio, Catalyst support effect on the activity and durability of magnetic nanoparticles: toward design of advanced electrocatalyst for full water splitting, ACS Appl. Mater. Interfaces (2018), https://doi.org/10.1021/acsami.8b08830.
[224] L. Zhang, H. Zhao, S. Xu, Q. Liu, T. Li, Y. Luo, S. Gao, X. Shi, A.M. Asiri, X. Sun, Recent advances in 1D electrospun nanocatalysts for electrochemical water splitting, Small Struct. (2021), https://doi.org/10.1002/sstr.202000048.
[225] H. Gu, G. Shi, H.C. Chen, S. Xie, Y. Li, H. Tong, C. Yang, C. Zhu, J.T. Mefford, H. Xia, W.C. Chueh, H.M. Chen, L. Zhang, Strong catalyst-support interactions in electrochemical oxygen evolution on Ni-Fe layered double hydroxide, ACS Energy Lett. 5 (2020) 3185–3194, https://doi.org/10.1021/acsenergylett.0c01584.
[226] Z. Zeng, K.C. Chang, J. Kubal, N.M. Markovic, J. Greeley, Stabilization of ultrathin (hydroxy)oxide films on transition metal substrates for electrochemical energy conversion, Nat. Energy 2 (2017) 1–9, https://doi.org/10.1038/nenergy.2017.70.
[227] P. Chakthranont, J. Kibsgaard, A. Gallo, J. Park, M. Mitani, D. Sokaras, T. Kroll, R. Sinclair, M.B. Mogensen, T.F. Jaramillo, Effects of gold substrates on the intrinsic and extrinsic activity of high-loading nickel-based oxyhydroxide oxygen evolution catalysts, ACS Catal. 7 (2017) 5399–5409, https://doi.org/10.1021/acscatal.7b01070.
[228] H. Sun, Z. Yan, F. Liu, W. Xu, F. Cheng, J. Chen, Self-supported transition-metal-based electrocatalysts for hydrogen and oxygen evolution, Adv. Mater. 1806326 (2019) 1–18, https://doi.org/10.1002/adma.201806326.
[229] C. Panda, P.W. Menezes, M. Zheng, S. Orthmann, M. Driess, In situ formation of nanostructured core-shell Cu 3 N-CuO to promote alkaline water electrolysis, ACS Energy Lett. 4 (2019) 747–754, https://doi.org/10.1021/acsenergylett.9b00091.
[230] T. ul Haq, Y. Bicer, A. Munir, S.A. Mansour, Y. Haik, Surface assembling of highly interconnected and vertically aligned porous nanosheets of Gd−CoB on TiO2 nanoflowers for durable methanol oxidation reaction, ChemCatChem 12 (2020) 3585–3597, https://doi.org/10.1002/cctc.202000392.
[231] L. Yu, L. Wu, S. Song, B. McElhenny, F. Zhang, S. Chen, Z. Ren, Hydrogen generation from seawater electrolysis over a sandwich-like NiCoN|NixP|NiCoN microsheet array catalyst, ACS Energy Lett. 5 (2020) 2681–2689, https://doi.org/10.1021/acsenergylett.0c01244.
[232] D. Chen, R. Lu, Z. Pu, J. Zhu, H.W. Li, F. Liu, S. Hu, X. Luo, J. Wu, Y. Zhao, S. Mu, Ru-doped 3D flower-like bimetallic phosphide with a climbing effect on overall water splitting, Appl. Catal. B Environ. (2020), https://doi.org/10.1016/j.apcatb.2020.119396.
[233] A. Tahir, F. Arshad, T. Haq, I. Hussain, S.Z. Hussain, Roles of Metal Oxide Nanostructure-Based Substrates in Sustainable Electrochemical Water Splitting: Recent Development and Future Perspective, , 2023. ⟨doi:10.1021/acsanm.2c04580⟩.
[234] M. Abbas, T. ul Haq, S.N. Arshad, M. Zaheer, Fabrication of cobalt doped titania for enhanced oxygen evolution reaction, Mol. Catal. 488 (2020), 110894, https://doi.org/10.1016/j.mcat.2020.110894.
[235] A. Munir, T. ul Haq, I. Hussain, I. Ullah, S.Z. Hussain, A. Qurashi, J. Iqbal, A. Rehman, I. Hussain, Controlled assembly of Cu/Co-oxide beaded nanoclusters on thiolated graphene oxide nanosheets for high-performance oxygen evolution catalysts, Chem. - A Eur. J. 26 (2020) 11209–11219, https://doi.org/10.1002/chem.202000491.
[236] F. Arshad, T. ul Haq, A. Khan, Y. Haik, I. Hussain, F. Sher, Multifunctional porous NiCo bimetallic foams toward water splitting and methanol oxidation-assisted hydrogen production, Energy Convers. Manag. (2022), https://doi.org/10.1016/j.enconman.2022.115262.
[237] F. Arshad, A. Tahir, T. ul Haq, H. Duran, I. Hussain, F. Sher, Fabrication of NiCu interconnected porous nanostructures for highly selective methanol oxidation coupled with hydrogen evolution reaction, Int. J. Hydrog. Energy 47 (2022) 36118–36128, https://doi.org/10.1016/j.ijhydene.2022.08.187.
[238] M. Bele, P. Jovanovič, Ž. Marinko, S. Drev, V.S. Šelih, J. Kovač, M. Gaberšček, G. Koderman Podboršek, G. Dražić, N. Hodnik, A. Kokalj, L. Suhadolnik, Increasing the oxygen-evolution reaction performance of nanotubular titanium oxynitride-supported ir nanoparticles by a strong metal-support interaction, ACS Catal. (2020), https://doi.org/10.1021/acscatal.0c03688.
[239] J. Zhang, Y. Wang, C. Zhang, H. Gao, L. Lv, L. Han, Z. Zhang, Self-supported porous NiSe2 nanowrinkles as efficient bifunctional electrocatalysts for overall water splitting, ACS Sustain. Chem. Eng. (2018), https://doi.org/10.1021/acssuschemeng.7b03657.
[240] C. Zhang, Y. Zhang, S. Zhou, C. Li, Self-supported iron-doping NiSe2 nanowrinkles as bifunctional electrocatalysts for electrochemical water splitting, J. Alloy. Compd. (2020), https://doi.org/10.1016/j.jallcom.2019.152833.
[241] D. Wang, Q. Li, C. Han, Q. Lu, Z. Xing, X. Yang, Atomic and electronic modulation of self-supported nickel-vanadium layered double hydroxide to accelerate water splitting kinetics, Nat. Commun. (2019), https://doi.org/10.1038/s41467-019-11765-x.
[242] J. Kang, J. Sheng, J. Xie, H. Ye, J. Chen, X.Z. Fu, G. Du, R. Sun, C.P. Wong, Tubular Cu(OH)2 arrays decorated with nanothorny Co-Ni bimetallic carbonate hydroxide supported on Cu foam: A 3D hierarchical core-shell efficient electrocatalyst for the oxygen evolution reaction, J. Mater. Chem. A (2018), https://doi.org/10.1039/c8ta02492h.
[243] L. Yin, X. Du, C. Di, M. Wang, K. Su, Z. Li, In-situ transformation obtained defect-rich porous hollow CuO@CoZn-LDH nanoarrays as self-supported electrode for highly efficient overall water splitting, Chem. Eng. J. (2021), https://doi.org/10.1016/j.cej.2021.128809.
[244] H. Sun, C. Tian, G. Fan, J. Qi, Z. Liu, Z. Yan, F. Cheng, J. Chen, C.P. Li, M. Du, Boosting activity on Co4N porous nanosheet by coupling CeO2 for efficient electrochemical overall water splitting at high current densities, Adv. Funct. Mater. (2020), https://doi.org/10.1002/adfm.201910596.
[245] F. Arshad, T.U. Haq, I. Hussain, F. Sher, Recent advances in electrocatalysts toward alcohol-assisted, energy-saving hydrogen production, ACS Appl. Energy Mater. (2021), https://doi.org/10.1021/acsaem.1c01932.
[246] F. Diao, W. Huang, G. Ctistis, H. Wackerbarth, Y. Yang, P. Si, J. Zhang, X. Xiao, C. Engelbrekt, Bifunctional and self-supported NiFeP-layer-coated NiP rods for electrochemical water splitting in alkaline solution, ACS Appl. Mater. Interfaces (2021), https://doi.org/10.1021/acsami.1c03089.
[247] Q. Zhang, W. Xiao, W.H. Guo, Y.X. Yang, J.L. Lei, H.Q. Luo, N.B. Li, Macroporous array induced multiscale modulation at the surface/interface of Co(OH)2/NiMo self-supporting electrode for effective overall water splitting, Adv. Funct. Mater. (2021), https://doi.org/10.1002/adfm.202102117.
[248] Q. Fu, T. Wu, G. Fu, T. Gao, J. Han, T. Yao, Y. Zhang, W. Zhong, X. Wang, B. Song, Skutterudite-type ternary Co1- xNixP3 nanoneedle array electrocatalysts for

enhanced hydrogen and oxygen evolution, ACS Energy Lett. (2018), https://doi.org/10.1021/acsenergylett.8b00908.
[249] G. Chen, Y. Zhao, G. Fu, P.N. Duchesne, L. Gu, Y. Zheng, X. Weng, M. Chen, P. Zhang, C.W. Pao, J.F. Lee, N. Zheng, Interfacial effects in iron-nickel hydroxide-platinum nanoparticles enhance catalytic oxidation, Sci. (80-.) (2014), https://doi.org/10.1126/science.1252553.
[250] H. Wang, Y.K. Tzeng, Y. Ji, Y. Li, J. Li, X. Zheng, A. Yang, Y. Liu, Y. Gong, L. Cai, Y. Li, X. Zhang, W. Chen, B. Liu, H. Lu, N.A. Melosh, Z.X. Shen, K. Chan, T. Tan, S. Chu, Y. Cui, Synergistic enhancement of electrocatalytic CO_2 reduction to C2 oxygenates at nitrogen-doped nanodiamonds/Cu interface, Nat. Nanotechnol. (2020), https://doi.org/10.1038/s41565-019-0603-y.
[251] J. Zhang, T. Wang, D. Pohl, B. Rellinghaus, R. Dong, S. Liu, X. Zhuang, X. Feng, Interface engineering of MoS 2 /Ni 3 S 2 heterostructures for highly enhanced electrochemical overall-water-splitting activity, Angew. Chem. (2016), https://doi.org/10.1002/ange.201602237.
[252] T. ul Haq, M. Pasha, Y. Tong, S.A. Mansour, Y. Haik, Au nanocluster coupling with Gd-Co2B nanoflakes embedded in reduced TiO2 nanosheets: Seawater electrolysis at low cell voltage with high selectivity and corrosion resistance, Appl. Catal. B Environ. (2022), https://doi.org/10.1016/j.apcatb.2021.120836.
[253] O. Diaz-Morales, F. Calle-Vallejo, C. De Munck, M.T.M. Koper, Electrochemical water splitting by gold: evidence for an oxide decomposition mechanism, Chem. Sci. (2013), https://doi.org/10.1039/c3sc50301a.
[254] N. Takei, C. Sommer, C. Genes, G. Pupillo, H. Goto, K. Koyasu, H. Chiba, M. Weidemüller, K. Ohmori, Direct observation of ultrafast many-body electron dynamics in an ultracold Rydberg gas, Nat. Commun. (2016), https://doi.org/10.1038/ncomms13449.
[255] F. Zhang, Y. Liu, L. Wu, M. Ning, S. Song, X. Xiao, V.G. Hadjiev, D.E. Fan, D. Wang, L. Yu, S. Chen, Z. Ren, Efficient alkaline seawater oxidation by a three-dimensional core-shell dendritic NiCo@NiFe layered double hydroxide electrode, Mater. Today Phys. 27 (2022), 100841, https://doi.org/10.1016/j.mtphys.2022.100841.
[256] F. Dionigi, T. Reier, Z. Pawolek, M. Gliech, P. Strasser, Design criteria, operating conditions, and nickel-iron hydroxide catalyst materials for selective seawater electrolysis, ChemSusChem 9 (2016) 962–972, https://doi.org/10.1002/cssc.201501581.
[257] X.H. Wang, Y. Ling, B. Wu, B.L. Li, X.L. Li, J.L. Lei, N.B. Li, H.Q. Luo, Doping modification, defects construction, and surface engineering: Design of cost-effective high-performance electrocatalysts and their application in alkaline seawater splitting, Nano Energy 87 (2021), 106160, https://doi.org/10.1016/j.nanoen.2021.106160.
[258] C. Wei, R.R. Rao, J. Peng, B. Huang, I.E.L. Stephens, M. Risch, Z.J. Xu, Y. Shao-Horn, Recommended practices and benchmark activity for hydrogen and oxygen electrocatalysis in water splitting and fuel cells, Adv. Mater. 31 (2019) 1–24, https://doi.org/10.1002/adma.201806296.
[259] E.M. KAPP, The precipitation of calcium and magnesium from sea water by sodium hydroxide, Biol. Bull. (1928), https://doi.org/10.2307/1536800.
[260] Y. Kuang, M.J. Kenney, Y. Meng, W.H. Hung, Y. Liu, J.E. Huang, R. Prasanna, P. Li, Y. Li, L. Wang, M.C. Lin, M.D. McGehee, X. Sun, H. Dai, Solar-driven, highly sustained splitting of seawater into hydrogen and oxygen fuels, Proc. Natl. Acad. Sci. U. S. A. (2019), https://doi.org/10.1073/pnas.1900556116.
[261] T. ul Haq, Y. Haik, Strategies of anode design for seawater electrolysis: recent development and future perspective, Small Sci. 2 (2022) 2200030, https://doi.org/10.1002/smsc.202200030.
[262] W. Wang, Z. Wang, Y. Hu, Y. Liu, S. Chen, A potential-driven switch of activity promotion mode for the oxygen evolution reaction at Co3O4/NiOxHy interface, EScience 2 (2022) 438–444, https://doi.org/10.1016/j.esci.2022.04.004.
[263] T. Ma, W. Xu, B. Li, X. Chen, J. Zhao, S. Wan, K. Jiang, S. Zhang, Z. Wang, Z. Tian, Z. Lu, L. Chen, The critical role of additive sulfate for stable alkaline seawater oxidation on nickel-based electrodes, Angew. Chem. Int. Ed. (2021), https://doi.org/10.1002/anie.202110355.
[264] J. Chang, G. Wang, Z. Yang, B. Li, Q. Wang, R. Kuliiev, N. Orlovskaya, M. Gu, Y. Du, G. Wang, Y. Yang, Dual-doping and synergism toward high-performance seawater electrolysis, Adv. Mater. (2021), https://doi.org/10.1002/adma.202101425.
[265] B. Xiong, L. Chen, J. Shi, Anion-containing noble-metal-free bifunctional electrocatalysts for overall water splitting, ACS Catal. (2018), https://doi.org/10.1021/acscatal.7b04286.
[266] L. Wu, L. Yu, B. McElhenny, X. Xing, D. Luo, F. Zhang, J. Bao, S. Chen, Z. Ren, Rational design of core-shell-structured CoPx@FeOOH for efficient seawater electrolysis, Appl. Catal. B Environ. (2021), https://doi.org/10.1016/j.apcatb.2021.120256.
[267] C. Wang, M. Zhu, Z. Cao, P. Zhu, Y. Cao, X. Xu, C. Xu, Z. Yin, Heterogeneous bimetallic sulfides based seawater electrolysis towards stable industrial-level large current density, Appl. Catal. B Environ. (2021), https://doi.org/10.1016/j.apcatb.2021.120071.
[268] Y. Li, X. Wu, J. Wang, H. Wei, S. Zhang, S. Zhu, Z. Li, S. Wu, H. Jiang, Y. Liang, Sandwich structured Ni3S2-MoS2-Ni3S2@Ni foam electrode as a stable bifunctional electrocatalyst for highly sustained overall seawater splitting, Electrochim. Acta (2021), https://doi.org/10.1016/j.electacta.2021.138833.
[269] Z. Chen, W. Wei, L. Song, B.-J. Ni, Hybrid water electrolysis: a new sustainable avenue for energy-saving hydrogen production, Sustain. Horiz. (2022), https://doi.org/10.1016/j.horiz.2021.100002.
[270] N.A. Burton, R.V. Padilla, A. Rose, H. Habibullah, Increasing the efficiency of hydrogen production from solar powered water electrolysis, Renew. Sustain. Energy Rev. (2021), https://doi.org/10.1016/j.rser.2020.110255.
[271] B.H.R. Suryanto, Y. Wang, R.K. Hocking, W. Adamson, C. Zhao, Overall electrochemical splitting of water at the heterogeneous interface of nickel and iron oxide, Nat. Commun. (2019), https://doi.org/10.1038/s41467-019-13415-8.
[272] P. Zhai, Y. Zhang, Y. Wu, J. Gao, B. Zhang, S. Cao, Y. Zhang, Z. Li, L. Sun, J. Hou, Engineering active sites on hierarchical transition bimetal oxides/sulfides heterostructure array enabling robust overall water splitting, Nat. Commun. (2020), https://doi.org/10.1038/s41467-020-19214-w.
[273] H. Wang, H.W. Lee, Y. Deng, Z. Lu, P.C. Hsu, Y. Liu, D. Lin, Y. Cui, Bifunctional non-noble metal oxide nanoparticle electrocatalysts through lithium-induced conversion for overall water splitting, Nat. Commun. (2015), https://doi.org/10.1038/ncomms8261.
[274] T. Tang, W.J. Jiang, S. Niu, N. Liu, H. Luo, Y.Y. Chen, S.F. Jin, F. Gao, L.J. Wan, J. S. Hu, Electronic and morphological dual modulation of cobalt carbonate hydroxides by Mn doping toward highly efficient and stable bifunctional electrocatalysts for overall water splitting, J. Am. Chem. Soc. (2017), https://doi.org/10.1021/jacs.7b03507.
[275] J. Liang, X. Han, Y. Qiu, Q. Fang, B. Zhang, W. Wang, J. Zhang, P.M. Ajayan, J. Lou, A low-cost and high-efficiency integrated device toward solar-driven water splitting, ACS Nano (2020), https://doi.org/10.1021/acsnano.9b09053.
[276] J. Luo, J.H. Im, M.T. Mayer, M. Schreier, M.K. Nazeeruddin, N.G. Park, S. D. Tilley, H.J. Fan, M. Grätzel, Water photolysis at 12.3% efficiency via perovskite photovoltaics and earth-abundant catalysts, Science (2014), https://doi.org/10.1126/science.1258307.
[277] Y. Qiu, W. Liu, W. Chen, G. Zhou, P.C. Hsu, R. Zhang, Z. Liang, S. Fan, Y. Zhang, Y. Cui, Efficient solar-driven water splitting by nanocone BiVO4-perovskite tandem cells, Sci. Adv. (2016), https://doi.org/10.1126/sciadv.1501764.
[278] H. Zhang, X. Li, A. Hähnel, V. Naumann, C. Lin, S. Azimi, S.L. Schweizer, A. W. Maijenburg, R.B. Wehrspohn, Bifunctional heterostructure assembly of NiFe LDH nanosheets on NiCoP nanowires for highly efficient and stable overall water splitting, Adv. Funct. Mater. (2018), https://doi.org/10.1002/adfm.201706847.
[279] H. Liu, Q. Jia, S. Huang, L. Yang, S. Wang, L. Zheng, D. Cao, Ultra-small Ru nanoparticles embedded on Fe-Ni(OH)2nanosheets for efficient water splitting at a large current density with long-term stability of 680 h, , J. Mater. Chem. A. (2022), https://doi.org/10.1039/d1ta10546a.
[280] A. Sivanantham, S. Shanmugam, Nickel selenide supported on nickel foam as an efficient and durable non-precious electrocatalyst for the alkaline water electrolysis, Appl. Catal. B Environ. (2017), https://doi.org/10.1016/j.apcatb.2016.10.050.
[281] Y. Pi, Q. Shao, P. Wang, F. Lv, S. Guo, J. Guo, X. Huang, Trimetallic oxyhydroxide coralloids for efficient oxygen evolution electrocatalysis, Angew. Chem. - Int. Ed. (2017), https://doi.org/10.1002/anie.201701533.
[282] X. Wu, J. Li, Y. Li, Z. Wen, NiFeP-MoO2 hybrid nanorods on nickel foam as high-activity and high-stability electrode for overall water splitting, Chem. Eng. J. (2021), https://doi.org/10.1016/j.cej.2020.128161.
[283] S. Hao, L. Chen, C. Yu, B. Yang, Z. Li, Y. Hou, L. Lei, X. Zhang, NiCoMo Hydroxide nanosheet arrays synthesized via chloride corrosion for overall water splitting, ACS Energy Lett. 4 (2019) 952–959, https://doi.org/10.1021/acsenergylett.9b00333.
[284] N.K. Oh, C. Kim, J. Lee, O. Kwon, Y. Choi, G.Y. Jung, H.Y. Lim, S.K. Kwak, G. Kim, H. Park, In-situ local phase-transitioned MoSe 2 in La 0.5 Sr 0.5 CoO 3-δ heterostructure and stable overall water electrolysis over 1000 h, Nat. Commun. 10 (2019) 1–12, https://doi.org/10.1038/s41467-019-09339-y.
[285] J. Parrondo, M. George, C. Capuano, K.E. Ayers, V. Ramani, Pyrochlore electrocatalysts for efficient alkaline water electrolysis, J. Mater. Chem. A. (2015), https://doi.org/10.1039/c5ta01771h.
[286] G. Li, L. Anderson, Y. Chen, M. Pan, P.Y.Abel Chuang, New insights into evaluating catalyst activity and stability for oxygen evolution reactions in alkaline media, Sustain. Energy Fuels. (2018), https://doi.org/10.1039/c7se00337d.
[287] W. Li, X. Gao, D. Xiong, F. Wei, W.G. Song, J. Xu, L. Liu, Hydrothermal synthesis of monolithic Co3Se4 nanowire electrodes for oxygen evolution and overall water splitting with high efficiency and extraordinary catalytic stability, Adv. Energy Mater. (2017), https://doi.org/10.1002/aenm.201602579.
[288] Y. Liu, X. Liang, L. Gu, Y. Zhang, G.D. Li, X. Zou, J.S. Chen, Corrosion engineering towards efficient oxygen evolution electrodes with stable catalytic activity for over 6000 h, Nat. Commun. 9 (2018) 1–10, https://doi.org/10.1038/s41467-018-05019-5.
[289] J. Zhang, Y. Bai, C. Zhang, H. Gao, J. Niu, Y. Shi, Y. Zhang, M. Song, Z. Zhang, Hybrid Ni(OH)2/FeOOH@NiFe nanosheet catalysts toward highly efficient oxygen evolution reaction with ultralong stability over 1000 h, ACS Sustain. Chem. Eng. (2019), https://doi.org/10.1021/acssuschemeng.9b02296.
[290] C. Liang, P. Zou, A. Nairan, Y. Zhang, J. Liu, K. Liu, S. Hu, F. Kang, H.J. Fan, C. Yang, Exceptional performance of hierarchical Ni-Fe oxyhydroxide@NiFe alloy nanowire array electrocatalysts for large current density water splitting, Energy Environ. Sci. (2020), https://doi.org/10.1039/c9ee02388g.
[291] K. Wan, J. Luo, X. Zhang, P. Subramanian, J. Fransaer, Sulfur-modified nickel selenide as an efficient electrocatalyst for the oxygen evolution reaction, J. Energy Chem. (2021), https://doi.org/10.1016/j.jechem.2021.03.013.
[292] T. ul Haq, Y. Haik, NiO x –FeO x nanoclusters anchored on g-C 3 N 4 sheets for selective seawater oxidation with high corrosion resistance, ACS Sustain. Chem. Eng. 10 (2022) 6622–6632, https://doi.org/10.1021/acssuschemeng.2c00359.
[293] Y. Gao, N. Zhang, C. Wang, F. Zhao, Y. Yu, Construction of Fe2O3@CuO heterojunction nanotubes for enhanced oxygen evolution reaction, ACS Appl. Energy Mater. (2020), https://doi.org/10.1021/acsaem.9b01866.
[294] X. Yue, Y. Jin, P.K. Shen, Highly stable and efficient non-precious metal electrocatalysts of tantalum dioxyfluoride used for the oxygen evolution reaction, J. Mater. Chem. A. (2017), https://doi.org/10.1039/c7ta01838j.

[295] W. Yaseen, N. Ullah, M. Xie, W. Wei, Y. Xu, M. Zahid, C.J. Oluigbo, B.A. Yusuf, J. Xie, Cobalt–Iron nanoparticles encapsulated in mesoporous carbon nanosheets: A one-pot synthesis of highly stable electrocatalysts for overall water splitting, Int. J. Hydrog. Energy (2021), https://doi.org/10.1016/j.ijhydene.2020.11.041.
[296] S. Anantharaj, S.R. Ede, K. Karthick, S. Sam Sankar, K. Sangeetha, P.E. Karthik, S. Kundu, Precision and correctness in the evaluation of electrocatalytic water splitting: revisiting activity parameters with a critical assessment, Energy Environ. Sci. 11 (2018) 744–771, https://doi.org/10.1039/c7ee03457a.
[297] D. Voiry, M. Chhowalla, Y. Gogotsi, N.A. Kotov, Y. Li, R.M. Penner, R.E. Schaak, P.S. Weiss, Best practices for reporting electrocatalytic performance of nanomaterials, ACS Nano (2018), https://doi.org/10.1021/acsnano.8b07700.
[298] E. Fabbri, A. Habereder, K. Waltar, R. Kötz, T.J. Schmidt, Developments and perspectives of oxide-based catalysts for the oxygen evolution reaction, Catal. Sci. Technol. (2014), https://doi.org/10.1039/c4cy00669k.
[299] S. Anantharaj, P.E. Karthik, S. Noda, The significance of properly reporting turnover frequency in electrocatalysis research, Angew. Chem. - Int. Ed. (2021), https://doi.org/10.1002/anie.202110352.
[300] Y. Li, Y. Sun, Y. Qin, W. Zhang, L. Wang, M. Luo, H. Yang, S. Guo, Recent advances on water-splitting electrocatalysis mediated by noble-metal-based nanostructured materials, Adv. Energy Mater. 10 (2020) 1–20, https://doi.org/10.1002/aenm.201903120.
[301] H. Xue, H. Zhang, S. Fricke, M. Lüther, Z. Yang, A. Meng, W. Bremser, Z. Li, Scalable and energy-efficient synthesis of CoxP for overall water splitting in alkaline media by high energy ball milling, Sustain. Energy Fuels. (2020), https://doi.org/10.1039/c9se00607a.
[302] Y. Zhai, X. Ren, B. Wang, S. Liu, High-entropy catalyst—a novel platform for electrochemical water splitting, Adv. Funct. Mater. (2022), https://doi.org/10.1002/adfm.202207536.
[303] E.T. Nguyen, I.A. Bertini, A.J. Ritz, R.A. Lazenby, K. Mao, J.R. McBride, A. V. Mattia, J.E. Kuszynski, S.F. Wenzel, S.D. Bennett, G.F. Strouse, A single source, scalable route for direct isolation of earth-abundant nanometal carbide water-splitting electrocatalysts, Inorg. Chem. 61 (2022) 13836–13845, https://doi.org/10.1021/acs.inorgchem.2c01713.
[304] T. Tran-Phu, R. Daiyan, J. Leverett, Z. Fusco, A. Tadich, I. Di Bernardo, A. Kiy, T. N. Truong, Q. Zhang, H. Chen, P. Kluth, R. Amal, A. Tricoli, Understanding the activity and stability of flame-made Co3O4 spinels: a route towards the scalable production of highly performing OER electrocatalysts, Chem. Eng. J. (2022), https://doi.org/10.1016/j.cej.2021.132180.
[305] S. Liu, G. Han, J. Zhang, H. Wang, X. Huang, Ultrafast, scalable and green synthesis of amorphous iron-nickel based durable water oxidation electrode with very high intrinsic activity via potential pulses, Chem. Eng. J. (2022), https://doi.org/10.1016/j.cej.2021.130688.
[306] F.Y. Chen, Z.Y. Wu, Z. Adler, H. Wang, Stability challenges of electrocatalytic oxygen evolution reaction: from mechanistic understanding to reactor design, Joule 5 (2021) 1704–1731, https://doi.org/10.1016/j.joule.2021.05.005.
[307] S. Jeong, H.D. Mai, K.H. Nam, C.M. Park, K.J. Jeon, Self-healing graphene-templated platinum-nickel oxide heterostructures for overall water splitting, ACS Nano (2022), https://doi.org/10.1021/acsnano.1c08506.
[308] S. Tao, Q. Wen, W. Jaegermann, B. Kaiser, Formation of highly active NiO(OH) thin films from electrochemically deposited Ni(OH)2 by a simple thermal treatment at a moderate temperature: a combined electrochemical and surface science investigation, ACS Catal. (2022), https://doi.org/10.1021/acscatal.1c04589.
[309] D. Zabelin, A. Zabelina, E. Miliutina, A. Trelin, R. Elashnikov, D. Nazarov, M. Maximov, Y. Kalachyova, P. Sajdl, J. Lancok, M. Vondracek, V. Svorcik, O. Lyutakov, Design of hybrid Au grating/TiO2 structure for NIR enhanced photo-electrochemical water splitting, Chem. Eng. J. 443 (2022), 136440, https://doi.org/10.1016/j.cej.2022.136440.
[310] Z. Yang, C. Zhao, Y. Qu, H. Zhou, F. Zhou, J. Wang, Y. Wu, Y. Li, Trifunctional self-supporting cobalt-embedded carbon nanotube films for ORR, OER, and HER triggered by solid diffusion from bulk metal, Adv. Mater. 31 (2019) 1–8, https://doi.org/10.1002/adma.201808043.
[311] J. Wang, W. Cui, Q. Liu, Z. Xing, A.M. Asiri, X. Sun, Recent progress in cobalt-based heterogeneous catalysts for electrochemical water splitting, Adv. Mater. (2016), https://doi.org/10.1002/adma.201502696.
[312] Y. Yang, M. Forster, Y. Ling, G. Wang, T. Zhai, Y. Tong, A.J. Cowan, Y. Li, Acid treatment enables suppression of electron-hole recombination in hematite for photoelectrochemical water splitting, Angew. Chem. - Int. Ed. (2016), https://doi.org/10.1002/anie.201510869.
[313] B. Zhang, C. Xiao, S. Xie, J. Liang, X. Chen, Y. Tang, Iron-nickel nitride nanostructures in situ grown on surface-redox-etching nickel foam: Efficient and ultrasustainable electrocatalysts for overall water splitting, Chem. Mater. (2016), https://doi.org/10.1021/acs.chemmater.6b02610.
[314] F. Guo, Y. Wu, H. Chen, Y. Liu, L. Yang, X. Ai, X. Zou, High-performance oxygen evolution electrocatalysis by boronized metal sheets with self-functionalized surfaces, Energy Environ. Sci. 12 (2019) 684–692, https://doi.org/10.1039/c8ee03405b.
[315] Y.J. Wang, D.P. Wilkinson, J. Zhang, Noncarbon support materials for polymer electrolyte membrane fuel cell electrocatalysts, Chem. Rev. (2011), https://doi.org/10.1021/cr100060r.
[316] S. Sharma, B.G. Pollet, Support materials for PEMFC and DMFC electrocatalysts - a review, J. Power Sources (2012), https://doi.org/10.1016/j.jpowsour.2012.02.011.
[317] D. Zheng, L. Yu, W. Liu, X. Dai, X. Niu, W. Fu, W. Shi, F. Wu, X. Cao, Structural advantages and enhancement strategies of heterostructure water-splitting electrocatalysts, Cell Rep. Phys. Sci. (2021), https://doi.org/10.1016/j.xcrp.2021.100443.
[318] S. Yang, J.Y. Zhu, X.N. Chen, M.J. Huang, S.H. Cai, J.Y. Han, J. Sen Li, Self-supported bimetallic phosphides with artificial heterointerfaces for enhanced electrochemical water splitting, Appl. Catal. B Environ. (2022), https://doi.org/10.1016/j.apcatb.2021.120914.
[319] K. Chhetri, A. Muthurasu, B. Dahal, T. Kim, T. Mukhiya, S.H. Chae, T.H. Ko, Y. C. Choi, H.Y. Kim, Engineering the abundant heterointerfaces of integrated bimetallic sulfide-coupled 2D MOF-derived mesoporous CoS2 nanoarray hybrids for electrocatalytic water splitting, Mater. Today Nano. (2022), https://doi.org/10.1016/j.mtnano.2021.100146.
[320] A. Shukla, S.C. Singh, C.S. Saraj, G. Verma, C. Guo, Ni-based overall water splitting electrocatalysts prepared via laser-ablation-in-liquids combined with electrophoretic deposition, Mater. Today Chem. (2022), https://doi.org/10.1016/j.mtchem.2021.100691.
[321] S. Ligani Fereja, P. Li, Z. Zhang, J. Guo, Z. Fang, Z. Li, S. He, W. Chen, W-doping induced abundant active sites in a 3D NiS2/MoO2 heterostructure as an efficient electrocatalyst for urea oxidation and hydrogen evolution reaction, Chem. Eng. J. (2022), https://doi.org/10.1016/j.cej.2021.134274.
[322] D. Rathore, A. Banerjee, S. Pande, Bifunctional tungsten-doped Ni(OH)2/NiOOH nanosheets for overall water splitting in an alkaline medium, ACS Appl. Nano Mater. (2022), https://doi.org/10.1021/acsanm.1c04359.
[323] G. Zhao, B. Wang, Q. Yan, X. Xia, Mo-doping-assisted electrochemical transformation to generate CoFe LDH as the highly efficient electrocatalyst for overall water splitting, J. Alloy. Compd. (2022), https://doi.org/10.1016/j.jallcom.2022.163738.
[324] Y. Li, T. Dai, Q. Wu, X. Lang, L. Zhao, Q. Jiang, Design heterostructure of NiS–NiS2 on NiFe layered double hydroxide with Mo doping for efficient overall water splitting, Mater. Today Energy (2022), https://doi.org/10.1016/j.mtener.2021.100906.
[325] E. Jiang, J. Li, X. Li, A. Ali, G. Wang, S. Ma, P. Kang Shen, J. Zhu, MoP-Mo2C quantum dot heterostructures uniformly hosted on a heteroatom-doped 3D porous carbon sheet network as an efficient bifunctional electrocatalyst for overall water splitting, Chem. Eng. J. (2022), https://doi.org/10.1016/j.cej.2021.133719.
[326] J. Zhang, L. Dai, Nitrogen, phosphorus, and fluorine Tri-doped graphene as a multifunctional catalyst for self-powered electrochemical water splitting, Angew. Chem. - Int. Ed. (2016), https://doi.org/10.1002/anie.201607405.
[327] J.N. Tiwari, N.K. Dang, S. Sultan, P. Thangavel, H.Y. Jeong, K.S. Kim, Multi-heteroatom-doped carbon from waste-yeast biomass for sustained water splitting, Nat. Sustain. (2020), https://doi.org/10.1038/s41893-020-0509-6.
[328] H. Xu, H. Jia, B. Fei, Y. Ha, H. Li, Y. Guo, M. Liu, R. Wu, Charge transfer engineering via multiple heteroatom doping in dual carbon-coupled cobalt phosphides for highly efficient overall water splitting, Appl. Catal. B Environ. (2020), https://doi.org/10.1016/j.apcatb.2019.118404.
[329] W.J. Jiang, T. Tang, T. Tang, Y. Zhang, J.S. Hu, J.S. Hu, Synergistic modulation of non-precious-metal electrocatalysts for advanced water splitting, Acc. Chem. Res. (2020), https://doi.org/10.1021/acs.accounts.0c00127.
[330] D. Zheng, Z. Jing, Q. Zhao, Y. Kim, P. Li, H. Xu, Z. Li, J. Lin, Efficient Co-doped pyrrhotite Fe0.95S1.05 nanoplates for electrochemical water splitting, Chem. Eng. J. (2020), https://doi.org/10.1016/j.cej.2020.125069.
[331] X. Li, X. Hao, A. Abudula, G. Guan, Nanostructured catalysts for electrochemical water splitting: current state and prospects, J. Mater. Chem. A. (2016), https://doi.org/10.1039/c6ta02334g.
[332] X. Luo, P. Ji, P. Wang, R. Cheng, D. Chen, C. Lin, J. Zhang, J. He, Z. Shi, N. Li, S. Xiao, S. Mu, Interface engineering of hierarchical branched Mo-Doped Ni3S2/NixPy hollow heterostructure nanorods for efficient overall water splitting, Adv. Energy Mater. (2020), https://doi.org/10.1002/aenm.201903891.
[333] W. Kong, C. Bacaksiz, B. Chen, K. Wu, M. Blei, X. Fan, Y. Shen, H. Sahin, D. Wright, D.S. Narang, S. Tongay, Angle resolved vibrational properties of anisotropic transition metal trichalcogenide nanosheets, Nanoscale (2017), https://doi.org/10.1039/c7nr00711f.
[334] X. Li, H. Liu, C. Ke, W. Tang, M. Liu, F. Huang, Y. Wu, Z. Wu, J. Kang, Review of anisotropic 2D materials: controlled growth, optical anisotropy modulation, and photonic applications, Laser Photonics Rev. (2021), https://doi.org/10.1002/lpor.202100322.
[335] N.U.A. Babar, F. Hussain, M.N. Ashiq, K.S. Joya, Engineered modular design of a nanoscale CoNP/aunanohybrid assembly for high-performance overall water splitting, ACS Appl. Energy Mater. (2021), https://doi.org/10.1021/acsaem.1c01221.
[336] M.T. Chen, J.J. Duan, J.J. Feng, L.P. Mei, Y. Jiao, L. Zhang, A.J. Wang, Iron, rhodium-codoped Ni2P nanosheets arrays supported on nickel foam as an efficient bifunctional electrocatalyst for overall water splitting, J. Colloid Interface Sci. (2022), https://doi.org/10.1016/j.jcis.2021.07.101.
[337] C.R. Dhas, S.E.S. Monica, K. Jothivenkatachalam, A.J. Nathanael, V. Kavinkumar, R. Venkatesh, D. Arivukarasan, Direct-grown nebulizer-sprayed nickel-copper mixed metal oxide nanocomposite films as bifunctional electrocatalyst for water splitting, Ion. (Kiel.). ((2022), https://doi.org/10.1007/s11581-021-04285-6.
[338] L. Li, D. Yu, P. Li, H. Huang, D. Xie, C.C. Lin, F. Hu, H.Y. Chen, S. Peng, Interfacial electronic coupling of ultrathin transition-metal hydroxide nanosheets with layered MXenes as a new prototype for platinum-like hydrogen evolution, Energy Environ. Sci. (2021), https://doi.org/10.1039/d1ee02538d.
[339] W. Li, S. Mukerjee, B. Ren, R. Cao, R.A. Fischer, Open framework material based thin films: electrochemical catalysis and state-of-the-art technologies, Adv. Energy Mater. (2022), https://doi.org/10.1002/aenm.202003499.

[340] K. Wang, G. Liu, N. Hoivik, E. Johannessen, H. Jakobsen, Electrochemical engineering of hollow nanoarchitectures: pulse/step anodization (Si, Al, Ti) and their applications, Chem. Soc. Rev. (2014), https://doi.org/10.1039/c3cs60150a.
[341] H. Zhang, Y. Liu, H. Wu, W. Zhou, Z. Kou, S.J. Pennycook, J. Xie, C. Guan, J. Wang, Open hollow Co-Pt clusters embedded in carbon nanoflake arrays for highly efficient alkaline water splitting, J. Mater. Chem. A. (2018), https://doi.org/10.1039/c8ta07101b.
[342] Q. Wang, H. Zhao, F. Li, W. She, X. Wang, L. Xu, H. Jiao, Mo-doped Ni2P hollow nanostructures: highly efficient and durable bifunctional electrocatalysts for alkaline water splitting, J. Mater. Chem. A. (2019), https://doi.org/10.1039/c9ta01015g.
[343] E. Hu, J. Ning, D. Zhao, C. Xu, Y. Lin, Y. Zhong, Z. Zhang, Y. Wang, Y. Hu, A room-temperature postsynthetic ligand exchange strategy to construct mesoporous Fe-Doped CoP hollow triangle plate arrays for efficient electrocatalytic water splitting, Small (2018), https://doi.org/10.1002/smll.201704233.
[344] G. Prieto, H. Tüysüz, N. Duyckaerts, J. Knossalla, G.H. Wang, F. Schüth, Hollow nano- and microstructures as catalysts, Chem. Rev. 116 (2016) 14056–14119, https://doi.org/10.1021/acs.chemrev.6b00374.
[345] C. Wang, H. Xu, Y. Wang, H. Shang, L. Jin, F. Ren, T. Song, J. Guo, Y. Du, Hollow V-Doped CoMx(M = P, S, O) nanoboxes as efficient OER electrocatalysts for overall water splitting, Inorg. Chem. (2020), https://doi.org/10.1021/acs.inorgchem.0c01832.